Halogen (F, Cl and Br) systematics in alkaline to peralkaline magmatic rocks and their constituting minerals

Dissertation

der Mathematisch-Naturwissenschaftlichen Fakultät

der Eberhard Karls Universität Tübingen

zur Erlangung des Grades eines

Doktors der Naturwissenschaften

(Dr. rer. nat.)

vorgelegt von

Lianxun Wang

aus Hebei, China

Tübingen

2014

Tag der mündlichen Qualifikation:	15.08.2014
Dekan:	Prof. Dr. Wolfgang Rosenstiel
1. Berichterstatter:	Prof. Dr. Gregor Markl
2. Berichterstatter:	Dr. Michael Marks

Acknowledgement

Hereby I would like to extend my sincere gratitude to all those who helped me in the past four years.

Prof. Dr. Gregor Markl provided me the precious opportunity to study here. His continuous helps before and after my acceptance as a Ph.D. student and his expert suggestions and stimulating discussions for my research are always highly appreciated. Specially, his excellent and efficient work, seriously scientific spirit and strong love in geology career have always inspirited me, the past, present and future.

Dr. Michael Marks intensively guided my work during my entire Ph.D. study in Tübingen. I would like to owe my deepest gratitude to him for his patient supervising, kind advising and technical support. I learned from him not only the knowledge but also a scientific attitude, and many other basic skills. I can't imagine if everything would go such well without his great help.

My sincere thanks also go to my colleague, **Holger Teiber**, who kindly helped me a lot in both lab works and private stuff. Translation of the German abstract in this thesis has just been done with his help, which is highly acknowledged.

PD Dr. Thomas Wenzel is thanked for his technical support on the microprobe analysis and his efforts on our collaborated publications.

Prof. Dr. Jörg Keller, **PD Dr. Meinert Rahn, Dr. Anette von der Handt, Dr. Udo Neumann** and **Prof. Dr. Helmut Schleicher** are highly appreciated for providing several sample materials and for insightful discussions.

Special thanks to the committee members: **Prof. Dr. Gregor Markl, Dr. Michael Marks, PD Dr. Thomas Wenzel** and **Prof. Dr. Markus Novak.**

I also want to express my sincere appreciation to the following people for their various helps in laboratory and/or in office: **Sara Ladenburger, Kai Hettmann, Susanne Göb, Martin Mangler, Gabriele Stoschek, Tobias Fuβwinkel, Christopher Giehl, Benjamin Walter,**

Anselm Loges, Seinhilber Bernd, Hartmut Schulz, Nils Nolde, Eroqlu Sümeyya and **Oliver Preuβ.**

My sincere gratitude also goes to **my parents, my sister, my wife** and **my daughter** for their unconditional support, understanding and love, as well as to **my friends** in Tübingen and elsewhere, without whom life would be boring.

Last but not least, the **China Scholarship Council (CSC)** is thanked for granting scholarship and **Deutsche Forschungsgemeinschaft (grant MA 2563/3-1)** is acknowledged for partially funding the analytical work.

Table of Contents

Zusammenfassung

In dieser kumulativen Doktorarbeit wurden umfangreiche Untersuchungen zu Gehalten und Verteilungen von Halogenen (F, Cl und Br) in alkalinen bis peralkalinen Gesteinensproben durchgeführt, sowie an den jeweils enthalten gesteinsbildenden und halogenhaltigen Mineralen (z.B.: Apatit, Biotit, Amphibole, Titanit, etc.). Die untersuchten Proben wurden entsprechend gewählt, um repräsentative alkaline Komplexe weltweit abzudecken, was die Lokalitäten des Kaiserstuhls, Tamazeght, Hegau und Urach beinhaltet. Das Pyrohydrolyseextraktionsverfahren in Kombination mit Ionenchromatographie (PHIC), als auch Total-Reflexion-Röntgen-Fluoreszenz (TXRF) Analysen wurden durchgeführt, um die Halogengehalte in den Gesamtgesteinsproben zu ermitteln. Elektronenstrahlmikrosondenanalysen (EPMA) wurden zur Quantifizierung von F- und Cl-Gehalten in den verschiedenen Mineralen ausgeführt. TXRF Analysen von Mineralseparaten wurden durchgeführt um die Br-Gehalte zu quantifizieren.

Die Halogengehalte der 51 untersuchten alkalinen Gesteinen aus dem Kaiserstuhl, Hegau und Urach zeigen, dass primitive Olivin-Melilithite und Olivin-Nephilinite geringere Mengen an Cl und Br enthalten (gewöhnlich < 100 µg/g, bzw. < 0.3 µg/g), im Vergleich zu höher entwickelten Gesteinen wie Tephrite und Phonolithe (bis zu 7600 µg/g Cl und 34 µg/g Br). Signifikante Unterschiede können dabei in den F-Gehalten nicht gefunden werden (900-1100 µg/g, bzw. 400-2100 µg/g von primitive und entwickelten Gesteinen). Das Cl/Br Massenverhältnis der meisten untersuchten Gesteine ist relative einheitlich (370 ± 120), unabhängig vom Gesteinstyp oder der beprobten Lokalität. Dies lässt darauf schließen, dass partielles Aufschmelzen, fraktionierende Kristallisation und Entgasungsprozesse einen begrenzten Einfluss auf die Fraktionierung von Cl zu Br haben. Das beobachtete, durchschnittliche Cl/Br Massenverhältnis ist sehr ähnlich den Werten, die bisher für Mittelozeanischenrücken-Basalte (MORB) und Ozeaninsel-Basalte (OIB) berichtet wurden. Die niedrigen Cl- und Br-Gehalte der Olivin-Melilithite und Olivin-Nephilinite sind ähnlich der bestehenden Abschätzungen für den primitiven Mantel und den niedrigsten, bekannten Werte für MORB und OIB. Die F-Gehalte dieser Proben sind hingegen deutlich höher als bisherige Abschätzungen für den MORB und OIB Mantel. Dies könnte auf einen verhältnismäßig F-reichen Mantel unter Zentraleuropa hinweisen.

Apatite aus alkalinen Gesteinen des Kaiserstuhl-Komplexes weisen höhere Cl-, Br-, S-, Fe-, Mn-, Th-, U- und Si-Gehalte auf, jedoch geringere Sr- und Nb-Gehalte als Apatite aus assoziierten Karbonatiten. Apatite aus einer Bergalitprobe (Karbonat haltiges, melilititisches Ganggestein) und einer Schlotbrekzienprobe (Karbonate und Silikatfragmente enthalten) zeigen eine systematische Kern-Rand-Zonierung, bzw. Austauschzonierung. Chlor-, S-, Sr- und Si-Gehalte der Kernzone des bergalitischen Apatits und den Reliktbereichen des Apatits aus der Schlotbrekzie sind in ihrer Zusammensetzung ähnlich der Apatite aus den assoziierten, silikatischen Gesteinen. Im Gegensatz dazu haben die Randbereiche des bergalitischen Apatits und die ersetzten Bereiche des Apatits aus der Schlotbrekzie eine ähnliche Zusammensetzung wie Apatite aus assoziierten Karbonatite. Diese Beobachtungen werden als eine genetischer Link der alkalinen Gesteine und den damit assoziierten Karbonatiten des Kaiserstuhl-Komplexes interpretiert, welche durch den jeweiligen Apatitzusammensetzungen wiedergegeben wird. Cl- sowie Br-Gehalte von Apatiten könnten dabei potentiell ideale Indikatoren für diese Interpretation sein.

Die Halogengehalte von Apatit, Biotit, Amphibole und Titanit aus Gesteinen des Tamazeght Komplexes sind variable. Im Allgemeinen sind die Cl-Gehalte dieser Minerale aus Gabbros und Monzoniten höher als diejenigen aus Pyroxeniten und syenitischen Gesteinen. Die Berechnungen von Verteilungskoeffizienten (z.B.: $K_{D,F}^{Ap/Bt} = (\frac{X_F}{X_{OH}})^{Ap} / (\frac{X_F}{X_{OH}})^{Bt}$) für F und Cl zwischen koexistierendem Biotit und Amphibol zeigen relative konstante Werte von 1.1, bzw. 0.3. Die K_D-Werte für F und Cl für andere koexistierende Mineralpaare sind jedoch sehr variabel, was von der Kristallchemie des Minerals, den Halogengehalten und der vorherrschenden Temperatur der Schmelz abhängt. Die allgemein beobachtete und bevorzugte F-Partitionierungsabfolge ist Apatit ≫ Biotit, Amphibole und Titanit. Im Fall von Cl ist es Apatit > Amphibol > Biotit**.** Zusätzlich zu diesen herkömmlichen, halogenführenden Mineralen sind Sodalith, Fluorit und Eudialyt weitere beobachtete stabile Phasen in einigen untersuchten Gesteinstypen. Basierend auf den Daten dieser Arbeit steigen die F-Gehalte bei Anwesenheit von Fluorit in allen herkömmlichen, halogenführenden Mineralen an. Im Gegensatz dazu nehmen die Cl-Gehalte von allen herkömmlichen, halogenführenden Mineralen bei dem Auftreten von Sodalith und Eudialyt deutlich ab. Diese Beobachtungen werden auf die extrem stark bevorzugte Partitionierung von Cl in Sodalith und Eudialyt im Vergleich zu anderen halogenführenden Minerale zurückgeführt.

Abstract

In this cumulative thesis, comprehensive investigations were conducted on halogen (F, Cl and Br) contents and distributions in alkaline to peralkaline rock samples and their constituting halogen-bearing minerals (e.g., apatite, biotite, amphibole, titanite, etc.). The investigated samples were chosen to cover representative alkaline complexes worldwide which include the localities of the Kaiserstuhl, Hegau, Urach and Tamazeght. The pyrohydrolysis extraction technique combined with ion chromatography (PHIC) and the total reflection X-ray fluorescence (TXRF) analyses were performed to determine halogen contents in whole rock samples. Electric microprobe analysis (EMPA) were carried out to quantify F and Cl contents in various minerals and TXRF analyses were performed to quantify Br contents in mineral separates.

The halogen contents of 51 investigated alkaline rocks from Kaiserstuhl, Hegau and Urach reveal that primitive olivine melilitites and olivine nephelinites contain small amounts of Cl and Br (generally below 100 µg/g and below 0.3 µg/g, respectively) with respect to evolved rocks such as tephrites and phonolites (up to 7600 µg/g Cl and 34 µg/g Br). Significant differences are not found in F contents (900-1100 µg/g and 400-2100 µg/g for primitive and evolved rocks, respectively). The Cl/Br ratios of most investigated samples are relatively uniform (370 ± 120, mass ratio), regardless of rock type and sample locality. This suggests that partial melting, fractional crystallization, and degassing processes might have limited effects on the fractionation of Cl from Br. The observed average Cl/Br ratio is similar to previously reported values of mid-ocean-ridge basalts (MORB) and ocean-island basalts (OIB). The low Cl and Br contents of olivine melilitites and olivine nephelinites are similar to estimates for the primitive mantle and the lower end of values known for MORB and OIB samples. However, the F contents of these samples are much higher than previous estimates for the MORB and OIB mantle. This might indicate a relatively F-rich mantle beneath Central Europe.

Apatites from alkaline rocks of the Kaiserstuhl complex are found containing higher Cl, Br, S, Fe, Mn, Th, U and Si contents but lower Sr and Nb contents than apatites from associated carbonatites. Apatites from a bergalite sample (carbonate-bearing melilititic dyke rock) and a diatreme breccias (containing both carbonatitic and silicate fragments) show systematic core-rim and replaced zonations, respectively. The core zone of apatites from bergalite and the relic part

of apatites from diatreme breccias have similar compositions as apatites from silicate rocks in terms of Cl, S, Sr and Si contents. In contrast, those for the rim zones of apatites from bergalite and the repaced part of apatites from diatreme breccias are similar to the composition of apatites from carbonatites. These observations imply that a genetic link of alkaline rocks and associated carbonatites in the Kaiserstuhl complex were recorded by the respective apatite compositions. Thereby, Cl and Br contents of apatite might be potentially ideal indicators for that interpretation.

Halogen concentrations of apatite, biotite, amphibole and titanite from a series of alkaline rocks in Tamazeght complex are rather variable. In general, the Cl contents of these minerals from gabbros and monzonites are higher than those from pyroxenites and syenitic rocks. Calculations of the partitioning coefficients (e.g., $K_{D,F}^{Ap/Bt} = (\frac{X_F}{X_{OH}})^{Ap} / (\frac{X_F}{X_{OH}})^{Bt}$) for F and Cl between coexisting biotite and amphibole show relatively constant values of 1.1 and 0.3, respectively. However, the K_D values of F and Cl for other coexisting mineral pairs are highly variable which depend on the crystal chemistry of mineral, halogen contents and prevailing temperature of melt. The generally observed and preferred partitioning sequence for F is apatite ≫ biotite, amphibole, titanite, whereas for Cl it is apatite > amphibole > biotite. In addition to these common halogen-bearing minerals, sodalite, fluorite and eudialyte are further observed stable phases in some studied rock types. Based on our data, F contents in apatite, titanite, biotite and amphibole generally increase with the presence of fluorite. Conversely, with the presence of sodalite and eudialyte, the Cl contents of these common halogen-bearing minerals obviously decrease. These observations are attributed to the extremely strong partitioning preference of Cl to sodalite and eudialyte with respect to others.

Introduction

Halogens (usually F, Cl and Br) are non-negligible constitutes of volatiles. Despite their smaller amounts found in magmatic systems than water, carbon dioxide and sulfur-species, halogens play essential roles in many igneous processes. During mineralization, chlorine anions can be strongly complexed with numerous metal cations such as Pb, Zn, Cu, Ni, Co and Ag as chloride complexes, and thus making these metals highly mobile in saline hydrothermal fluids (Seward and Barnes, 1997; Coulson et al., 2001; Kendrick et al., 2005; Fuβwinkel, 2013; Johnson et al., 2013). During partial melting and crystallization, F and Cl can exert important effects on phase equilibria, solidus temperature and magma viscosity and rheology (Foley et al., 1986; Luth, 1988; Filiberto and Treiman, 2009; Filiberto et al., 2012; Baasner et al., 2013; Giehl et al., 2014). As an output of volcanic eruptions, hydrogen chloride is often one of the most abundant species which have detrimental effects on the behavior of our ecosystems (Aiuppa et al., 2009; Edmonds et al., 2009; Pyle and Mather, 2009; Marks et al., 2014).

Our knowledge on the chemical property, storage and cycle of halogens in the solid earth are far too fragmentary, mainly due to the analytical difficulties in these elements (Aiuppa et al., 2009; Pyle and Mather, 2009). In the recent years, with the development of analytical techniques particularly in measuring low abundances of heavy halogens (e.g., Br and I), blooming interests have been attracted on this issue (e.g., Webster et al., 2009; Zhang et al., 2012; Kendrick, 2012; Kendrick et al. 2012, 2013, 2014; Giehl et al., 2014; Mangler et al., 2014; Marks et al., 2014; Teiber et al., 2014; Wang et al., 2014). On one hand, the establishment of TXRF methods and the advance in PH-IC and Pyrohydrolysis combined Inductively Coupled Plasma Mass Spectrometry have allowed precise measurement of Br in rock and mineral powder materials (e.g., Chai and Muramatsu, 2007; Balcone- Boissard et al., 2009; Marks et al., 2012; Mangler et al., 2014; Wang et al., 2014). On the other hand, approaches of the Secondary Ion Mass Spectrometry technique open new perspectives for in-situ reliable quantification of halogens in minerals (Marks et al., 2012; Beyer et al., 2012; Bernini, et al., 2013).

As stated in the recent reviews of Aiuppa et al. (2009) and Pyle and Mather (2009), several key questions are urgently required to answer in the study of halogen geochemistry, including (1) halogen distributions in various geological materials, of particular in rocks and minerals from the

mantle; (2) halogen behaviors during partial melting, fractional crystallization, degassing and other geological processes; and (3) halogen partitioning in mineral-fluid-melt systems and between co-existing mineral phases.

Alkaline-peralkaline rocks are found having high solubility of halogens in comparison with cal-alkaline rocks (e.g., Kogarko, 1974; Carroll, 2005; Giehl et al., 2014). Retention of these halogens in rocks accordingly requires largely crystallization of halogen-rich minerals including both common halogen-bearing minerals (e.g., apatite, mica, amphibole and titanite) and less common ones, such as sodalite, eudialyte and fluorite (Giel et al., 2014; Wang et al., 2014). As a result, alkaline-peralkaline rocks and their constituting halogen-bearing minerals are potentially ideal objects for the study of halogen behaviors in magmatic systems.

In this Ph.D. work, comprehensive investigations were carried out on the distribution and variation of halogens (F, Cl and Br) in a large variety of alkaline to peralkaline rocks and their constituting halogen-bearing minerals from several representative alkaline complexes worldwide (Kaiserstuhl, Hegau, Urach and Tamazeght). This work was aimed to fundamentally improve our understanding on the halogen systematics in alkaline-peralkaline magmatism. As an introduction to the thesis, previous studies, recent major advances, and remaining scientific questions on several fundamental aspects related to this study were reviewed in the following sections.

Halogen abundances in earth's mantle

Several studies imply that a large proportion of halogen elements are trapped in modern earth's surface, resulting in a halogen-depleted interior in earth (e.g., Dong, 2005; Wishkerman, 2006; Pyle and Mather, 2009). For example, the ocean contains 19000 mg/l Cl and 65 mg/l Br in average (Yasushi, 1975; Kendrick et al., 2012), occupying ca. 73% and 51% of their total amounts in earth (Kramers, 2003). Accordingly, modern sediments and sedimentary rocks are also found rich in Cl and Br (see Pyle and Mather, 2009 and references therein).

Investigations of halogen abundances in mantle-related rocks are rather scarce (Pyle and Marther, 2009). Rough estimates of the primitive mantle imply low halogen concentrations (F = 18-28 µg/g, Cl = 1-38 µg/g, Br = 0.004-0.5 µg/g; e.g., Lyubetskaya and Korenaga, 2007; Newsom,

1995; Pyle and Marther, 2009). Similar low concentrations were observed in the melt inclusions from Siqueiros MORB samples (F = 50-135 µg/g; Cl = 1-21 µg/g; Saal et al., 2002). However, many other MORB and OIB rock and glass samples show variable halogen concentrations (Schilling et al., 1980; Michael and Schilling, 1989; Jambon et al., 1995; Kent et al., 2002; Coombs et al., 2004; Le Roux et al., 2006; Kenderick et al., 2012, 2013). These variations have been interpreted by the assimilation of seawater (Michael and Schilling, 1989; Kent et al., 2002; Coombs et al., 2004; Sumino et al., 2010; Kenderick et al., 2012, 2013), variable degrees of degassing, and mantle-derived heterogeneities in halogens (Schilling et al., 1980).

In contrast to the oceanic basaltic rocks, the continental rift-related alkaline to peralkaline rocks generally contain higher concentrations of F. For example, rift-related alkaline silicate rocks from Greenland, Oldoinyo Lengai (Tanzania) and Hawaii display F contents up to 1.2 wt %, which are partially interpreted to reflect mantle halogen abundances (Aoki et al., 1981; Köhler et al., 2009; Mangler et al., 2014). However, it is not clear whether these high halogen abundances really reflect the composition of a metasomatised source mantle or caused by low-degree partial melting in the mantle source.

The knowledge of halogen distribution in mantle minerals is extremely lacking (Aiuppa et al., 2009). Earlier works demonstrated that common hydrous minerals such as apatite and phlogopite are dominant mineral hosts of halogens in earth's mantle (Aoki et al., 1981; Smith et al., 1981; Foley et al., 1986; Edgar and Pizzolato, 1995; O'Reilly and Griffin, 2000). Complete melting of F-rich apatite could fulfill the F concentrations in basaltic rocks, whereas in alkaline rocks such as kimberlites additional F is required from phlogopite (Smith et al., 1981). However, recent studies argued that F-apatite may be only stable in strongly metasomatised mantle and anhydrous minerals such as olivine and pyroxene could be the major hosts for F in depleted mantle (Beyer et al., 2012 and references therein). Although these minerals have low F concentrations (2-10 ppm for olivine; 2-20 ppm for pyroxene; Beyer et al., 2012; Bernini, et al., 2013), their high modal proportion in the upper mantle make them as important fluorine reservoirs (Beyer et al., 2012).

Halogen behavior in magmatic processes

The behavior of halogens during magmatic processes, such as partial melting, fractional crystallization and degassing, primarily depends on their incompatible characters and their partitioning coefficients between melt and exsolved fluid. Fluorine has a small ionic radius similar to oxygen and thus can easily substitute hydroxyl and oxygen in many silicate minerals (e.g., apatite, amphibole, mica and titanite), resulting in moderate incompatibility during partial melting and fractional crystallization. Conversely, due to the larger ionic radii, Cl and Br are highly incompatible for these common hydrous silicate minerals and preferably partition into fluid during fluid exsolution. As a result, theoretically, F could be largely fractionated from Cl and Br by the magmatic processes mentioned above.

Numerous studies have demonstrated that during degassing Cl and Br could be efficiently emitted from magma, whereas the emission for F is much less pronounced (e.g., Villemant and Boudon, 1999; Balcone-Boissard et al., 2010; Aiuppa et al., 2009). However, experimental observations by Chevychelov et al. (2008) showed that high partition coefficients for F also exists between fluid and phonolitic melt at 200 MPa. Likewise, in some plutons significant quantities of F extracted by late-stage hydrothermal fluids from magma are also reported (e.g., Webster et al., 2004; Thomas et al., 2005). These contradictions have been interpreted by slow cooling process (Aiuppa et al., 2009) and by the effects of magma compositions (Chevychelov et al., 2008).

Comprehensive investigation focusing on the F and Cl variations through a differentiated rock sequence is rare. Two early works observed increasing F and Cl contents with increasing SiO_2 contents in natural rocks (Greenland and Lovering, 1966; Coradossi and Martini, 1981). A recent experimental study implies that both F and Cl contents increase with fractional crystallization in phonolitic melts and the F/Cl ratios remain constant until halogen-bearing minerals occur (Giehl et al., 2014). Thus, ignoring the influences by degassing, F/Cl ratios in melts strongly depend on the F/Cl ratios and abundances of stable halogen-bearing minerals during partial melting and magma differentiation.

Chlorine and Br are considered having similar geochemical behaviors and being not fractionated from each other in magmatic processes (Jambon et al., 1995; Balcone-Boissard et al., 2010; Kendrick et al., 2012; 2013). The Cl/Br ratios of pristine MORB and OIB samples have been observed showing only little variations, independent of rock type and sample locality (Schilling

et al., 1980; Jambon et al., 1995; Kendrick et al., 2012; 2013). Nevertheless, such information is extremely scarce for continental rocks due to the lack of a precise dataset for Br (Teiber et al., 2014; Mangler et al., 2014; Marks et al., 2012). To my knowledge, systematic study of Cl/Br ratios in alkaline to peralkaline rocks, which is essential to understand the Cl and Br distribution in the mantle beneath continental rift, has not yet been conducted so far.

Halogen distribution in volatile-bearing minerals

The F and Cl abundances in common volatile-bearing minerals (e.g., apatite, mica, amphibole and titanite) and their partitioning behaviors between mineral, melt and fluid have been investigated in a large number of studies since decades (e.g., Ekström, 1972; Munoz, 1984; Volfinger et al., 1985; Zhu and Sverjensky, 1992; Brenan, 1993; Edgar and Pizzolato, 1995; Icenhower and London, 1997; Mathez and Webster, 2005; Chevychelov et al., 2008; Webster, 2009; Zhang et al., 2012; Teiber et al., 2014). On one hand, incorporation of F and Cl in these minerals depended on a number of factors, including crystal chemistry of minerals, composition of melts/fluids, temperature and pressure. On the other hand, the F and Cl contents in minerals are in general positively correlated with the halogen contents of melt (Chevychelov et al., 2008; Webster et al., 2009; Doherty et al., 2014).

Few studies focus on F and Cl partitioning between coexisting volatile-bearing minerals mentioned above and quantitatively calculation or estimation of the inter-mineral partitioning coefficients of F and Cl are even rare (Ekström, 1972; Munoz, 1984; Zhu and Sverjensky, 1992; Markl et al., 1998). Ekström (1972) and Markl (1998) found that partitioning coefficients for F and Cl between co-existing biotite and amphibole are fairly uniform. Zhu and Sverjensky (1992) conducted experimental work and thermodynamic calculations and documented that partitioning of F and Cl between co-existing apatite and biotite is a complex function of temperature, pressure, and X_{Fe} of biotite. However, to our knowledge, no quantitative studies visited the partitioning of F and Cl in coexisting apatite-amphibole and titanite-apatite/biotite/amphibole pairs.

Due to the analytical difficulties, reliable Br data for volatile-bearing minerals are extremely scarce and rare of them focus on the Br partitioning between co-existing volatile-bearing

minerals (Ionov et al., 1997; O'Reilly and Griffin, 2000; Kendrick, 2012; Marks et al., 2012; Teiber et al., 2014; Wang et al., 2014). Furthermore, knowing the Cl/Br ratios of these minerals could improve our understanding on the fairly uniform Cl/Br ratios in rocks, such as MORB and OIB samples.

Contributions of this study

Chapter 1 presents halogen (F, Cl and Br) concentrations in a large series of alkaline rocks from the Kaiserstuhl, Hegau and Urach areas of the Upper Rhine graben region (South Germany). The investigated samples are very representative alkaline rocks and have been well-studied petrologically and geochemically by a large series of publications (e.g., Wimmenauer, 1966, 1974, 2003; Hubberten et al., 1988; Keller et al., 1990; Schleicher et al., 1990; 1991; Grapes and Keller, 2010). The halogen contents in these rocks are found variable from primitive ones (olivine nephelinites and olivine melilitites) to evolved ones (e.g., tepheritic and phonolitic rocks). Details are shown in the paper "Halogen variations in alkaline rocks from the Upper Rhine Graben (SW Germany): insights into F, Cl and Br behavior during magmatic processes" (Appendix 1) published in *CHEMICAL GEOLOGY*. Therein, the halogen behaviors during alkaline magmatic processes and the halogen abundances in the source mantle of these rocks were thoroughly discussed.

Chapter 2 presents compositional data, including F, Cl, Br and many other major and trace elemental contents, of apatites from the Kaiserstuhl alkaline volcanic complex (SW Germany). As one of the most important halogen-bearing mineral, apatites from alkaline silicate rocks display obviously distinct Cl and Br contents from those in associated carbonatites. More interestingly, the genetic links between these silicate rocks and carbonatites has been recorded in the compositional zonations of apatites from a bergalite (carbonate-bearing melilititic dyke rock) and a diatreme breccias (containing both carbonatitic and silicate fragments). The article "Apatites from the Kaiserstuhl Volcanic Complex, Germany: new constraints on the relationship between carbonatite and associated silicate rocks" (Appendix 2) published in *EUROPEAN JOURNAL OF MINERALOGY* goes into detail of the results.

In chapter 3, a large dataset of halogen (F, Cl, and Br) concentrations in volatile-bearing minerals from the alkaline-peralkaline rocks of the Tamazeght Complex, Morocco is present. This complex is also a well-known alkaline complex composed of a large variety of alkaline to peralkaline rocks from ultramafic to intermediate. The related manuscript entitled "Halogen partitioning between co-existing minerals from alkaline-peralkaline rocks: a case study of the Tamazeght Complex" (Appendix 3) is now prepared for submission. In this work, quantitative calculations and evaluations on the halogen partitioning between co-existing common volatile-bearing minerals (e.g., apatite, biotite, amphibole and titanite) and their influence factors have been conducted. Further discussions on some less common halogen-bearing minerals (e.g., sodalite, eudialyte and fluorite) were also involved, for example, the stability of these minerals and the distribution of halogens between these minerals and other common halogen-bearing minerals.

1. Halogen (F, Cl and Br) systematics in alkaline rocks from the Upper Rhine Graben, SW Germany

Geological settings and sample description

The Upper Rhine Graben (URG) located in southwest Germany is one of the largest branches of the Cenozoic rift system in western and central Europe (Illies, 1972, 1975; Wilson and Downes, 1991, 2006; Lustrino and Wilson, 2007). Along the graben and in its closer vicinity, Tertiary/Cenozoic volcanic centers, dykes, pipes, necks and diatremes are widespread (e.g., Wimmenauer, 1974; Keller et al., 1990; Wilson and Downes, 2006). The dominant rock types are alkaline basic rocks of sodic affinity and their more evolved differentiation products (e.g., trachytes, phonolites). Strongly silica-undersaturated olivine nephelinites and olivine melilitites characterize the southern sector of the URG as the only primitive mantle melts (e.g., Wimmenauer, 1974; Keller et al., 1990; Dunworth and Wilson, 1998; Keller, 2008). Samples of the present study are from three main volcanic fields in Southwest Germany, namely the Kaiserstuhl, Hegau and Urach areas.

The Kaiserstuhl is the largest volcanic to subvolcanic complex of the Upper Rhine Graben and was active between 18 and 13 Ma (Kraml et al., 1995; 2006; Keller et al., 2002). The main rock types exposed are tephrites, essexites, phonolites, basanites (limburgites), olivine nephelinites, hauynophyres, carbonatites and unusual carbonate- and melilite-bearing dyke rocks called bergalites which are considered as transitional between alkaline silicate rocks and carbonatites (Wimmenauer, 1966, 1974, 2003; Hubberten et al., 1988; Keller et al., 1990; Schleicher et al., 1990; Keller, 1997). Small occurrences of olivine melilitites are additionally present in the surrounding area, for example at Mahlberg and Lehen (Keller et al., 1990; Dunwoth and Wilson 1998). Spinel lherzolite nodules are found in some of the olivine nephelinites and olivine melilitites which are considered to represent relatively primitive mantle-derived melts (Keller et al., 1990; Schleicher et al., 1990, 1991; Dunworth and Wilson, 1998; Ulianov et al., 2007). Other evolved rocks, such as basanites, tephrites, essexites, phonolites and hauynophyres, are assumed

to reflect variable degrees of fractionation, potentially combined with minor amounts of crustal contamination (Keller et al., 1990; Schleicher et al., 1990).

The Hegau and Urach volcanic fields are situated in the adjacent regions east of the URG. Volcanic activity in both regions took place between about 16 and 7 Ma (Lippolt et al., 1973; Lippolt, 1983; Keller et al., 1990). Olivine melilitites (and melilite-bearing olivine nephelinites) and phonolites are two major rock types exposed in the Hegau area (Keller et al., 1990). The Urach field is known for its more than 350 diatreme centers consisting of olivine melilitites and (olivine) nephelinitites and lack of more evolved rocks (e.g., Mäusenest, 1974). Mineralogical, petrological and geochemical studies show that these primitive rocks are very similar to the olivine melilitites and olivine nephelinites from the Kaiserstuhl and its surroundings (Alibert et al., 1983; Keller et al., 1990; Kramm et al., 1990; Schleicher, 1990; Dunwoth and Wilson, 1998; Blusztajn and Hegner, 2002).

For this study we investigated 51 powdered whole-rock samples from alkaline igneous rocks of the Kaiserstuhl, Hegau and Urach areas, including 13 relatively primitive olivine nephelinites and olivine melilitites and 38 variably evolved alkaline rocks. Detailed petrographic descriptions of the investigated rocks are given by Blusztajn and Hegner (2002), Ulianov et al. (2007) and Wimmenauer (1966, 2003).

Summary of the results and discussion

The thirteen olivine nephelinites and olivine melilitites reveal a narrow range of F concentrations (900-1300 µg/g), with no significant differences among sample localities. Their Cl contents are low (10-100 µg/g), except for two outliers from the Kaiserstuhl (900 and 2200 µg/g, respectively). Bromine concentrations correlate with Cl, showing low contents (<0.3 µg/g) in Cl-poor samples and relatively higher ones (2 and 5 µg/g, respectively) in the two Cl-rich outliers. In contrast, the evolved alkaline rocks display larger variations in all halogens. Their F contents generally vary from 400 to 1400 µg/g, whereas Cl and Br vary largely from 50 to 7700 µg/g and from 0.4 to 34 µg/g, respectively, and are clearly higher than that of the primitive rocks.

Variation of halogen contents in bulk rocks are predominantly related with the constituting halogen-bearing minerals. The F contents in most investigated rocks roughly increase with increasing CIPW-calculated apatite abundance, indicating that apatite is an important F-carrier in these samples. However, contributions from other halogen-bearing minerals are also not neglected. For example, the phonolitic rocks are relatively poor in apatite but contain abundant titanite and thus show the most pronounced deviation in the Bulk F contents vs. apatite volume correlation diagram. For Cl and Br, the highest concentrations are present in hauynophyres, phonolites and bergalites, due to the significant amounts of sodalite-group minerals in these samples.

Considered as the most primitive mantle-derived melts (Hubberten et al., 1988; Keller et al., 1990; Schleicher et al., 1990; Dunworth and Wilson, 1998; Wilson, 2006), olivine nephelinitic and olivine melilititic samples are used to constrain the composition of their source mantle based on their halogen signatures. Since Cl and Br is strongly incompatible and is preferably enriched in melts than residual solids during partial melting, the low Cl and Br concentrations (10-100 µg/g for Cl and < 0.3 µg/g for Br) of the olivine nephelinites and olivine melilitites place an upper limit to the Cl and Br abundances of the source mantle. However, this conclusion is given on the ignoring of halogen emission during degassing. Two evidences seems support the missing of degassing processes to these samples: (1) their low Cl and Br concentrations are similar to previous estimates for the primitive mantle and the lower end of values reported for MORB and OIB samples (Schilling et al., 1978, 1980; Jambon et al., 1995; Saal et al., 2002; Kendrick et al., 2013); (2) These low Cl values are much lower than the reported Cl solubility in phonolitic melts (0.6-0.8 wt%; Signorelli and Carroll, 2000; Giehl et al., 2014). The F concentrations of the investigated olivine nephelinites and olivine melilitites are fairly constant (around 1100 ± 100 µg/g) and are much higher than estimates for the primitive and depleted mantle (Schilling et al, 1980; Newsom, 1995; Saal et al., 2002; Salters and Stracke, 2004; Lyubetskaya and Korenaga, 2007; Pyle and Mather, 2009). This indicates that mantle-derived nephelinitic and melilititic rocks are much higher in F than typical MORB and OIB samples, which could be caused by high F concentrations of the source mantle, or alternatively, by different degrees of mantle melting.

Displaying large variations, the halogen concentrations of evolved rocks could be undergone various modifications during fractional crystallization and degassing and thus are used to

constrain the halogen behavior during magmatic processes. Modeling of magma/crystal fractionation generally shows that F, Cl and Br concentrations increase with magma evolution because of their incompatible behavior. For our sample suite, however, there is no clear indication that halogen concentrations vary systematically with magma differentiation, which could be attributed to the retention and emission of halogens before and during degassing (Schilling et al., 1980; Webster et al., 1999; Harford et al., 2003; Lowenstern et al., 2012; Giehl et al., 2014). For example, high amounts of Cl and Br were incorporated by the sodalite-group minerals during an early stage, preventing them from late-stage degassing and thus resulting in the Cl- and Br- rich hauynophyres. In contrast, variable amounts of F were released in these samples due to the lack of effective mineral storage. This implies that halogens can be protected from degassing if they are incorporated in appropriate minerals. A series of tephritic samples with variable crystallinity (glassy tephrite, extrusive lavas and sub-volcanic essexites) showed positive correlations between their F, Cl and Br contents. Since these samples have similar geochemical and isotopic signatures with the only difference being textural: they vary from glassy to phanerocrystalline, we suggest that these correlations record halogen degassing due to crystallization of the matrix (c.f. second boiling; e.g., Webster et al., 1999). Simplified calculations imply that about 50 % F and 90 % Cl and Br were released during the crystallization process.

Despite the large variation over more than two orders of magnitude, Cl (from 50 to 7700 µg/g) and Br (from 0.3 to 34 µg/g) show a clear linear positive correlation for most of the investigated samples and the Cl/Br ratios generally vary from 200 to 600, with an average of 371 ± 120 (N =35, except for four outliers). This value is very similar to that from previous estimates for the MORB and OIB samples (Schilling et al., 1978, 1980; Jambon et al., 1995; Kendrick et al., 2012, 2013) as well as the alkaline silicate rocks from Oldoinyo Lengai volcano (Mangler et al., 2014). This demonstrates that variable degrees of partial melting, fractional crystallization and degassing have no large effect on Cl/Br ratios during the formation and evolution of sub-continental mantle-derived alkaline magmas and that no large heterogeneities in terms of Cl/Br ratios exist between different mantle reservoirs. Conversely, the F/Cl ratios vary largely over more than three orders of magnitude (from <0.1 to >100), implying F could be strongly fractionated from Cl and Br during magmatic processes.

2. Variation of halogens and other elements in apatites from the Kaiserstuhl alkaline volcanic complex, Germany

Geological settings and sample description

Geological setting of the Kaiserstuhl Volcanic Complex (KVC) could be found in Chapter 1. Hereby we mainly specify the petrology of the complex and the samples selected in this study.

Volcanism of the Kaiserstuhl complex is a sequence of early intrusion and extrusion of alkaline silicate rocks followed by late formation of carbonatites (Keller et al., 1990, 2008; Wimmenauer, 2003). The silicate rocks are dominated by tephrites, essexites and phonolites. Sub-dominant rock types include olivine-melilitites, olivine-nephelinites, limburgites (olivine + augite + glassy groundmass), hauynophyres, syenites, shonkinite porphyries, and mondhaldeites (Wimmenauer, 2003; Keller, 2008). Shonkinite porphyry and mondhaldeite are fractionated dyke rocks from the tephritic magma. Carbonatites consist of sövite intrusions (Badberg and Orberg), alvikitic dykes and rare extrusive carbonatites (Keller, 1981; Hubberten et al., 1988). These are spatially and temporally associated with (1) magmatic diatreme breccias, some of which are polygenic mixtures consisting of mafic cumulates, carbonatite and silicate rock fragments, fill pipe structures in the sövite bodies (Baranyi, 1977; Katz and Keller, 1981; Hubberten et al., 1988; Keller et al., 1990; Sigmund, 1996) and (2) bergalite dyke rocks (Hubberten et al., 1988; Schleicher et al., 1990; Keller, 1991, 1997), which are carbonate-bearing and silica-undersaturated rocks with a mineral assemblage of melilite + sodalite + perovskite + biotite ± nepheline + apatite + magnetite + calcite (Keller, 2008).

In this study we investigate apatite separates from twelve KVC rocks, including four sövitic carbonatites from surface outcrops and drill cores, one diatreme breccia, one bergalite, and six alkaline silicate rocks (one essexite, one mondhaldeite, one shonkinitic porphyry, and three

phonolitic rocks). Details on the petrography, mineralogy and geochemistry of these samples are given in Hubberten et al. (1988), Keller et al. (1990) and Schleicher et al. (1990).

Summary of the results and discussion

Compositional analysis shows that the Cl and Br concentrations in apatites from carbonatitic rocks (C.Ap) are always lower than those from alkaline silicate rocks (S.Ap), whereas the F values are largely overlapping. This agrees well with previous studies where apatites from carbonatite complexes were reported Cl-poor with mostly less than 0.1 wt% Cl (e.g., Eby, 1975; Hogarth, 1989; Seifert et al., 2000; Patiño Douce et al., 2011). The depleted Cl was explained by Cl partitioning into an aqueous fluid phase, which generally coexisted with the carbonatitic melt (Gittins, 1989; Seifert et al., 2000). The consistent behavior of Cl and Br contents in all apatites is also consistent with previously reported positive correlations between Cl and Br (O'Reilly and Griffin, 2000; Marks et al., 2012), implying Cl and Br behave similar while incorporated by apatite.

Beyond halogens, S, Fe, Mn, Th, U and Si contents in C.Ap are found generally lower than those in S.Ap, whereas Sr and Nb contents are higher in C.Ap. These chemical variations are mainly controlled by apatite-melt partitioning coefficients, melt composition, and the substitution mechanisms of apatite (e.g., Peng et al., 1997; Sha and Chappell, 1999; Harlov et al., 2002). For instance, the partitioning coefficient $D^{apatite\text{-}melt}$ value of Nb in apatite-carbonatitic melt system is found higher than that in apatite-silicate melt system, resulting in the relatively higher Nb contents in C.Ap. However, the higher Sr contents in C.Ap are most likely buffered by the melt composition, since carbonatitic melts are usually much richer in Sr than silicate melts (e.g., Hubberten et al., 1988; Keller et al., 1990). Besides, the positive correlations between S and Si and between La+Ce and Si for C.Ap and S.Ap imply that the substitutions of $Si^{4+} + S^{6+} = 2P^{5+}$ and $REE^{3+} + Si^{4+} = Ca^{2+} + P^{5+}$ play dominant roles for the variation of S and Si contents in C.Ap and S.Ap.

Apatites from bergalite show a systematic and discontinuous core-rim zonation under cathodoluminescence (CL) condition, with the core being compositionally similar to S.Ap and

the rim corresponding to C.Ap. This observation probably reflects the evolution of magma composition during cooling and crystallization of bergalite. The overgrowth of C.Ap-like rims on S.Ap-like cores imply that the bergalite apatites nucleated in a silicate melt and continued to crystallize from an evolving CO_2-enriched melt probably with carbonatitic affinity. The origin of carbonatitic melt could be principally explained by prolonged fractional crystallization of a melilite nephelinitic magma, which has been successfully conducted by early experimental works (Watkinson and Wyllie, 1971). The coherence of Cl contents in the rim zone of apatites from bergalite and C.Ap indicate that Cl is a good tracer for magma evolution.

Apatites from the diatreme breccia comprise three populations: (1) similar to S.Ap, (2) similar to C.Ap and (3) resembling apatite population (1) partially replaced by apatite (2). These observations are consistent with the mixing components of this sample which comprise both silicate and carbonatitic fragments. The replacement texture found in the apatites probably represents a late-stage fluid/melt reequilibration product and caused by metasomatism of late-injected carbonatitic melt on early crystallized apatites from silicate rock fragments. Overall, we conclude that apatite (1) is derived from silicate rock fragments and apatite (2) is crystallized from a later intruding carbonatitic melt, which metasomatized the silicate rock fragments and caused the replacement textures as observed in apatite population (3).

3. Halogen partitioning between coexisting minerals from alkaline to peralkaline rocks in Tamazeght Complex, Morocco

Geological settings and sample description

The Tamazeght (also known as Tamazert) complex is located in the northern margin of the High Altlas Mountain Range of Morocco. It intruded into Liassic to Cretaceous limestones within a Mesozoic graben-like structure that formed as a result of the continental collision between Africa and Europe and and the opening of Atlantic Ocean (Tisserant et al., 1976; Laville and Harmand, 1982). The Tamazeght complex is a multiphase plutonic to sub-volcanic complex with an outcrop area of around 70 km^2 and an intrusive depth of less than 3 km (Salvi et al., 2000). Chronology studies imply that the complex was emplaced between 44 to 35 Ma (Tisserant et al., 1976; Klein and Harmand, 1985; Marks et al., 2008; Wu et al., 2010).

The complex consists of a wide range of silica-undersaturated alkaline-peralkaline rocks and carbonatites as well as subsequent dyke swarms. The alkaline rocks include ultramafic pyroxenite (also known as jacupirangite and in some places change to foidolite with abundant nepheline; Kchit, 1990), glimmerite, shonkinite, gabbro, monzonite, monzosyenite (or plagisyenite; Kchit, 1990), nepheline syenite and malignite. Based on petrography, mineral chemisty and petrology (Marks et al., 2008, 2009), these rocks are classified into several rock groups, namely the ultramafic, shonkinitic, monzonitic and syenitic group. Petrogenesis of these rocks are assumed as products of variable degrees of fractional crystallization by a common parental magma with nephelinitic or monchiquitic composition, which was originated by low-degree partial melting of a carbonated amphibole-Iherzolite mantle source (Bouabdli et al., 1988; Kchit, 1990). However, Marks et al., (2008, 2009) proposed that the large variety of lithologies in the Tamazeght complex results from successive melting of compositionally heterogeneous mantle source region followed by different amounts of fractional crystallization processes.

For this study, 15 representative samples were chosen from major rock units in Tamazeght Complex. The geochemical and petrographic characteristics of these rocks are briefly summarized below. More details on the petrography and petrology of these rocks can be found in Marks et al. (2008, 2009) and Schilling et al. (2009).

Ultramafic rocks (pyroxenites and glimmerites) contain the lowest SiO_2 contents and the highest MgO contents. The halogen-bearing minerals observed include various amounts of biotite, minor titanite and abundant apatite. Shonkinites are petrographically similar to pyroxenites, except for the presence of amphibole and alkali feldspar. The halogen-bearing minerals (apatite, amphibole, biotite and titanite) all reach appreciable amounts and generally coexist with each other in these rocks. The monzonitic unit consists of gabbros, monzonites and foid monzosyenites. Their SiO_2 and MgO contents are variable, partly overlapping with that of the shonkinites, but reaching relatively high SiO_2 and alkali alkali ($Na_2O + K_2O$) and low MgO contents. In this rock group, coexisting of halogen-bearing minerals (amphibole, biotite, titanite and apatite) is common. In one sample (TMZ 157) sodalite is present. The syenitic rocks include nepheline syenites, miaskitic malignites and agpaitic malignites. They are the most evolved rocks of the complex, showing very high alkali ($Na_2O + K_2O$) and low MgO contents. Small amounts of amphibole and/or biotite occur in nepheline syenites but absent in malignites. Sodalite and fluorite are present in all samples of this rock group. Apatite and titanite are common in most rocks except the agpaitic malignite, where rare of them occur only as tiny inclusions in clinopyroxene. Additional eudialyte is present in the agpaitic malignite.

Summary of the results and discussion

The F and Cl contents of common halogen-bearing minerals (apatite, biotite, amphibole and titatnite) show considerable variation among the various rock groups. Apatites from syenitic rocks contain the highest amounts of F (3.0-3.4 wt %), followed by ultramafic rocks (2.8 to 2.9 wt %) and shonkinitic rocks (2.3-2.6 wt %). Apatites from monzonitic rocks are highly variable (2.5-3.2 wt %). Similarly, biotite and amphibole from syenitic rocks contain the highest F contents, whereas those from ultramafic and shonkinitic rocks generally show intermediate and the lowest F contents, respectively. Those from mozonitic rocks are highly variable. Similar

variation tendency of F are observed in the titanite from these rocks except an ultramafic sample. The Cl contents in these minerals mentioned above are rather low (maximum of 0.4 wt %). In general, apatites, biotites and amphiboles from monzonitic rocks and shonikinitic rocks contain relatively higher Cl contents than those from ultramafic rocks and syenitic rocks. Sodalites from a monzonitic rock and several syenitic rocks contain the highest Cl contents (aroud 6-7 wt %) and eudialyte from an agpaitic maliggnite are also Cl-rich (around 1.2 wt %). The Br contents are roughly correlated with Cl contents among minerals. A sodalite sample shows 75 μg/g Br, followed by the eudialyte (7 μg/g Br) and the apatite, biotite and amphibole (< 3 μg/g Br).

Consistent with recent studies on halogen-bearing minerals from calc-alkaline plutonic rocks (e.g., Zhang et al., 2012; Teiber et al., 2014), our data from alkaline to peralkaline rocks show that F contents generally decrease from apatite, through biotite, to amphibole and in a given sample, F-rich apatite is normally associated with F-rich biotite and F-rich amphibole. The F content in titanite is significantly lower than that in apatite but undistinguishable with biotite and amphibole and similarly F-rich titanite coexisted with F-rich apatite, biotite and amphibole except one ultramafic sample. The variation of Cl is more complex partly due to its low concentration in these minerals of this study. But in many samples, Cl-rich apatite is normally associated with Cl-rich biotite and/or Cl-rich amphibole as well as relatively Cl-rich sodalite. The Cl content in amphibole is always higher than that in coexisting biotite.

Calculation of the partitioning coefficients of F and Cl between coexisting minerals (e.g., $K_{D,F}^{Ap/Bt} = (\frac{X_F}{X_{OH}})^{Ap} / (\frac{X_F}{X_{OH}})^{Bt}$) according to Zhu and Sverjensky (1992) show that partitioning of F and Cl between coexisting biotite and amphibole are fairly constant with K_D values of 1.1 and 0.3, respectively, similar to previous studies (Ekström 1972; Markl et al., 1998). However, other partitioning coefficients (e.g., $K_{D,F}^{Ap/Bt}$, $K_{D,Cl}^{Ap/Bt}$, $K_{D,F}^{Ap/Am}$, $K_{D,Cl}^{Ap/Am}$, $K_{D,F}^{Bt/Ttn}$ and $K_{D,F}^{Am/Ttn}$) are largely variable and mainly controlled by temperature and mineral chemistry at constant pressure. For example, the partitioning coefficients between coexisting biotite and apatite decrease largely with increasing Mg contents in biotite, temperature and F contents in both apatite and biotite. These observations are rather similar with the thermodynamic calculations by Zhu and Sverjensky (1992) where he claim that the partitioning coefficients between coexisting biotite and apatite is a complex function of X_{Fe} of biotite, temperature and pressure.

Stability of fluorite in syenitic rocks indicate that the parental magma is rich in and F (e.g., Scaillet and Macdonard, 2004; Dplejs and Baker, 2006; Giehl et al., 2014), which could be further constrained by the relatively F-rich apatite, biotite, amphibole and/or titanite in the same samples. However, with the stability of sodalite in these rocks which suggests higher Cl in the magma (Stormer and Carmichael, 1971; Sharp et al., 1989; Giehl et al., 2014), the coexisting apatite, biotite and amphibole are relatively Cl-poor. This might indicate that extremely strong partitioning coefficients exist between sodalite and other common Cl-bearing minerals (Stormer and Carmichael, 1971).

Recent studies imply that during high-temperature magmatic processes Br shows a very similar geochemical behavior as Cl and therefore Cl/Br ratios in mantle-derived rocks, glasses and melt inclusions show a relatively narrow range (Jambon et al., 1995; Balcone-Boissard et al., 2010; Kendrick et al., 2012, 2013a, 2013b; Mangler et al., 2014; Wang et al., 2014). However, our data show that the Cl/Br ratios of investigated biotite, amphibole, sodalite and eudialyte are rather scattering than those fairly constant values found in the rock samples. It is therefore unclear to us why Cl/Br ratios for bulk halogens are fairly constant particularly in alkaline rocks where the halogen-bearing mineral abundances in alkaline rocks are highly variable (e.g., Wang et al., 2014). Obviously further work on this topic is needed.

Quantitatively evaluation of the F and Cl abundances in the alkaline magmas were conducted based on their concentrations in halogen-bearing minerals (apatite, biotite and amphibole). The results imply that F increase from shonkinitic magma (1600-2000 μg/g), through ultramafic magma (2000-2100 μg/g) to syenitic magma (2300-2600 μg/g) with a large variation in monzonitic magma (1800-2400 μg/g). The calculated Cl contents in sodalite-free magmas are generally in a similar level with the analyzed Cl contents of alkaline rocks from Upper Rhine Graben (Wang et al., 2014). However, the calculated Cl contents in sodalite-bearing magmas are significantly lower than those analyzed in sodalite-bearing phonolitic rocks of the Kaiserstuhl, Germany (54 μg/g vs. 1200-7600 μg/g; Wang et al., 2014). This could result from the extremely strong partitioning preference of Cl to sodalite with respect to apatite, biotite and amphibole as we mentioned above. As a result, in sodalite-bearing rocks, one needs to take more care when using apatite, biotite or amphibole to model the Cl concentrations in melts.

References

Aiuppa, A., Baker, D.R., Webster, J.D., 2009. Halogens in volcanic systems. Chemical Geology 263(1), 1-18.

Alibert, C., Michard, A., Albarede, F., 1983. The transition from alkali basalts to kimberlites: isotope and trace element evidence from melilitites. Contributions to Mineralogy and Petrology 82(2-3), 176-186.

Baasner, A., Schmidt, B.C., Webb, S.L., 2013. Compositional dependence of the rheology of halogen (F, Cl) bearing aluminosilicate melts. Chemical Geology 346, 172-183.

Balcone- Boissard, H., Michel, A., Villemant, B., 2009. Simultaneous determination of fluorine, chlorine, bromine and iodine in six geochemical reference materials using pyrohydrolysis, ion chromatography and inductively coupled plasma- mass spectrometry. Geostandards and Geoanalytical Research 33(4), 477-485.

Balcone-Boissard, H., Villemant, B., Boudon, G., 2010. Behavior of halogens during the degassing of felsic magmas. Geochemistry, Geophysics, Geosystems 11, Q09005, doi:10.1029/

2010GC003028.

Baranyi, I., 1977. Petrography and geochemistry of the subvolcanic breccias of the Kaiserstuhl volcano (SW-Germany). Neues Jahrbuch für Mineralogie Abhandlungen 128, 254-284.

Bernini, D., Wiedenbeck, M., Dolejš, D., Keppler, H., 2013. Partitioning of halogens between mantle minerals and aqueous fluids: implications for the fluid flow regime in subduction zones. Contributions to Mineralogy and Petrology 165(1), 117-128.

Beyer, C., Klemme, S., Wiedenbeck, M., Stracke, A., Vollmer, C., 2012. Fluorine in nominally fluorine-free minerals: Experimental partitioning of F between olivine, orthopyroxene and silicate melts with implications for magmatic processes. Earth and Planetary Science Letters 337-338, 1-9.

Blusztajn, J., Hegner, E., 2002. Osmium isotopic systematics of melilitites from the Tertiary Central European Volcanic province in SW Germany. Chemical Geology 189(1), 91-103.

Brenan, J.M., 1993. Partitioning of fluorine and chlorine between apatite and aqueous fluids at high pressure and temperature: implications for the F and Cl content of high P-T fluids. Earth and Planetary Science Letter 117, 251-263.

Carroll, M.R., 2005. Chlorine solubility in evolved alkaline magmas. Annals of Geophysics 48(4-5), 619-631.

Chai, J.Y., Muramatsu, Y., 2007. Determination of bromine and iodine in twenty- three geochemical reference materials by ICP- MS. Geostandards and Geoanalytical Research 31(2), 143-150.

References

Chevychelov, V.Y., Botcharnikov, R.E., Holtz, F., 2008. Experimental study of fluorine and chlorine contents in mica (biotite) and their partitioning between mica, phonolite melt, and fluid. Geochemistry International 46(11), 1081-1089.

Coombs, M.L., Sisson, T.W., Kimura, J.I., 2004. Ultra-high chlorine in submarine Kılauea glasses: evidence for direct assimilation of brine by magma. Earth and Planetary Science Letters 217(3), 297-313.

Coradossi, N., Martini, M., 1981. Fluorine, Chlorine and lithium distribution in igneous rocks of Lipari and Vulcano (Aeolian Islands, Italy). Bulletin Volcanologique 44(3), 565-571.

Coulson, I.M., Dipple, G.M., Raudsepp, M., 2001. Evolution of HF and HCl activity in magmatic volatiles of gold-mineralized Emerald Lake Pluton, Yurkon Territory, Canada. Mineralium Deposita 26, 594-606.

Doherty, A.J., Webster, J.D., Goldoff, B.A., Piccoli, P.M., 2014. Partitioning behavior of chlorine and fluorine in felsic melt-fluid(s)-apatite systems at 50 MPa and 850-950 ℃. Chemical Geology Doi: 10.1016/j.chemgeo. 2014.06.023.

Dong, P., 2005. Halogen- element (F, Cl and Br) behavior in apatites, scapolite, and sodalite: an experimental investigation with field applications. Ph. D. thesis, pp 1-234.

Dunworth, E.A., Wilson, M., 1998. Olivine melilitites of the SW German Tertiary volcanic province: mineralogy and petrogenesis. Journal of Petrology 39, 1805-1836.

Eby, G.N., 1975. Abundance and distribution of the rare-earth elements and yttrium in the rocks and minerals of the Oka carbonatite complex. Geochima et Cosmochima Acta 39, 597-620.

Edgar, A.D., Pizzolato, L.A., 1995. An experimental study of partitioning of fluorine between K-richterite, apatite, phlogopite, and melt at 20 kbar. Contributions to Mineralogy and Petrology 121(3), 247-257.

Edmonds, M., Gerlach, T.M., Herd, R.A., 2009. Halogen degassing during ascent and eruption of water-poor basaltic magma. Chemical Geology 263, 122-130.

Ekström,T.K., 1972. The distribution of fluorine among some coexisting minerals. Contributions to Mineralogy and Petrology 34(3), 192-200.

Filiberto, J., Treiman, A.H., 2009. The effect of chlorine on the liquidus of basalt: first results and implications for basalt genesis on Mars and Earth. Chemical Geology 263, 60-68.

Filiberto, J., Wood, J., Dasgupta, R., Shimizu, N., Le, L., Treiman, A.H., 2012. Effect of fluorine on near-liquidus phase equilibria of an Fe-Mg rich basalt. Chemical Geology 312-313, 118-126.

Foley, S.F., Taylor, W.R., Green, D.H., 1986. The effect of fluorine on phase relationships in the system $KAlSiO_4$-Mg_2SiO_4-SiO_2 at 28 kbar and the solution mechanism of fluorine in silicate melts. Contributions to Mineralogy and Petrology 93(1), 46-55.

Fuβwinkel, T., Wagner, T., Wälle, M., Wenzel, T., Heinrich, C.A., Markl, G., 2013. Fluid mixing forms basement-hosted Pb-Zn deposits: Insight from metal and halogen geochemistry of individual fluid inclusions. Geology 41(6), 679-682.

Gittins, J., 1989. The origin and evolution of carbonatite magmas. in "Carbonatites: Genesis and Evolution", K. Bell ed., Unwin Hyman, London, 580-600.

Grapes, R., Keller, J., 2010. Fe^{2+} dominant rhönite in undersaturated alkaline basaltic rocks, Kaiserstuhl volcanic complex, Upper Rhine Graben, SW Germany. European Journal of Mineralogy 22(2), 285-292.

Greenland, L., Lovering, J.F., 1966. Fractionation of fluorine, chlorine and other trace elements during differentiation of a tholeiitic magma. Gechimica et Cosmochimica Acta 30, 963-982.

Harford, C.L., Sparks, R.S.J., Fallick, A.E., 2003. Degassing at the Soufrière Hills Volcano, Montserrat, recorded in matrix glass compositions. Journal of Petrology 44(8), 1503-1523.

Harlov, D.E., Förster, H.J., Nijland, T.G., 2002. Fluid-induced nucleation of (Y+ REE)-phosphate minerals within apatite: nature and experiment. Part I. Chlorapatite. American Mineralogist 87(2-3), 245-261.

Hogarth, D.D., 1989. Pyrochlore, apatite and amphibole: distinctive minerals in carbonatite. in "Carbonatites: Genesis and Evolution", K. Bell ed., Unwin Hyman, London, 105-148.

Hubberten, H.W., Katz-Lehnert, K., Keller, J., 1988. Carbon and oxygen isotope investigations in carbonatites and related rocks from the Kaiserstuhl, Germany. Chemical Geology 70, 257-274.

Icenhower, J.P., London, D., 1997. Partitioning of fluorine and chlorine between biotite and granitic melt: experimental calibration at 200 MPa H_2O. Contributions to Mineralogly and Petrology 127(1-2), 17-29.

Illies, J.H., 1972. The Rhine graben rift system-plate tectonics and transform faulting. Geophysical Surveys 1(1), 27-60.

Illies, J.H., 1975. Recent and paleo-intraplate tectonics in stable Europe and the Rhinegraben rift system. Tectonophysics 29(1), 251-264.

Ionov, D.A., Griffin, W.L., O'Reilly, S.Y., 1997. Volatile-bearing minerals and lithophile trace elements in the upper mantle. Chemical Geology 14(3), 153-184.

Jambon, A., Déruelle, B., Dreibus, G., Pineau, F., 1995. Chlorine and bromine abundance in MORB: the contrasting behaviour of the Mid-Atlantic Ridge and East Pacific Rise and implications for chlorine geodynamic cycle. Chemical Geology 126(2), 101-117.

Johnson, E.R., Kamenetsky, V.S., Mcphie, J., 2013. The behavior of metals (Pb, Zn, As, Mo, Cu) during crystallization and degassing of rhyolites from the Okataina volcanic center, Taupo volcanic zone, New Zealand. Journal of Petrology 54, 1641-1659.

Katz, K., Keller, J., 1981. Comb-layering in carbonatite dykes. Nature 294, 350-352.

Kchit, A., 1990. Le complexe plutonique alcalin du Tamazert, Haut-Atlas de Midelt (Maroc): pétrologie et structurologie. Toulouse 3.

Keller, J., 1981. Carbonatitic volcanism in the Kaiserstuhl alkaline complex: Evidence for highly fluid carbonatitic melts at the earth's surface. Journal of Volcanology Geothermal Research 9, 423-431.

Keller, J., 1997. Bergalite-Okaite-Turjaite: The carbonatite-melilitite connection. Geol.Ass. /Mineral. Ass. Annual Meeting Ottawa. Abstracts, A77.

Keller, J., 2008. Tertiary Rhinegraben volcanism: Kaiserstuhl and Hegau. 9th International Kimberlite Conference. Field Trip Guide 38.

Keller, J., Brey, G., Lorenz, V., Sachs, P., 1990. IAVCEI 1990 Pre-conference Excursion 2A: Volcanism and Petrology of the Upper Rhinegraben (Urach-Hegau-Kaiserstuhl). 1-60.

Keller, J., Kraml, M., Henjes-Kunst, F., 2002. $^{40}Ar/^{39}Ar$ single crystal laser dating of early volcanism in the Upper Rhine Graben and tectonic implications. Schweizerische Mineralogische und Petrographische Mitteilungen 82, 121-130.

Kendrick, M.A., 2012. High precision Cl, Br and I determinations in mineral standards using the noble gas method. Chemical Geology 292-293, 116-126.

Kendrick, M.A., Arculus, R.J., Danyushevsky, L.V., Kamenetsky, V.S., Woodhead, J.D., Honda, M., 2014. Subduction-related halogen (Cl, Br and I) and H_2O in magmatic glasses from Southwest Pacific Backarc Basins. Earth and Planetary Science Letters 400, 165-176.

Kendrick, M.A., Burgess, R., Harrison, D., Bjørlykke, A., 2005. Noble gas and halogen evidence for the origin of Scandinavian sandstone-hosted Pb-Zn deposits. Geochimica et cosmochimica acta 69(1), 109-129.

Kendrick, M.A., Honda, M., Pettke, T., Scambelluri, M., Phillips, D., Giuliani, A., 2013. Subduction zone fluxes of halogens and noble gases in seafloor and forearc serpentinites. Earth and Planetary Science Letters 365, 86-96.

Kendrick, M.A., Kamenetsky, V.S., Phillips, D., Honda, M., 2012. Halogen systematics (Cl, Br, I) in mid-ocean ridge basalts: A Macquarie Island case study. Geochimica et Cosmochimica Acta 81, 82-93.

Kent, A.J., Peate, D.W., Newman, S., Stolper, E.M., Pearce, J.A., 2002. Chlorine in submarine glasses from the Lau Basin: seawater contamination and constraints on the composition of slab-derived fluids. Earth and Planetary Science Letters 202(2), 361-377.

Klein, J.L., Harmand, C., 1985. Le volcanisme de la région de Zebzate; age relations avec le complex alcalin a carbonatites du Tamazert (Haut-Atlas de Midelt, Maroc). 110e Congrès National de la Société Sav., Montpellier, Sci., Fascicule VII, 147-152.

Kogarko, L.N., 1974. Role of volatiles. In Sørensen, H. (ed) The alkaline rocks. Wiley, London, pp 474-487.

Kramers, J.D., 2003. Volatile element abundance patterns and an early liquid water ocean on Earth. Precambrain Research 126, 379-394.

Kraml, M., Keller, J., Henjes-Kunst, F., 1995. New K/Ar, $^{40}Ar/^{39}Ar$ step-heating and 40Ar/39Ar laser fusion dates for the Kaiserstuhl volcanic complex (Upper Rhine Graben; Germany). European Journal of Mineralogy Beihefte 7(1), 142.

Kraml, M., Pik, R., Rahn, M., Selbekk, R., Carignan, J., Keller, J., 2006. A new multi-mineral age reference material for $^{40}Ar/^{39}Ar$, (U-Th)/He and Fission Track dating methods: The Limberg t3 tuff. Geostandards and Geoanalytical Research 30, 73-86.

Laville, E., Harmand, C., 1982. Evolution magmatique et tectonique du bassin intracontinental mésozoique du Haut-Atlas (Maroc): un modèle de mise en place synsédimentaire de massifs "anorogeniques" liés a des dérochements. Bulletin de la Société Géologique de France 7, 221-227.

Le Roux, P.J., Shirey, S.B., Hauri, E.H., Perfit, M.R., Bender, J.F., 2006. The effects of variable sources, processes and contaminants on the composition of northern EPR MORB (8–10° N and 12–14° N): Evidence from volatiles (H_2O, CO_2, S) and halogens (F, Cl). Earth and Planetary Science Letters 251(3), 209-231.

Lippolt, H.J., 1983. K/Ar age determinations and the correlation of Tertiary volcanic activity in Central Europe. Geologisches Jahrbuch, D52, 113-135.

Lippolt, H.J., Todt, W., Baranyi, I., 1973. K-Ar ages of basaltic rocks from the Urach volcanic district SW-Germany. Fortschr Miner 50 Beiheft 3, 101-102.

Lowenstern, J.B., Bleick, H., Vazquez, J.A., Castro, J.M., Larson, P.B., 2012. Degassing of Cl, F, Li, and Be during extrusion and crystallization of the rhyolite dome at Volcán Chaitén, Chile during 2008 and 2009. Bulletin of volcanology 74(10), 2303-2319.

Lustrino M, Wilson M., 2007. The circum-Mediterranean anorogenic Cenozoic igneous province. Earth-Science Reviews 81(1): 1-65.

Luth, R.W., 1988. Effects of F on phase equilibria and liquid structure in the system NaAlSiO4-CaMgSi2O6-SiO2. American Mineralogist 87(7), 813-821.

Lyubetskaya, T., Korenaga, J., 2007. Chemical composition of Earth's primitive mantle and its variance: 1. Method and results. Journal of Geophysical Research: Solid Earth 112(B3), 1978–2012.

Mangler, M.F., Marks, M.A.W., Zaitzev, A.N., Eby, G.N., Markl, G., 2014. Halogen (F,Cl, and Br) at Oldoinyo Lengai volcano (Tanzania): Effects of magmatic differentiation, silicate – natrocarbonatite melt separation and surface alteration of natrocarbonatite. Chemical Geology 365, 43-53.

Markl, G., Piazolo, S., 1998. Halogen-bearing minerals in syenites and high-grade marbles of Dronning Maud Land, Antarctica: monitors of fluid compositional changes during late-magmatic fluid-rock interaction processes. Contributions to Mineralogy and Petrology 132 (3), 246-268.

Marks, A.W.M., Wenzel, T., Whitehouse, M.J., Loose, M., Zack, T., Barth, M., Worgard, L., Krasz, V., Eby, G.N., Stosnach, H., Markl, G., 2012. The volatile inventory (F, Cl, Br, S, C) of magmatic apatite: an integrated analytical approach. Chemical Geology 291, 241-255.

Marks, M.A.W., Neukirchen, F., Vennemann, T., Markl, G., 2009. Textural, chemical, and isotopic effects of late-magmatic carbonatitic fluids in the carbonatite–syenite Tamazeght complex, High Atlas Mountains, Morocco. Mineralogy and Petrology 97(1-2), 23-42.

Marks, M.A.W., Schilling, J., Coulson, I.M., Wenzel, T., Markl, G., 2008. The alkaline–peralkaline Tamazeght complex, High Atlas Mountains, Morocco: mineral chemistry and petrological constraints for derivation from a compositionally heterogeneous mantle source. Journal of Petrology 49(6), 1097-1131.

Mathez, E.A., Webster, J.D., 2005. Partitioning behavior of chlorine and fluorine in the system apatite-silicate melt-fluid. Geochimica et Cosmochimica Acta 69(5), 1275-1286.

Mäussnest, O., 1974. Die Eruptionspunkte des Schwäbischen Vulkans. Zeitschrift der Deutschen Gologischen Gesellschaft Band 125, 23-54.

Michael P.J, Schilling J.G., 1989. Chlorine in mid-ocean ridge magmas: evidence for assimilation of seawater-influenced components. Geochimica et Cosmochimica Acta 53(12), 3131-3143.

Munoz, J.L., 1984. F-OH and Cl-OH exchange in micas with applications to hydrothermal ore deposits. Reviews in Mineralogy and Geochemistry 13(1), 469-493.

Munoz, J.L., Ludington, S.D., 1974. Fluoride-hydroxyl exchange in biotite. American Journal of Science 274(4), 396-413.

Newsom, H.E., 1995. Composition of the solar system, planets, meteorites, and major terrestrial reservoirs. Global Earth Physics, 159-189.

O'Reilly, S.Y., Griffin, W.L., 2000. Apatite in the mantle: implications for metasomatic processes and high heat production in Phanerozoic mantle. Lithos 53(3), 217-232.

Patiño Douce, A.E., Roden, M.F., Chaumba, J., Fleisher, C., Yogodzinski, G., 2011. Compositional variability of terrestrial mantle apatites, thermodynamic modeling of apatite volatile contents, and the halogen and water budgets of planetary mantles. Chemical Geology 288, 14-31.

Peng, G., Luhr, J.F., McGee, J.J., 1997. Factors controlling sulfur concentrations in volcanic apatite. American Mineralogist 82, 1210-1224.

Pyle, D.M., Mather, T.A., 2009. Halogens in igneous processes and their fluxes to the atmosphere and oceans from volcanic activity: A review. Chemical Geology 263(1), 110-121.

Salters, V.J., Stracke, A., 2004. Composition of the depleted mantle. Geochemistry, Geophysics, Geosystems 5(5).

Salvi, S., Fontan, F., Monchoux, P., Williams-Jones, A.E., Moine, B., 2000. Hydrothermal mobilization of high field strength elements in alkaline igneous systems: evidence from the Tamazeght Complex (Morocco). Economic Geology 95(3), 559-576.

Scaillet, B., Macdonald, R., 2004. Fluorite stability in silicic magmas. Contributions to Mineralogy and Petrology 147(3): 319-329.

Schilling, J., Marks, M.A.W., Wenzel, T., Markl, G., 2009. Reconstruction of magmatic to subsolidus processes in an agpaitic system using eudialyte textures and composition: a case study from Tamazeght, Morocco. The Canadian Mineralogist 47(2), 351-365.

Schilling, J.G., Bergeron, M.B., Evans, R., Smith, J.V., 1980. Halogens in the Mantle Beneath the North Atlantic. Philosophical Transactions of the Royal Society of London. Series A, Mathematical and Physical Sciences 297, 147-178.

Schleicher, H., Baumann, A., Keller, J., 1991. Pb isotopic systematics of alkaline volcanic rocks and carbonatites from the Kaiserstuhl, upper Rhine rift valley, FRG. Chemical geology 93, 231-243.

Schleicher, H., Keller, J., Kramm, U., 1990. Isotope studies on alkaline volcanics and carbonatites from the Kaiserstuhl, Federal Republic of Germany. Lithos 26, 21-35.

Seifert, W., Kämpf, H., Wasternack, J., 2000. Compositional variation in apatite, phlogopite and other accessory minerals of the ultramafic Delitzsch complex, Germany: implication for cooling history of carbonatites. Lithos 53, 81-100.

Seward, T.M., Barnes, H.L., 1997. Metal transport by hydrothermal ore fluids. In: H.L. Barnes (Ed.), Geochemistry of hydrothermal ore deposits. New York, John Wiley & Sons, pp. 435-486.

Sha, L.K., Chappell, B.W., 1999. Apatite chemical composition, determined by electron microprobe and laser-ablation inductively coupled plasma mass spectrometry, as a probe into granite petrogenesis. Geochimica et Cosmochima Acta 63, 3861-3881.

Sharp, Z.D., Helffrich, G.R., Bohlen, S.R., Essene, E.J., 1989. The stability of sodalite in the system $NaAlSiO_4$ - NaCl. Geochimica et Cosmochimica Acta 53(8), 1943-1954.

Sigmund, J., 1996. Diatrembreccien, Mantelxenolithe und Karbonatite in der Kernbohrung KB2 im Kaiserstuhl. PhD thesis Universität Freiburg.

Signorelli, S., Carroll, M.R., 2000. Solubility and fluid-melt partitioning of Cl in hydrous phonolitic melts. Geochimica et Cosmochimica Acta 64(16), 2851-2862.

Stormer, J.C., Carmichael, I.S.E., 1971. The free energy of sodalite and the behavior of chloride, fluoride and sulfate in silicate magmas. American Mineralogist 56, 292-306.

Sumino, H., Burgess, R., Mizukami, T., Wallis, S. R., Holland, G., Ballentine, C.J., 2010. Seawater-derived noble gases and halogens preserved in exhumed mantle wedge peridotite. Earth and Planetary Science Letters 294(1), 163-172.

Teiber, H., Marks, M.A., Wenzel, T., Siebel, W., Altherr, R., Markl, G., 2014. The distribution of halogens (F, Cl, Br) in granitoid rocks. Chemical Geology 374, 92-109.

Thomas, R., Förster, H.J., Rickers, K., Webster, J.D., 2005. Formation of extremely F-rich hydrous melt fractions and hydrothermal fluids during differentiation of highly evolved tin-granite magmas: a complex melt/fluid-inclusion study. Mineralium Deposita 148, 582-601.

Tisserant, D., Thuizat, R., Agard, J., 1976. Données géochronologiques sur le complexe de roches alcalines du Tamazeght (Haut Atlas de Midelt, Maroc). Bureau des Recherches Géologiques Minière Bulletin, Section 23, 279-283.

Ulianov, A., Müntener, O., Ulmer, P., Pettke, T., 2007. Entrained macrocryst minerals as a key to the source region of olivine nephelinites: Humberg, Kaiserstuhl, Germany. Journal of Petrology 48(6), 1079-1118.

Villemant, B., Boudon, G., 1999. H2O and halogen (F, Cl, Br) behavior during shallow magma degassing processes. Earth and Planetary Science Letters 168, 271-286.

Volfinger, M., Robert, J.L., Vielzeuf, D., Neiva, A.M.R., 1985. Structural control of the chlorine content of OH-bearing silicates (micas and amphiboles). Geochimica et Cosmochimica Acta 49(1), 37-48.

Wang, L.X., Marks, M.A.W., Keller, J., Markl, G., 2014. Halogen variations in alkaline rocks from the Upper Rhine Graben (SW Germany): Insights into F, Cl and Br behavior during magmatic processes. Chemical Geology 380, 133-144.

Watkinson, D.H., Wyllie, P.J., 1971. Experimental study of the composition join $NaAlSiO_4$-$CaCO_3$-H_2O and the genesis of alkali rock-carbonatite complexes. Journal of Petrology 12, 357-378.

Webster, J.D., Kinzler, R.J., Mathez, E.A., 1999. Chloride and water solubility in basalt and andesite melts and implications for magmatic degassing. Geochimica et Cosmochimica Acta 63(5), 729-738.

Webster, J.D., Tappen, C.M., Mandeville, C.W., 2009. Partitioning behavior of chlorine and fluorine in the system apatite–melt–fluid II: Felsic silicate systems at 200MPa. Geochimica et Cosmochimica Acta 73(3), 559-581.

Webster, J.D., Thomas, R., Förster, H.J., Seltmann, R., Tappen, C., 2004. Geochemical evolution of halogen-enriched, granite magmas and mineralizing fluids of the Zinnwald tin-tungsten mining district, Erzgebirge, Germany. Mineralium Deposita 39, 452-472.

Wilson, M., Downes, H., 1991. Tertiary—Quaternary Extension-Related Alkaline Magmatism in Western and Central Europe. Journal of Petrology 32(4), 811-849.

Wilson, M., Downes, H., 2006. Tertiary-Quaternary intra-plate magmatism in Europe and its relationship to mantle dynamics. Geological Society of London.

Wimmenauer, W., 1966. The eruptive rocks and carbonatites of the Kaiserstuhl, Germany. Carbonatites. Wiley, London, 183-204.

Wimmenauer, W., 1974. The alkaline province of central Europe and France. In: H Sørensen (ed) The Alkaline Rocks. John Wiley & Sons Ltd., London, 238-271.

Wimmenauer, W., 2003. Geologische Karte von Baden-Württemberg 1:25.000 Erläuterungen zum Blatt Kaiserstuhl, Landesamt für Geologie, Rohstoffe und Bergbau Baden-Württemberg, Freiburg i. Br., 47-130.

Wishkerman, A., 2006. Bromine and iodine in plant-soil systems. Ph. D. thesis, pp 1-179.

Wu, F.Y., Yang, Y.H., Marks, M.A.W., Liu, Z.C., Zhou, Q., Ge, W.C., Yang, J.H., Zhao, Z.F., Mitchell, R.H., Markl, G. 2010. In situ U–Pb, Sr, Nd and Hf isotopic analysis of eudialyte by LA-(MC)-ICP-MS. Chemical Geology 273(1), 8-34.

Yasushi, K., 1975. Geochemistry of Water. Dowden, Hutchinson and Ross, New York, 455p.

Zhang, C., Holtz, F., Ma, C., Wolff, P.E., Li, X., 2012. Tracing the evolution and distribution of F and Cl in plutonic systems from volatile-bearing minerals: a case study from the Liujiawa pluton (Dabie orogen, China). Contributions to Mineralogy and Petrology 164(5), 859-879.

Zhu, C., Sverjensky, D.A., 1992. F-Cl-OH partitioning between biotite and apatite. Geochimica et Cosmochimica Acta 56(9), 3435-3467.

Appendix 1

Halogen variations in alkaline rocks from the Upper Rhine Graben (SW Germany): Insights into F, Cl and Br behavior during magmatic processes

Authors

Lian-Xun Wang, Michael A.W. Marks, Jörg Keller, Gregor Markl

Status

Published in *CHEMICAL GEOLOGY* (2014), v. 380, p.133-144

Editor

Donald B. Dingwell

Reviewer

Mark Kendrick and one anonymous reviewer

Contributions of the candidate

Scientific ideas	50%
Data acquisition	100%
Analysis and interpretation	70%
Preparation of manuscript	70%

Chemical Geology 380 (2014) 133–144

Contents lists available at ScienceDirect

Chemical Geology

journal homepage: www.elsevier.com/locate/chemgeo

Halogen variations in alkaline rocks from the Upper Rhine Graben (SW Germany): Insights into F, Cl and Br behavior during magmatic processes

Lian-Xun Wang [a,*], Michael A.W. Marks [a], Jörg Keller [b], Gregor Markl [a]

[a] Universität Tübingen, Mathematisch-Naturwissenschaftliche Fakultät, FB Geowissenschaften, 72074 Tübingen, Germany
[b] Albert-Ludwigs-Universität Freiburg, Institut für Geowissenschaften-Mineralogie-Geochemie, 79104 Freiburg, Germany

ARTICLE INFO

Article history:
Received 8 January 2014
Received in revised form 28 April 2014
Accepted 2 May 2014
Available online 10 May 2014

Editor: D.B. Dingwell

Keywords:
Halogens
Alkaline rocks
Upper Rhine Graben
Magmatic processes
Cl/Br ratio
Degassing

ABSTRACT

We present halogen compositions in a series of alkaline rocks from the Kaiserstuhl, Hegau and Urach areas of the Upper Rhine Graben region (South Germany). Most primitive rocks (olivine melilitites and olivine nephelinites) have lower Cl and Br concentrations (generally below 100 μg/g and below 0.3 μg/g, respectively) compared to more evolved tephrites, phonolites and related rocks (up to 7600 μg/g Cl and 34 μg/g Br). However, the Cl/Br ratios of the majority of the investigated samples are relatively uniform (371 ± 120), regardless of rock type and sample locality, suggesting that partial melting, fractional crystallization, and degassing have limited effects on the fractionation of Cl from Br. The mean value of the Cl/Br ratio is similar to previous estimates for basaltic rocks representing MORB and OIB mantle signatures.

Fluorine concentrations of the primitive rocks show limited variations (900–1100 μg/g) and are within the range defined by the evolved rocks (400–2100 μg/g), but are much higher than previous estimates for the MORB and OIB mantle (50–135 μg/g). This may indicate a relatively F-rich mantle source beneath the Rhine Graben region. In contrast to Cl/Br ratios, the F/Cl ratios vary significantly over three orders of magnitudes (from <0.1 to around 100) and decrease from primitive rocks to more evolved ones, implying that magmatic processes such as fractional crystallization and degassing strongly effect this ratio.

Positive correlations between F, Cl and Br contents in a series of tephritic rocks from Kaiserstuhl probably record degassing processes, since these samples have similar geochemical and isotopic signatures with the only difference being textural: they vary from glassy to phanerocrystalline. Simplified calculations imply that about 50% F and 90% Cl and Br were released during the crystallization process, resulting in increasing F/Cl, but relatively constant Cl/Br ratios.

1. Introduction

Besides water, carbon dioxide and sulfur, halogens (F, Cl and Br) are important volatile components in magmatic systems. They play essential roles in melting of the mantle, degassing of eruptive volcanoes and in transporting and depositing metals during hydrothermal processes (e.g., Kendrick et al., 2005; Aiuppa et al., 2009; Pyle and Mather, 2009; Fusswinkel et al., 2013; Johnson et al., 2013).

Our current understanding on how halogens are distributed between the Earth's geochemical reservoirs and how they are mobilized during magmatic processes is limited (e.g., Aiuppa et al., 2009; Pyle and Mather, 2009). Estimates of halogen abundances in the primitive mantle imply low concentrations (F = 18–28 μg/g, Cl = 1–38 μg/g, Br = 0.004–0.5 μg/g; e.g., Newsom, 1995; Lyubetskaya and Korenaga, 2007; Pyle and Mather, 2009). Similarly, studies on mid-ocean ridge basalts (MORB) imply that the MORB-mantle is relatively depleted in halogens (F = 50–135 μg/g; Cl = 1–21 μg/g; e.g., Saal et al., 2002). Detailed studies on MORB and ocean island basalts (OIB), however, generally show relatively high and variable halogen concentrations, partially attributed to the assimilation of seawater (e.g., Michael and Schilling, 1989; Schilling et al., 1980; Jambon et al., 1995; Kent et al., 2002; Saal et al., 2002; 2012; Kendrick et al., 2013a, 2013b; Coombs et al., 2004; Le Roux et al., 2006; Sumino et al., 2010).

Halogen abundance ratios (F/Cl, Cl/Br) in magmatic systems are considered as indicators for their origin and evolution (e.g., Jambon et al., 1995; Kent et al., 2002; Saal et al., 2002; Kendrick et al., 2012, 2013a, 2013b). Recent studies show that Cl/Br ratios of pristine MORB and OIB samples show only little variations, implying relatively similar geochemical behavior for Cl and Br during magmatic processes, such as partial melting, fractional crystallization and degassing (average of 360 ± 112; Jambon et al., 1995; Balcone-Boissard et al., 2010; Kendrick et al., 2012, 2013a, 2013b). However, much less is known on halogen

* Corresponding author. Tel.: +49 7071 29 730 77; fax: +49 7071 29 3060.
E-mail address: lian.x.wang@gmail.com (L.-X. Wang).

http://dx.doi.org/10.1016/j.chemgeo.2014.05.003
0009-2541/

systematics in rift-related alkaline magmatic systems (e.g., Köhler et al., 2009; Mangler et al., 2014). The detailed investigation of the halogen systematics of such rock series may help to constrain halogen signatures in the sub-continental mantle (e.g., Muramatsu and Wedepohl, 1979; Bailey and Hampton, 1990; Johnson et al., 2000; Burgess et al., 2002; Köhler et al., 2009). For example, rift-related alkaline silicate rocks from Greenland and Oldoinyo Lengai (Tanzania) reveal high F contents (up to 1.2 wt.%) and variable Cl contents (70–5000 μg/g) and are partially interpreted to reflect mantle halogen abundances (Köhler et al., 2009; Mangler et al., 2014).

In this contribution, we report F, Cl and Br abundance data for a suite of alkaline rocks from the Upper Rhine Graben area of southwest Germany, which is a part of the Cenozoic rift system in western and central Europe (Fig. 1a; e.g., Wilson and Downes, 1991, 2006; Lustrino and Wilson, 2007). Major halogen-bearing minerals in these rocks are apatite, titanite, fluorite, mica, amphibole, sodalite-group minerals (SGM) and götzenite (Keller et al., 1990; Wimmenauer, 1962). The main goals of this work are (1) to investigate the variation of halogen contents and ratios in alkaline rocks, (2) to understand the influences of magmatic differentiation and degassing on halogen variations, and (3) to constrain halogen signatures for the sub-continental mantle beneath Central Europe.

2. Geological setting

The Upper Rhine Graben (URG) in southwest Germany is one of the largest branches of the Cenozoic rift system in western and central Europe in the northern foreland of the Alpine orogenic belt (Fig. 1b; e.g., Illies, 1972, 1975; Wilson and Downes, 1991, 2006; Lustrino and Wilson, 2007). Along the graben and in its closer vicinity, Tertiary/Cenozoic volcanic centers, dykes, pipes, necks and diatremes occur (Fig. 1c; e.g., Wimmenauer, 1974; Keller et al., 1990; Wilson and Downes, 2006). The dominant rock types are alkaline basic rocks of sodic affinity and their more evolved differentiation products (e.g., trachytes, phonolites). Strongly silica-undersaturated olivine nephelinites and olivine melilitites characterize the southern sector of the URG as the only primitive mantle melts (e.g., Wimmenauer, 1974; Dunworth and Wilson, 1998; Keller et al., 1990; Keller, 2008). The generation of these primitive mafic magmas has been related to decompression-induced partial melting of the asthenospheric mantle (Wedepohl et al., 1994). However, more recent studies suggest the lithospheric mantle to be the main source region (Blusztajn and Hegner, 2002; Dunworth and Wilson, 1998). Samples of the present study are from three main volcanic fields in Southwest Germany, namely the Kaiserstuhl, Hegau and Urach areas (Fig. 1).

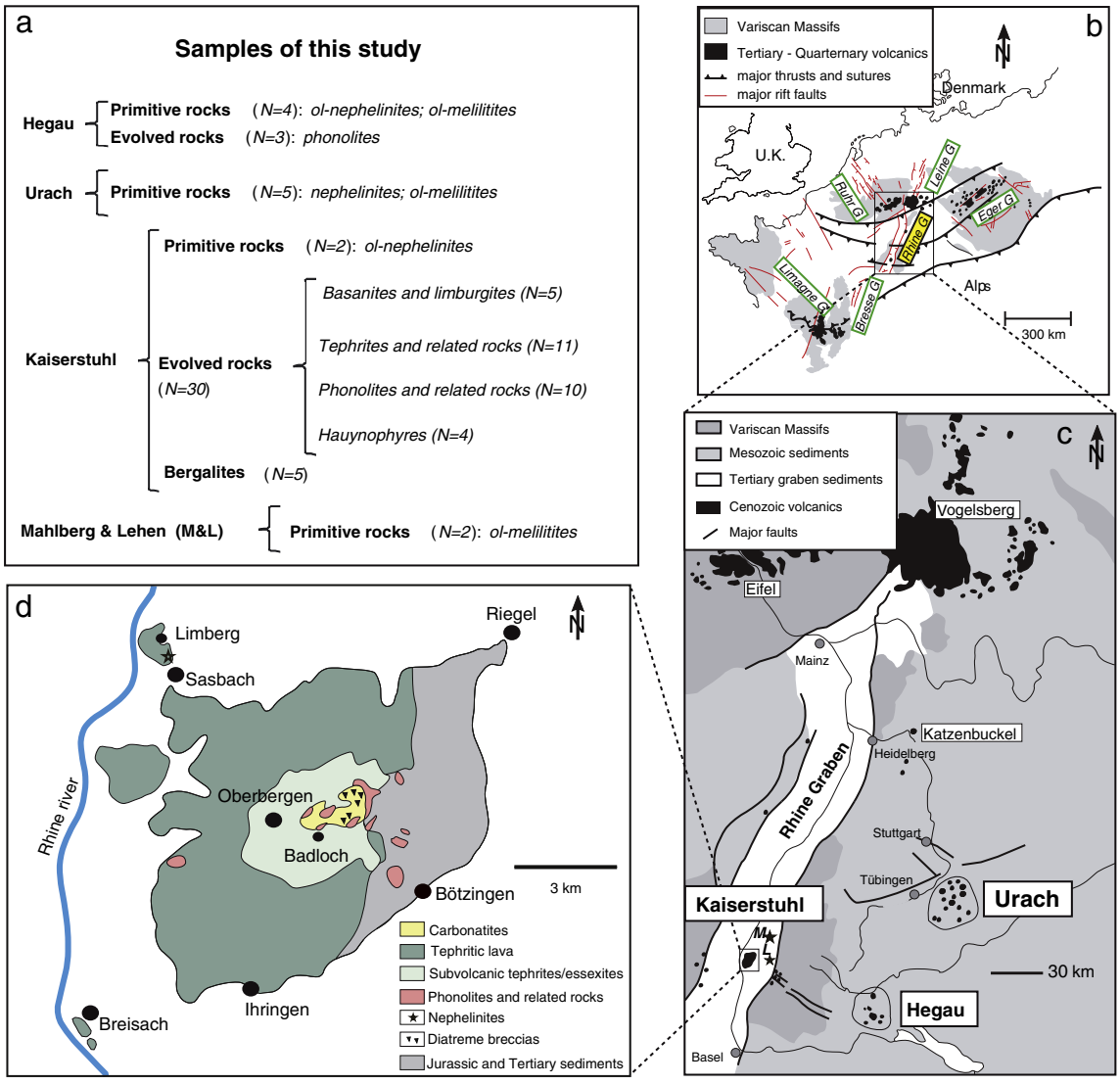

Fig. 1. (a) List of the investigated rocks from the Upper Rhine Graben area and geological sketch maps of (b) the Cenozoic rift system in western and central Europe (after Wilson and Downes, 1991), (c) the Miocene alkaline volcanic centers along the Rhine Graben and (d) the Kaiserstuhl volcanic complex (after Keller et al., 1990).

The Kaiserstuhl is the largest volcanic to subvolcanic complex of the Upper Rhine Graben (Fig. 1d) and was active between 18 and 13 Ma (Kraml et al., 1995; Keller et al., 2002; Kraml et al., 2006). The main rock types exposed are tephrites, essexites, phonolites, basanites (limburgites), olivine nephelinites, hauynophyres, carbonatites and unusual carbonate- and melilite-bearing dyke rocks called bergalites which are considered as transitional between alkaline silicate rocks and carbonatites (Wimmenauer, 1966, 1974; Hubberten et al., 1988; Keller, 1997; Keller et al., 1990; Schleicher et al., 1990; Wimmenauer, 2003). Small occurrences of olivine melilitites are additionally present in the surrounding area, for example at Mahlberg and Lehen (M- and L-marked stars in Fig. 1c; Keller et al., 1990; Dunworth and Wilson, 1998). Spinel lherzolite nodules are found in some of the olivine nephelinites and olivine melilitites occurrences. Based on the Mg numbers, high Cr and Ni contents and other geochemical characteristics, olivine nephelinites and olivine melilitites are considered to represent relatively primitive mantle-derived melts (e.g., Keller et al., 1990; Schleicher et al., 1990, 1991; Keller et al., 1997; Dunworth and Wilson, 1998; Ulianov et al., 2007). The more evolved rocks (basanites, tephrites, essexites, phonolites and hauynophyres) are assumed to reflect variable degrees of fractionation, potentially combined with minor amounts of crustal contamination (Keller et al., 1990; Schleicher et al., 1990).

The Hegau and Urach volcanic fields are situated in the adjacent regions east of the URG (Fig. 1c). Volcanic activity in both regions took place between about 16 and 7 Ma (Lippolt et al., 1973; Lippolt, 1983; Keller et al., 1990). Olivine melilitites (and melilite-bearing olivine nephelinites) and phonolites are two major rock types exposed in the Hegau area (Keller et al., 1990). The Urach field is known for its more than 350 diatreme centers consisting of olivine melilitites and (olivine) nephelinitites and lack of more evolved rocks (e.g., Mäussnest, 1974). Mineralogical, petrological and geochemical studies show that these primitive rocks are very similar to the olivine melilitites and olivine nephelinites from the Kaiserstuhl and its surroundings (Alibert et al., 1983; Keller et al., 1990; Schleicher et al., 1990); Dunworth and Wilson, 1998; Blusztajn and Hegner, 2002.

3. Sample material

For this study we investigated 51 powdered whole-rock samples from alkaline igneous rocks of the Kaiserstuhl, Hegau and Urach areas, including 13 relatively primitive olivine nephelinites and olivine melilitites and 38 variably evolved alkaline rocks (Fig. 1a). The classification of these rocks is illustrated in a TAS diagram (Fig. 2a). Detailed petrographic descriptions of the investigated rocks are given by Blusztajn and Hegner (2002), Ulianov et al. (2007) and Wimmenauer (2003, 1966). In summary, olivine nephelinites and olivine melilitites consist of variable amounts of forsteritic olivine, åkermanite, nepheline, analcime, Ti-augite, spinel, and minor amounts of glass, with accessory apatite, perovskite, magnetite, ilmenite, phlogopite and calcite. Tephrites and related rocks are rich in Ti-augite, magnetite, plagioclase, alkali feldspar and leucite/analcime, whereas basanites contain appreciable amounts of forsteritic olivine, besides Ti-augite, plagioclase and nepheline. Phonolites are dominated by alkali feldpar, nepheline, sodalite group minerals (sodalite-hauyne(ss); SGM), aegirine-augite, Ti-bearing andradite–schorlomite(ss), titanite ± calcite ± wollastonite ± götzenite ($Na_2Ca_5Ti(Si_2O_7)_2F_4$). Hauynophyres are rich in SGM and contain variable amounts of alkali feldspar, aegirine augite, Ti-bearing andradite–schorlomite(ss) and calcite. Bergalites contain significant amounts of carbonate and are generally dominated by åkermanite, SGM, nepheline, perovskite, biotite, apatite and magnetite.

The sample suite covers a large range of Mg numbers (78–13) and SiO_2 contents (31–56 wt.%; Fig. 2; Table 1). The primitive olivine nephelinites and olivine melilitites show the highest Mg-numbers (68–78) and the lowest SiO_2 concentrations (36–40 wt.%). Basanites and limburgites have lower Mg-numbers (56–66) and higher SiO_2 contents (42–43 wt.%), and tephrites and related rocks are even more evolved (Mg-numbers of 45–51) with SiO_2 contents between 43 and 45 wt.%.

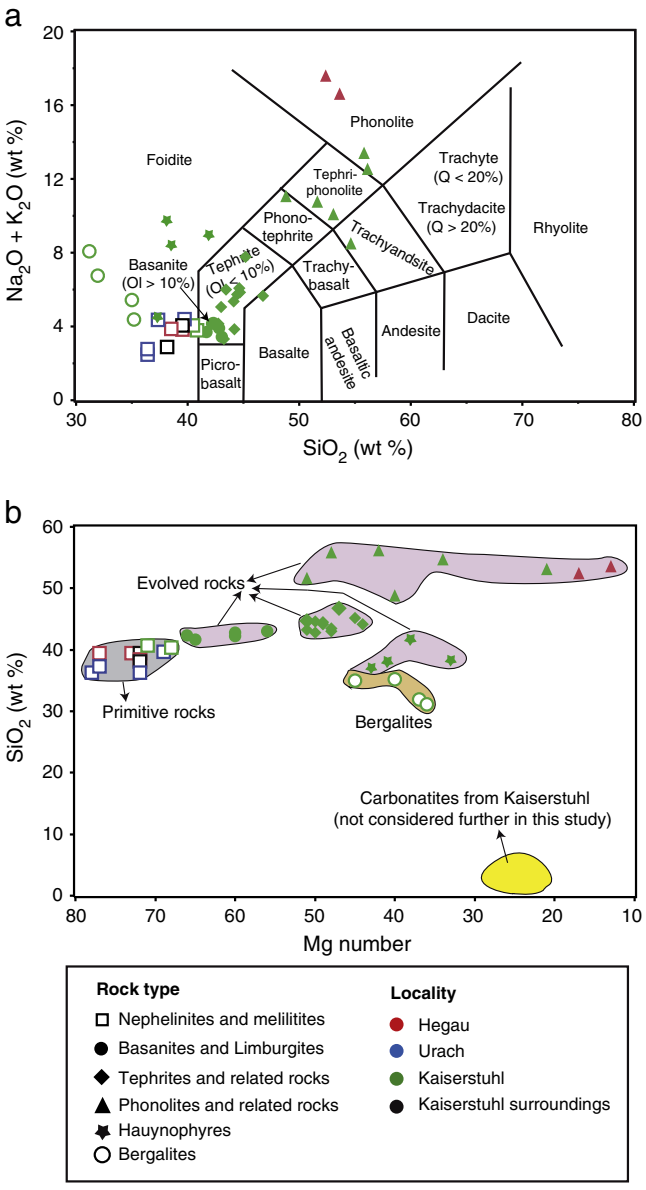

Fig. 2. Whole rock data for alkaline rocks from the Upper Rhine Graben area (Data from Keller et al. (1990) and unpublished). Mg number = molar $Mg/(Mg + Fe_{total})$.

The Mg numbers of hauynophyres and bergalites are both relatively low (33–45) with SiO_2 contents of 31–35 wt.% and 31–42 wt.%, respectively. Phonolites and related rocks reach the lowest Mg numbers (13–51) and highest SiO_2 contents (49–56 wt.%), representing some of the most evolved igneous rocks in the Upper Rhine graben.

4. Methods

Halogen analyses in this study were performed using a pyrohydrolysis extraction line combined with ion chromatography (PHIC) and Total Reflection X-ray Fluorescence Analysis (TXRF) at the Fachbereich Geowissenschaften, Universität Tübingen.

4.1. Pyrohydrolysis combined with Ion Chromatography

Around 50 to 100 mg of dried rock powders were mixed with approximately the same amount of V_2O_5 and placed into quartz containers, which were then inserted into a silica tube and heated to 1100 °C for 30 min. Throughout the heating procedure a constant

Table 1
Halogen concentrations and other information for the investigated alkaline rocks from the Upper Rhine Graben region.

Locality	Sample	Rock type	F	Cl	Br	Br	F/Cl	Cl/Br	SiO_2	Mg#	D.I.	Ap	Ttn	SGM
			PHIC ± 10% (μg/g)			TXRF(μg/g)	PHIC		(wt.%)					
Hegau	NH3	Ol-nephelinite	1106	79	<0.3	n.d.	13.9	>264	39	72	31	2.0		
	HE3	Ol-nephelinite	1108	25	<0.3	n.d.	43.9	>84	40	73	31	1.9		
	HE7	Ol-nephelinite	1168	48	<0.3	n.d.	24.2	>160	–	–	–	–		
	NH2	Ol-melilitite dyke	1042	103	<0.3	n.d.	10.1	>343	40	77	28	1.6		
	H3	Phonolite	911	2704	5.0	n.d.	0.3	539	–	–	–	–	‡‡‡	‡
	H2	Phonolite	1371	4007	8.2	n.d.	0.3	488	52	17	84	0.2	‡‡‡	‡
	NH1	Phonolite	698	1633	2.2	n.d.	0.4	747	54	13	86	0.1	‡‡‡	
Urach	NU1	Ol-nephelinite	1290	27	<0.3	n.d.	47.3	>91	40	69	32	1.6		
	NU4	Ol-nephelinite dyke	971	38	<0.3	n.d.	25.4	>127	36	72	27	2.5		
	NU3	Ol-melilitite	1223	10	<0.3	n.d.	116.6	>35	–	–	–	–		
	U2	Ol-melilitite	1200	24	< 0.3	n.d.	49.5	>81	37	77	27	1.9		
	NU2	Ol-melilitite	1232	46	< 0.3	n.d.	26.6	>154	36	78	25	2.1		
M&L	334.2	Ol-melilitite	1182	58	< 0.3	b.d.l.	20.4	>193	38	72	30	2.0		
	753	Ol-melilitite	1013	44	< 0.3	n.d.	23.3	>145	40	72	32	1.9		
Kaiserstuhl	L2	Ol-nephelinite	907	874	2.0	n.d.	1.0	436	41	71	36	1.8		
	462	Ol-nephelinite	1209	2230	5.2	3.7 ± 0.6	0.5	428	40	68	32	1.6		
	465	Limburgite	707	614	1.2	1.1 ± 0.2	1.2	505	42	66	41	1.7		
	G49	Limburgite	798	1058	2.1	1.3 ± 0.2	0.8	494	43	60	43	1.7		
	L1	Limburgite	747	454	0.8	1.1 ± 0.1	1.6	537	42	65	41	1.6		
	238	Basanite	963	223	0.5	n.d.	4.3	483	43	56	51	1.3		
	480	Basanite	853	2538	6.2	5.5 ± 0.3	0.3	413	42	60	46	1.2		–
	435	Glassy tephrite	1796	6813	25.1	n.d.	0.3	272	45	45	57	1.7		
	173	Essexite	859	101	0.6	1.0 ± 0.1	8.5	165	44	49	54	1.2		
	214	Essexite	905	163	2.9	3.7 ± 0.1	5.6	56	45	51	57	1.5		
	204	Essexite	1072	852	1.3	1.7 ± 0.1	1.3	647	44	49	53	1.1		
	436	Tephrite	1283	2784	9.0	6.4 ± 0.3	0.5	308	43	48	54	1.2		–
	476	Tephrite	1113	2699	5.0	5.8 ± 0.7	0.4	536	45	50	52	1.3		
	475	Tephrite	1062	105	0.4	0.6 ± 0.1	10.1	292	47	47	57	1.0		
	437	Tephrite	802	119	0.9	b.d.l.	6.8	132	43	48	53	1.5		
	200	Tephrite	992	282	1.0	0.9 ± 0.3	3.5	295	43	51	51	1.4		
	486	Shonkinite porphyry	713	300	1.1	1.0 ± 0.1	2.4	277	43	50	58	1.4		
	379	Monchiquite	1223	866	2.1	2.0 ± 0.1	1.4	408	44	44	67	1.5		
	287	Mela-phonolite	1068	954	3.2	3.0 ± 0.3	1.1	294	–	–	–	–		
	470	Mela-phonolite	1238	1663	3.1	3.2 ± 0.2	0.7	533	–	–	–	–		–
	464	Mela-phonolite	962	383	1.9	n.d.	2.5	205	–	–	–	–		
	B40	Phonolite dyke	1165	52	0.6	1.1 ± 0.2	22.2	91	53	21	76	0.5	‡‡‡	
	160	Phonolite dome	2151	90	2.3	2.6 ± 0.1	24.0	39	49	40	81	0.3	‡‡‡	
	494	Phonolite dome	1188	7691	20.9	19 ± 0.5	0.2	367	56	48	88	0.1	‡‡‡	‡‡‡
	156	Phonolite dome	471	7447	22.2	22.6 ± 1.0	0.1	336	56	42	90	0.1	‡‡‡	‡‡‡
	515	Phonolite dyke	956	2673	6.0	6.0 ± 0.3	0.4	448	52	51	89	0.1	‡‡‡	‡
	309	Mondhaldeite	873	139	0.4	b.d.l.	6.3	360	55	34	85	0.9	‡‡‡	
	B91	Alkali syenite	343	91	0.3	n.d.	3.8	269	–	–	–	–	‡‡‡	
	174	Hauynophyre	859	7634	33.5	n.d.	0.1	228	38	41	63	1.1		‡‡‡
	406	Hauynophyre	801	2936	11.8	11.5 ± 0.4	0.3	249	37	43	67	1.3		‡‡‡
	396	Hauynophyre	1446	6547	18.1	15.3 ± 0.7	0.2	362	38	33	58	1.1		‡‡‡
	166	Hauynophyre	413	6862	16.5	15 ± 0.4	0.1	416	42	38	73	0.4		‡‡‡
	229	Bergalite	1331	2640	6.6	5.9 ± 0.1	0.5	400	31	36	45	1.5		‡
	158	Bergalite	1748	6231	19.3	n.d.	0.3	322	–	–	–	–		–
	217	Bergalite	1484	1249	3.8	3.1 ± 0.3	1.2	326	32	37	49	1.6		‡
	263	Bergalite	1980	169	0.8	1.2 ± 0.3	11.7	222	35	40	47	2.4		
	340	Py-bergalite	1958	160	22.6	28.5 ± 0.4	12.2	7	35	45	44	2.6		
	M1	Titanite (phonolite)	4234	39	–	n.d.	–	–	–	–	–	–		

Ap* = percent apatite by CIPW norm calculation; SGM = sodalite group minerals; Mg# = Mg number Mg/(Mg + total Fe); D.I. = differentiation index, sum of Qz + Ab + Or + Ne + Kp + Lc in CIPW norm calculation. SiO_2 contents and Mg numbers from Keller et al. (1990) and unpublished data. n.d. = not detected; "–" = unknown; b.d.l. = below detection limit; "‡" = present; "‡‡‡" = abundant.

H_2O-vapor stream (60 ml/min) was maintained in order to collect the released halogens. The loaded stream was then cooled down using a Liebig condenser and collected in two vessels, containing 2 ml diluted NaOH solution (0.02 mol/l) and 4 ml MQ H_2O, respectively. Immediately after collection, the solutions were analyzed using a Dionex ICS-1000 ion chromatograph equipped with an IonPac AS9-HC 2-mm anion column. More details can be found in Marks et al. (2012) and Köhler et al. (2009). Effective detection limits for whole-rock samples are about 10 μg/g for F and Cl and about 0.3 μg/g for Br. The accuracy and precision for PHIC was assessed by analyzing various reference materials (Table 2). All samples were analyzed at least twice generally resulting in a reproducibility of >90%. The total errors for F and Cl measurements are around 10% depending on the absolute halogen concentrations, loss and contamination during pyrohydrolysis extraction, and peak combinations during IC measurements. Higher uncertainties generally occur at concentrations close to the detection limits, especially for Br.

4.2. Total Reflection X-ray Fluorescence Analysis

For comparison with the PHIC data, Br analysis was additionally performed by TXRF using an S2 PICOFOX spectrometer (Bruker AXS). From each sample, around 5 mg of whole-rock powder (grain size <15 μm) was dispersed in 1 ml of Triton X-100 solution (1 vol.%) and 10 μl of a 10 mg/l Se solution was added for internal standardization. These suspensions were homogenized for about 2 min and 10 μl aliquots were pipetted onto quartz disks and dried on a heating plate at 70 °C. The dried sample cakes were then analyzed for 1000 s (live time) using a Mo X-

Table 2
Halogen concentrations of reference materials as determined by Phyrohydrolysis combined with Ion Chromatography and Total Reflection X-ray Fluorescence Analysis and literature data.

		PYIC (μg/g)				TXRF (μg/g)		Literature data (μg/g)		
Sample no.	Rock type	F	Cl	Br		Br		F	Cl	Br
RGM-1	Rhyolite	309 ± 6	502 ± 83	1.5 ± 0.2	n = 3	2.0 ± 0.2	n = 5	280–342[a–c]	393–510[a,c]	1.3–1.9[a,c,d]
JR-1	Rhyolite	945 ± 98	919 ± 90	1.6 ± 0.3	n = 3	2.2 ± 0.3	n = 6	942–1034[c,e,f]	898–920[c,e,f,i]	1.7–2.4[c,f,g]
ACE	Granite	1962 ± 93	261 ± 22	0.7 ± 0.1	n = 2	0.7 ± 0.4	n = 6	1937–2100[a]	180–226[a]	0.5–0.7[a,d,j]
GH	Granite	3099 ± 376	84 ± 32	0.4 ± 0.2	n = 4	0.6 ± 0.2	n = 6	3300–3696[a,c]	100–120[a,c]	0.2–0.3[a,c,d]
GSN	Granite	932 ± 31	456 ± 32	1.9 ± 0.3	n = 2	2.4 ± 0.3	n = 6	890–1050[a,c,f]	349–450[a,c,h]	2.5–3.0[a,d,f,h]
AGV-1	Andesite	369 ± 7	129 ± 19	<0.3	n = 2	n.d.		425[c]	119–170[c,i]	0.2–0.3[c,d,k]
DRN	Diorite	567 ± 97	545 ± 25	1.5 ± 0	n = 2	1.5 ± 0.3	n = 6	500[c]	400[c]	1.5[c,d]
AN-G	Anorthosite	87 ± 21	262 ± 51	2.8 ± 0.3	n = 4	3.2 ± 0.4	n = 6	120–131[a,c]	197–300[a,c]	1.9–3.2[a,c,d,]

[a] Michel and Villemant (2003).
[b] Peterman and Cloke (2002).
[c] Govindaraju (1994).
[d] Korotev (1996)
[e] Shimizu et al. (2006).
[f] Balcone-Boissard et al. (2009).
[g] Ozaki and Ebihara (2007).
[h] Boulyga and Heumann (2005).
[i] Shinonaga et al.(1994).
[j] Maghraoui et al. (1999).
[k] Chai and Muramatsu (2007).

ray tube with an operating voltage of 50 kV and a beam current of 600 μA. The resulting spectra were fitted with the Spectra 6.2 software (Bruker Nano GmbH). Using this method, the detection limit for Br is around 0.3 μg/g. As shown by Marks et al. (2012) and Mangler et al. (2014), TXRF is well-suited for analyzing Br in solid samples and Br concentrations obtained by PHIC and TXRF in our study are very similar (Tables 1 & 2). Unfortunately, quantification of F is, however, not possible with TXRF and serious problems exist for Cl (see detailed discussions in Garcıa-Heras et al., 1997; Misra and Singh Mudher, 2002; Marks et al., 2012; Mangler et al., 2014).

5. Results

5.1. Halogen abundances

In olivine nephelinites and olivine melilitites, F concentrations show a narrow range (900–1300 μg/g), with no significant differences among sample localities (Fig. 3). Their Cl contents are low (10–100 μg/g), except for two olivine nephelinites from the Kaiserstuhl (samples L2 and 462), which show Cl contents of 900 and 2200 μg/g, respectively (Fig. 3a). Bromine concentrations correlate with those of Cl, as they are very low (<0.3 μg/g) in all Cl-poor olivine nephelinites and olivine melilitites but comparatively high (2 and 5 μg/g, respectively) in the two Cl-rich olivine nephelinites (Fig. 3b). Compared to the evolved rocks and bergalites, olivine nephelinites and olivine melilitites generally show lower Cl and Br contents, whereas their F concentrations are within the relatively large range defined by the evolved rocks and bergalites (Fig. 3).

Most of the evolved rocks from the Kaiserstuhl contain 400 to 1400 μg/g of F, except for a götzenite-bearing phonolite (sample 160) and a glassy tephrite (sample 435), with F contents of 2150 and 1800 μg/g, respectively. Their Cl and Br concentrations reveal very large variations (50–7700 μg/g for Cl; 0.4–34 μg/g for Br) and are clearly higher than that of the primitive rocks (Fig. 3). Three phonolites from the Hegau area have F (about 700–1400 μg/g), Cl (1600–4000 μg/g) and Br (2–8 μg/g) contents similar to those from the Kaiserstuhl.

Bergalites contain large amounts of F (1300–2000 μg/g), higher than most other samples (Fig. 3). Their Cl and Br contents are highly variable (160–6200 μg/g for Cl and 0.8–23 μg/g for Br; Table 1).

5.2. Halogen ratios

The F/Cl ratios of the investigated samples vary by more than three orders of magnitude from <0.1 to >100 (Fig. 3a). The primitive rocks generally show relatively high F/Cl ratios from 10 to 100, with the exception of two Cl-rich olivine nephelinites from the Kaiserstuhl, which have much lower F/Cl ratios (1.0 and 0.5). Evolved rocks and the bergalites, however, reveal relatively low F/Cl ratios, mainly ranging

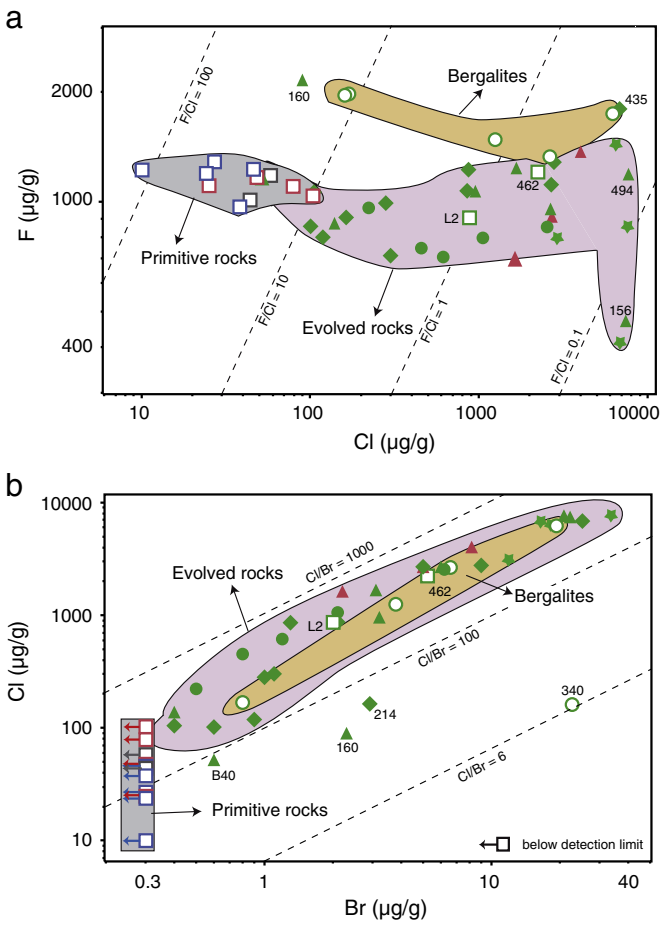

Fig. 3. Halogen (F, Cl, and Br) contents of the investigated samples. Symbols are the same as in Fig. 2. Samples L2 and 462 are olivine nephelinites from the Kaiserstuhl, samples 494 and 156 are SGM-bearing phonolites, sample 160 is a götzenite-bearing phonolite and sample 435 is a glassy tephrite.

from 0.1 to 10 (Fig. 3a; Table 1). Due to their extremely high Cl contents, samples being rich in sodalite group minerals (SGM; hauynophyres and phonolites 156 and 494) have some of the lowest F/Cl ratios. In contrast, Cl/Br ratios vary within a relatively narrow range from about 200 to 600 (Fig. 3b; Table 1) in the majority of the evolved rocks and bergalites. Four samples (phonolite 160 and B40; tephrite 214 and bergalite 340) show lower Cl/Br ratios <100.

6. Discussion

6.1. Mineralogical controls on whole rock halogen composition

The F contents in most investigated rocks roughly increase with increasing CIPW-calculated apatite abundance (Table 1), indicating that apatite is an important F-carrier in these samples. This is consistent with earlier studies as apatites from the Kaiserstuhl Volcanic Complex are fluorapatite to hydroxylapatite with low Cl contents (Sommerauer and Katz-Lehnert, 1985; Wang et al., in press). However, many data plot above the ideal fluorapatite line (Fig. 4), suggesting that additional F-contributors such as mica, amphibole, titanite, and halogen-rich volcanic glass fragments in some of the tephritic and basanitic samples (see details below) contribute to the total F-budget. Phonolitic rocks show the most pronounced deviation from the fluorapatite line. These rocks are relatively poor in apatite but contain abundant titanite (around 4000 μg/g F; Table 1) and in the case of sample 161 also F-rich götzenite (Keller et al., 1990). Furthermore, fluorite was described from some phonolites by Wimmenauer (1962).

The highest Cl and Br concentrations (up to about 7700 μg/g Cl and 34 μg/g Br) are present in hauynophyres and some phonolites and bergalites, which contain significant amounts of SGM (up to 28%, Keller et al., 1990; Table 1). This indicates that SGM are the major Cl- and Br-carriers in these samples, consistent with data from elsewhere (e.g., Krumrei et al., 2007; Markl et al., 2001). In SGM-free samples (e.g., basanites and tephrites) mica, amphibole and in some cases glassy groundmass may be important Cl and Br hosts.

6.2. Bulk-rock halogen concentration versus melt composition

Halogen concentrations of evolved alkaline rocks are probably different from that of their parental magma, since such rocks generally underwent various magmatic processes (e.g., fractional crystallization and degassing), which might modify their initial halogen contents. During magmatic differentiation, F behaves moderately incompatible, while

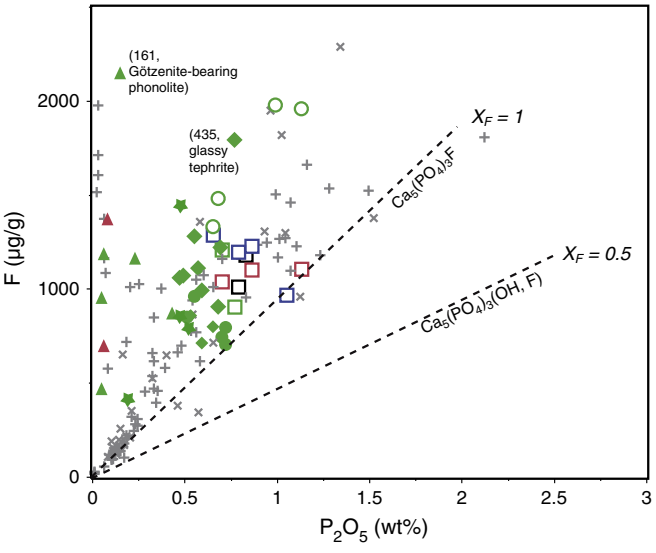

Fig. 4. Whole-rock F versus P_2O_5 contents of alkaline rocks from the Upper Rhine Graben area. The $Ca_5(PO_4)_3F$ line represents the ideal fluorapatite line and the $Ca_5(PO_4)_3(OH,F)$ represents fluor-hydrolapatite. Symbols are the same as in Fig. 2. "+" = volcanic rocks from Iceland and Jan Mayen after Stecher (1998); "×" = basalts and related rocks from Aoki et al. (1981).

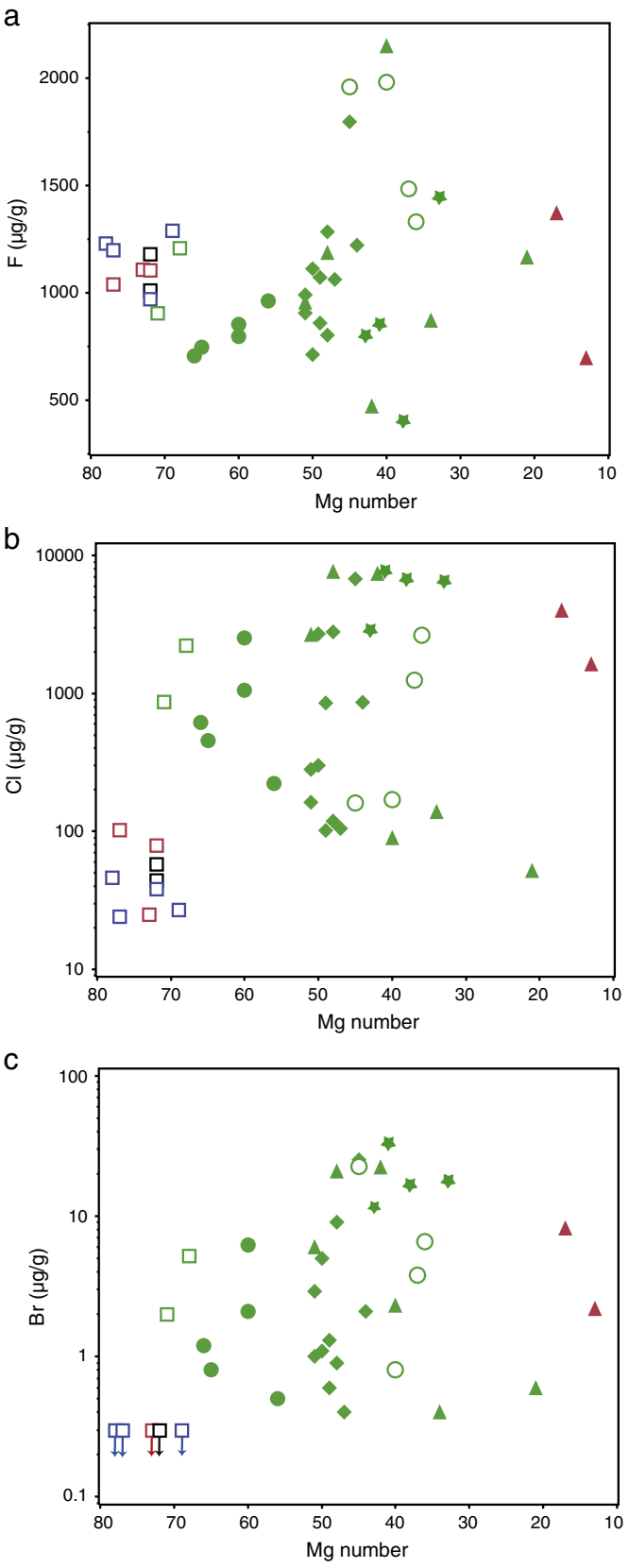

Fig. 5. Halogen concentrations versus Mg number of alkaline rocks from the Upper Rhine Graben area. Symbols are the same as in Fig. 2.

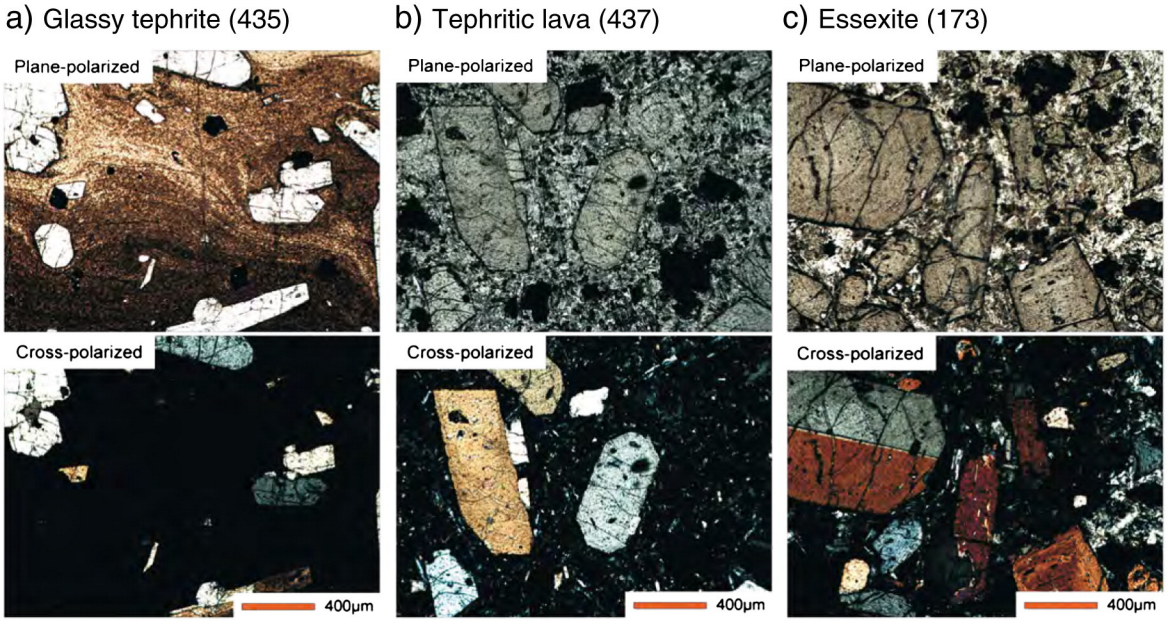

Fig. 6. Microscopic images of tephritic rocks, illustrating their variable crystallinity. (a) Flow texture and glassy matrix of the glassy tephrite (sample 435). (b) Tiny microphenocrysts of augite in the groundmass of a tephritic lava (sample 437). (c) Increase grain size of the microphenocrysts in the groundmass of subvolcanic essexite (sample 17).

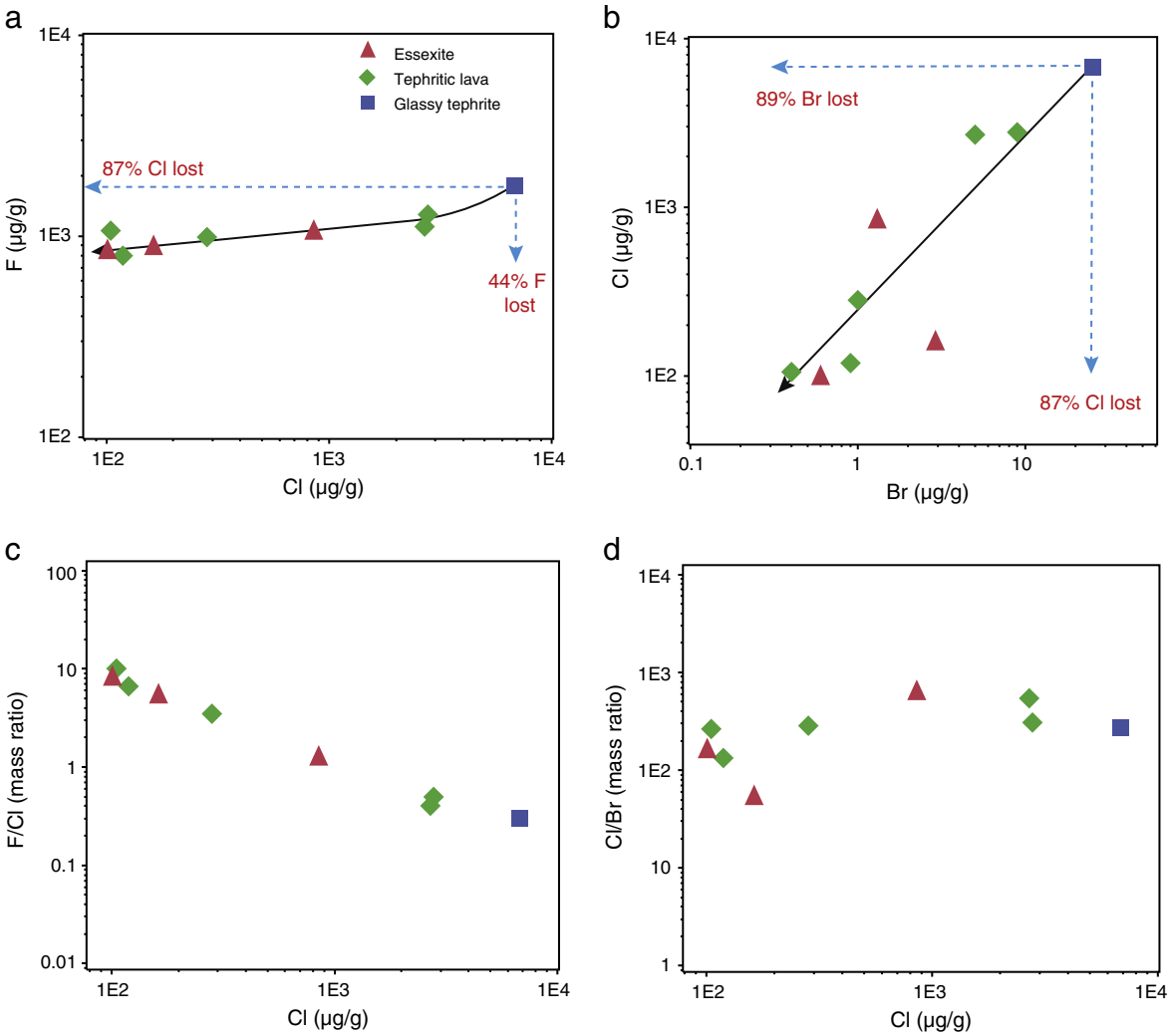

Fig. 7. Halogen variations in the tephritic sample suit from the Kaiserstuhl including one glassy tephrite, 5 tephritic lava and 3 essexites.

Cl and Br are highly incompatible and show very similar behavior (e.g., Schilling et al., 1980). Crystallization of halogen-free minerals will enrich halogens in the residual melt and the crystallization of halogen-bearing minerals may retain halogens in the rocks (e.g., Webster et al., 1999). When ascending to shallow depths, however, magmas may undergo variable degrees of degassing and the initial halogen signature could thereby change. During degassing F is less efficiently extracted compared to Cl and Br and the latter two are not largely fractionated from each other (e.g., Balcone-Boissard et al., 2010).

6.2.1. Halogen variation with magma differentiation

Modeling of magma/crystal fractionation generally shows that F, Cl and Br concentrations increase with magma evolution because of their incompatible behavior. For our sample suite, however, there is no clear indication that halogen concentrations vary systematically with magma differentiation (Fig. 5 and Supplementary figure). For example, basanites and limburgites, which are interpreted as differentiation products of the primitive rocks (e.g., Keller et al., 1990), are slightly lower in F, but higher in Cl and Br than olivine nephelinites and olivine melilitites. On the other hand, within the basanite group F increases with decreasing Mg number. This trend, however, is not as clear for Cl and Br. Also, there are no systematic differences in the halogen concentrations between the variably evolved basanitic, tephritic and phonolitic rocks. According to Schilling et al. (1980), variations in the extent of low-pressure fractional crystallization or partial melting are not the major cause for large halogen variations. Large differences in Cl contents between lava blocks and pumice clasts indicate that shallow-level processes dominate Cl (and possibly Br) variation (Harford et al., 2003). Similarly, Lowenstern et al. (2012) demonstrated that large amounts of halogens are released during near-surface crystallization of rhyolitic lavas. Consequently, the observed variations of halogen concentrations in our sample suite are probably caused by the additional modification exerted by shallow-level degassing which is relevant during matrix crystallization.

6.2.2. Halogen release during shallow-level degassing

A series of tephritic samples with variable crystallinity (one glassy tephrite, extrusive lavas and sub-volcanic essexites; Fig. 6) allow for investigating the effects of degassing during matrix crystallization. The glassy tephrite contains the highest amounts of F, Cl and Br (1800, 6800 and 25 μg/g, respectively), much higher than that of MORB and OIB glasses (50–135 μg/g for F and 1–21 μg/g for Cl; Saal et al., 2002). For phonolitic melts, Cl solubility was experimentally determined to around 0.6–0.8 wt.% (Signorelli and Carroll, 2000; Giehl et al., 2014), similar to the Cl concentrations of the glassy tephrite.

Positive correlations between F and Cl, and between Cl and Br among these tephritic samples exist, with the highest values observed in the glassy sample (Fig. 7a & b). We suggest that these correlations record halogen degassing due to crystallization of the matrix (c.f. second boiling; e.g., Webster et al., 1999). These samples are from the same rock unit and show similar geochemical and isotopic signatures (Keller et al., 1990; Schleicher et al., 1990, 1991). Their similar SiO_2 contents, Mg numbers and differentiation index (D.I.) argue against large amounts of fractional crystallization among these samples (Fig. 2; Table 1). The major difference between these samples is their variable crystallinity (Fig. 6). Extensive crystallization of halogen-free minerals, which dominate the matrix of these samples (e.g., augite, plagioclase, magnetite and leucite) results in increasing halogen contents in the residual melt. When reaching their solubility limit, excess halogens would exsolve and escape from the melt.

Assuming that the glassy tephrite represents the initial halogen composition before degassing, the other samples represent products of variable degrees of degassing. Using the sample with the lowest halogen contents, about 45% of the initial F, and about 90% of the initial Cl and Br escaped during crystallization of the matrix. These results fit well with observations made by Noble et al. (1967), who compared F and Cl contents of more than 200 tuffs and lavas from a similar rock suite and found that samples with crystallized groundmass generally contain much less F (around 50%) and Cl (around 80%) than the glasses. Likewise, Schilling et al. (1980) found that the F contents of MORB pillow interiors are around 40% lower than that of their glassy margins.

Variations of the F/Cl and Cl/Br ratios during degassing are shown in Fig. 7c & d. The negative correlation between F/Cl ratio and Cl content imply that F/Cl ratios of the melt increase with halogen degassing. Comparatively, the Cl/Br ratios are fairly constant with decreasing Cl. This indicates that the incompatibility of halogens during degassing can be expressed as Cl ≈ Br > F, in line with the conclusions by Balcone-Boissard et al. (2010) that Cl and Br are efficiently extracted but not fractionated from each other during degassing.

6.2.3. Halogen retention during crystallization

Hauynophyres as well as some phonolites and bergalites contain high amounts of SGM (see above), which indicates relatively Cl-rich magma compositions at quite early stages of magmatic evolution, since SGM occur mainly as euhedral phenocrysts in these rocks. Relatively variable F contents in SGM-rich rocks (400–1700 μg/g) may be

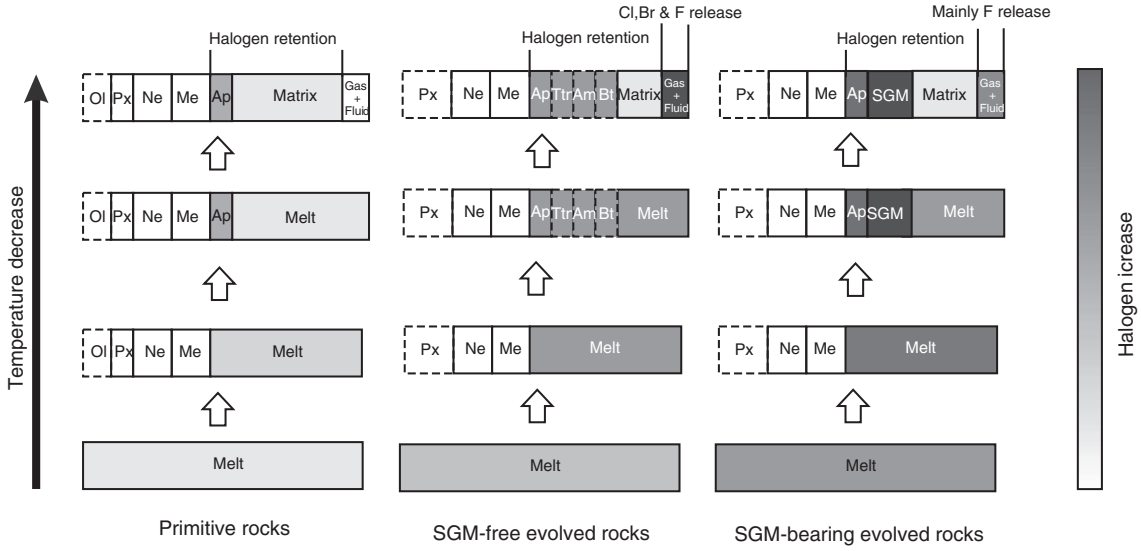

Fig. 8. Simplified models for the possible modifications of initial halogen contents of the magma during crystallization and cooling.

related to degassing events similar to the observations in the tephritic rocks. However, it is a little surprising that degassing apparently only affects F but not Cl and Br. We suggest that high amounts of Cl and Br were incorporated by the SGM during an early stage, preventing them from late-stage degassing. In contrast, variable amounts of F were released due to the lack of effective mineral storage. This implies that halogens can be protected from degassing if they are incorporated in appropriate minerals. This view could be further supported by the F-rich but Cl- and Br-variable bergalite samples. Their halogen systematics are mainly governed by the crystallization of fluorapatite (Wang et al., in press). Overall, we conclude that halogen release during second boiling may significantly modify the initial halogen composition of magmas. Crystallization of halogen-bearing minerals (e.g., SGM, apatite, titanite), however, could (at least partly) protect halogens from release during degassing (Fig. 8).

6.3. Constraints on halogen abundances of the source mantle

In contrast to the evolved rocks, olivine nephelinites and olivine melilitites investigated in this study are primitive mantle-derived melts and intense differentiation can be excluded for these rocks (e.g., Hubberten et al., 1988; Keller et al., 1990; Schleicher et al., 1990; Dunworth and Wilson, 1998; Wilson and Downes, 2006). As Cl and Br are strongly incompatible during partial melting, they are enriched in partial melts relative to their source rocks. Thus, the low Cl and Br concentrations (10–100 μg/g for Cl and <0.3 μg/g for Br) of these rocks could place an upper limit to the Cl and Br abundances in their source mantle. However, it is difficult to evaluate whether or not these rocks underwent degassing processes. On the one hand, the generally low Cl and Br data of the primitive samples are similar to previous estimates for the primitive mantle and the lower end of values reported for MORB and OIB samples (Fig. 9a). On the other hand, two olivine nephelinites out of thirteen olivine nephelinites and olivine melilitites show relatively high Cl and Br concentrations despite similar Mg-numbers (Table 1 and Fig. 9a) and are similar to the Cl and Br concentrations for olivine nephelinites and olivine melilitites from the Hessian Depression in Central Germany (Muramatsu and Wedepohl, 1979) and the Oldoinyo Lengai area in Tanzania (Mangler et al., 2014; Fig. 9a). This either implies significant heterogeneity with respect to halogen abundances in the mantle as suggested by Schilling et al. (1980), or one has to assume that the two high-Cl samples are much less degassed compositions and therefore approximate the halogen compositions of their parental melts.

The F concentrations of the investigated olivine nephelinites and olivine melilitites are fairly constant (around 1100 ± 100 μg/g; Fig. 9b) and are much higher than estimates for the primitive and depleted mantle (e.g., Newsom, 1995; Schilling et al, 1980; Saal et al., 2002; Salters and Stracke, 2004; Lyubetskaya and Korenaga, 2007; Pyle and Mather, 2009). Similarly high F abundances in nephelinites and melilitites (1000–3000 μg/g) were reported from Hawaii and Tanzania (Aoki et al., 1981; Mangler et al., 2014). This indicates that mantle-derived nephelinitic and melilititic rocks are much higher in F than typical MORB and OIB samples, which could be caused by high F concentrations of the source mantle, or alternatively, by different degrees of mantle melting. Foley et al. (1986) demonstrated that silica-undersaturated ultrapotassic rocks were generated from partial melting of a H_2O-poor, but F-rich mantle. Fluorine in the sub-continental lithospheric mantle could be stored in e.g. phlogopite and apatite (e.g., Aoki et al., 1981; Smith, 1981; Köhler et al., 2009). Indeed, phlogopite phenocrysts and phlogopite-bearing mantel xenoliths were found in the ultramafic diatreme breccias and some olivine melilitites from Urach and Hegau (Keller et al., 1990; Schleicher et al., 1990; Dunworth and Wilson, 1998). Besides, apatite is another potential F-carrier in the mantle beneath this region, as indicated by the relatively high P_2O_5 concentrations in the studied olivine nephelinites and olivine melilitites (Table 1, Fig. 4). Smith (1981) demonstrated that the F concentrations in many basaltic rocks are consistent with melting of F-rich apatite in the mantle and

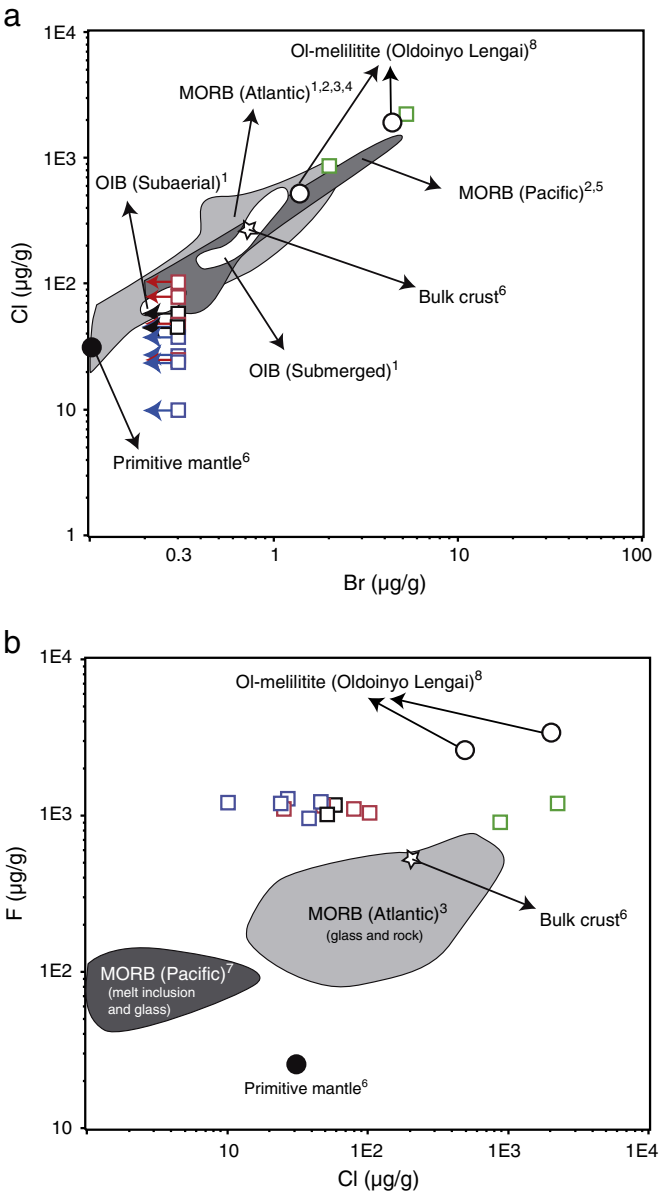

Fig. 9. Halogen abundances in the primitive olivine nephelinites and olivine melilitites from Upper Rhine Graben are compared to estimates of primitive mantle composition and MORB and OIB sample data. Symbols are the same as in Fig. 2. References are from: 1. Schilling et al. (1978); 2. Jambon et al. (1995); 3. Schilling et al. (1980); 4. Kendrick et al. (2013a, 2013b); 5. Kendrick et al. (2012); 6. Pyle and Mather (2009); 7. Saal et al. (2002); 8. Mangler et al. (2014).

Watson (1980) concluded based on experimental work that apatite is not likely to stay as a residual phase in the mantle source region, even during low degrees of partial melting. Thus, although our whole-rock data may overestimate the abundance in the source rock to a certain extent (as F is moderately incompatible during melting processes, see above), we suggest that this may indicate a relatively F-rich source mantle below the Uppler Rhine Graben.

6.4. Halogen ratios in the mantle

Despite their variation over more than two orders of magnitude, Cl (from 50 to 7700 μg/g) and Br (from 0.3 to 34 μg/g) show a clear linear positive correlation for most of the investigated samples and the Cl/Br ratios generally vary from 200 to 600, with an average of 371 ± 120 (N = 35, except for four outliers; Fig. 10a & b). Pan and Dong (2003)

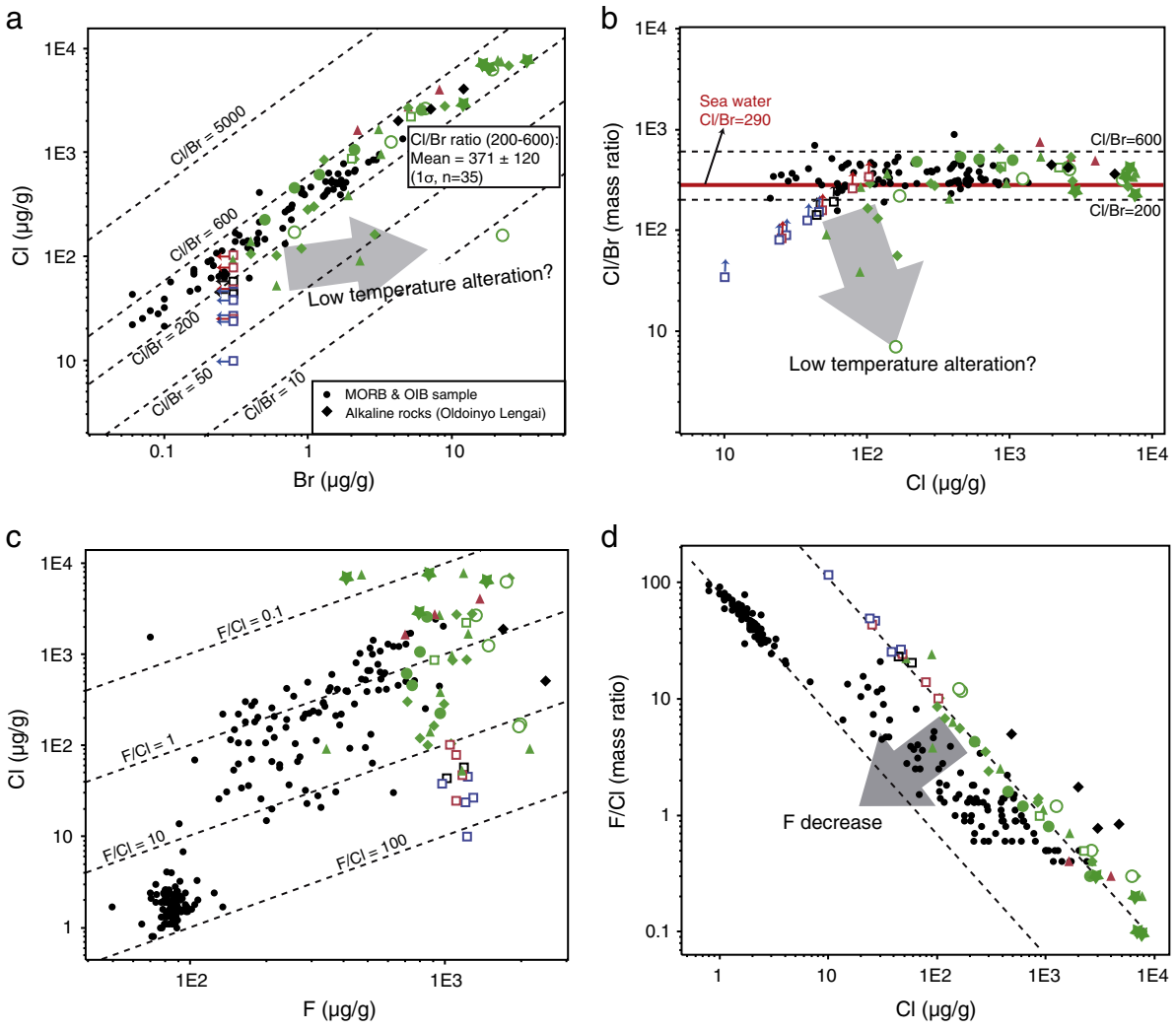

Fig. 10. Halogen ratios in the investigated alkaline rocks. Symbols are the same as in Fig. 2. Data for MORB and OIB samples are from Jambon et al. (1995), Schilling et al. (1980, 1978), Kendrick et al. (2012, 2013a, 2013b), Metrich (1990) and Saal et al. (2002). Data for alkaline silicate rocks of Oldoinyo Lengai are from Mangler et al. (2014).

demonstrated that the Cl/Br ratio in sodalite equals that of the coexisting melt. Our SGM-rich samples show a mean Cl/Br ratio of 378 ± 90 (N = 11), very similar to that from the SGM-free samples and indistinguishable from previous estimates for MORB and OIB samples (Jambon et al., 1995; Schilling et al., 1978, 1980; Kendrick et al., 2012, 2013a, 2013b) as well as the alkaline silicate rocks from Oldoinyo Lengai volcano (Mangler et al., 2014; Fig. 11). This demonstrates that variable degrees of partial melting, fractional crystallization and degassing have no large effect on Cl/Br ratios during the formation and evolution of sub-continental mantle-derived alkaline magmas and that no large heterogeneities in terms of Cl/Br ratios exist between different mantle reservoirs.

Several outliers in our study show much lower Cl/Br ratios down to about 10 (Fig. 10a & b). Whether these samples lost Cl or gained Br is not clear, but they show that Cl and Br can be largely fractionated from each other. However, based on what is known about Cl/Br fractionation, we attribute this to low-temperature alteration.

In contrast to Cl/Br ratios, F/Cl ratios of the investigated samples vary largely over more than three orders of magnitude (from <0.1 to >100; Fig. 10c). This large variation is similar to that recorded for basaltic samples (Schilling et al., 1980; Metrich, 1990; Saal et al., 2002), although our samples are much richer in F. Negative correlations between F/Cl ratios and Cl concentrations (Fig. 10d) show that F is strongly fractionated

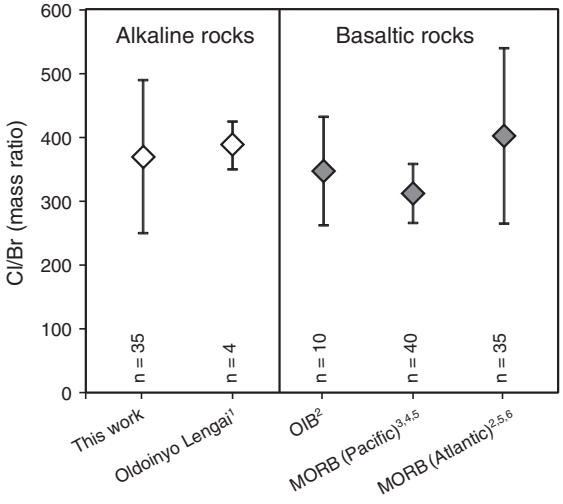

Fig. 11. Comparison between Cl/Br ratios of rift-related alkaline rocks, OIB and MORB samples. Data sources: 1 = Mangler et al. (2014), 2 = Schilling et al. (1978), 3 = Kendrick et al. (2012), 4 = Kendrick et al. (2013a, 2013b), 5 = Jambon et al. (1995) and 6 = Schilling et al. (1980).

from Cl. We suggest that this reflects the combined effects of (i) the different behavior of F and Cl during degassing processes (Fig. 7c), (ii) the crystallization of large amounts of Cl-rich minerals such as SGM in some rocks (Fig. 8) and (iii) different degrees of partial melting of the source rock.

7. Conclusions

Halogen (F, Cl and Br) concentrations were determined for primitive olivine nephelinites and olivine melilitites and associated evolved alkaline rocks from three Cenozoic volcanic fields along the Upper Rhine Graben in southwest Germany. Most olivine nephelinites and olivine melilitites have relatively low Cl (generally <100 μg/g) and Br concentrations (generally <0.3 μg/g). Their F contents are relatively high and constant (around 1100 ± 100 μg/g), much higher than that of primitive mantle and MORB samples (<200 μg/g). The halogen concentrations in the evolved alkaline rocks show variable F (300 to 2200 μg/g), Cl (50 to 7700 μg/g) and Br (from 0.3 to 34 μg/g) abundances.

The majority of the investigated samples show a positive correlation between Cl and Br, independent of rock type and sample locality. Their average Cl/Br ratio of 371 ± 120 is in accordance with previous studies on mantle-derived samples. We therefore suggest that no large heterogeneities in terms of Cl/Br ratios exist between different mantle reservoirs and that Cl and Br are not largely fractionated from each other during magmatic processes such as partial mantle melting, fractional crystallization and degassing. In contrast, a negative correlation between F/Cl ratios and Cl concentrations is present for the whole sample suite, showing that F is strongly fractionated from Cl (and Br) by the above-mentioned processes.

Acknowledgments

U. Neumann is thanked for providing some sample materials. G. Stoschek, S. Ladenburger, B. Steinhilber, H. Teiber and M. Mangler are acknowledged for their help and discussions concerning the PHIC measurements. We are grateful to Mark Kendrick and another anonymous reviewer for their thoughtful and critical reviews on this manuscript. Special thanks to Donald Dingwell for his editorial handling. The China Scholarship Council (CSC) is thanked for granting scholarship (2010641006) for the first author. This work is partially financially supported by Deutsche Forschungsgemeinschaft (grant MA 2563/3-1).

Appendix A. Supplementary data

Supplementary data to this article can be found online at http://dx.doi.org/10.1016/j.chemgeo.2014.05.003.

References

Aiuppa, A., Baker, D.R., Webster, J.D., 2009. Halogens in volcanic systems. Chem. Geol. 263 (1), 1–18.
Alibert, C., Michard, A., Albarede, F., 1983. The transition from alkali basalts to kimberlites: isotope and trace element evidence from melilitites. Contrib. Mineral. Petrol. 82 (2–3), 176–186.
Aoki, K., Ishiwaka, K., Kanisawa, S., 1981. Fluorine geochemistry of basaltic rocks from continental and oceanic regions and petrogenetic application. Contrib. Mineral. Petrol. 76 (1), 53–59.
Bailey, D.K., Hampton, C.M., 1990. Volatiles in alkaline magmatism. Lithos 26 (1), 157–165.
Balcone-Boissard, H., Michel, A., Villemant, B., 2009. Simultaneous determination of fluorine, chlorine, bromine and iodine in six geochemical reference materials using pyrohydrolysis, ion chromatography and inductively coupled plasma-mass spectrometry. Geostand. Geoanal. Res. 33 (4), 477–485.
Balcone-Boissard, H., Villemant, B., Boudon, G., 2010. Behavior of halogens during the degassing of felsic magmas. Geochem. Geophys. Geosyst. 11 (9). http://dx.doi.org/10.1029/2010GC003028.
Blusztajn, J., Hegner, E., 2002. Osmium isotopic systematics of melilitites from the Tertiary Central European Volcanic province in SW Germany. Chem. Geol. 189 (1), 91–103.
Boulyga, S.F., Heumann, K.G., 2005. Direct determination of halogens in powdered geological and environmental samples using isotope dilution laser ablation ICP-MS. Int. J. Mass Spectrom. 242 (2), 291–296.
Burgess, R., Layzelle, E., Turner, G., Harris, J.W., 2002. Constraints on the age and halogen composition of mantle fluids in Siberian coated diamonds. Earth Planet. Sci. Lett. 197 (3), 193–203.
Chai, J.Y., Muramatsu, Y., 2007. Determination of bromine and iodine in twenty-three geochemical reference materials by ICP-MS. Geostand. Geoanal. Res. 31 (2), 143–150.
Coombs, M.L., Sisson, T.W., Kimura, J.I., 2004. Ultra-high chlorine in submarine Kilauea glasses: evidence for direct assimilation of brine by magma. Earth Planet. Sci. Lett. 217 (3), 297–313.
Dunworth, E.A., Wilson, M., 1998. Olivine melilitites of the SW German Tertiary volcanic province: mineralogy and petrogenesis. J. Petrol. 39, 1805–1836.
Foley, S.F., Taylor, W.R., Green, D.H., 1986. The role of fluorine and oxygen fugacity in the genesis of the ultrapotassic rocks. Contrib. Mineral. Petrol. 94 (2), 183–192.
Fusswinkel, T., Wagner, T., Wälle, M., Wenzel, T., Heinrich, C.A., Markl, G., 2013. Fluid mixing forms basement-hosted Pb–Zn deposits: insight from metal and halogen geochemistry of individual fluid inclusions. Geology 41 (6), 679–682.
Garcıa-Heras, M., Fernández-Ruiz, R., Tornero, J.D., 1997. Analysis of archaeological ceramics by TXRF and contrasted with NAA. J. Archaeol. Sci. 24 (11), 1003–1014.
Giehl, C., Marks, M.A., Nowak, M., 2014. An experimental study on the influence of fluorine and chlorine on phase relations in peralkaline phonolitic melts. Contrib. Mineral. Petrol. 167 (3), 1–21.
Govindaraju, K., 1994. 1994 compilation of working values and sample description for 383 geostandards. Geostand. Newslett. 18 (S1), 1–158.
Harford, C.L., Sparks, R.S.J., Fallick, A.E., 2003. Degassing at the Soufrière Hills Volcano, Montserrat, recorded in matrix glass compositions. J. Petrol. 44 (8), 1503–1523.
Hubberten, H.W., Katz-Lehnert, K., Keller, J., 1988. Carbon and oxygen isotope investigations in carbonatites and related rocks from the Kaiserstuhl, Germany. Chem. Geol. 70, 257–274.
Illies, J.H., 1972. The Rhine graben rift system-plate tectonics and transform faulting. Geophys. Surv. 1 (1), 27–60.
Illies, J.H., 1975. Recent and paleo-intraplate tectonics in stable Europe and the Rhinegraben rift system. Tectonophysics 29 (1), 251–264.
Jambon, A., Déruelle, B., Dreibus, G., Pineau, F., 1995. Chlorine and bromine abundance in MORB: the contrasting behaviour of the Mid-Atlantic Ridge and East Pacific Rise and implications for chlorine geodynamic cycle. Chem. Geol. 126 (2), 101–117.
Johnson, L.H., Burgess, R., Turner, G., Milledge, H.J., Harris, J.W., 2000. Noble gas and halogen geochemistry of mantle fluids: comparison of African and Canadian diamonds. Geochim. Cosmochim. Acta 64 (4), 717–732.
Johnson, E.R., Kamenetsky, V.S., Mcphie, J., 2013. The behavior of metals (Pb, Zn, As, Mo, Cu) during crystallization and degassing of rhyolites from the Okataina volcanic center, Taupo volcanic zone, New Zealand. J. Petrol. 54, 1641–1659.
Keller, J., 1997. Bergalite–Okaite–Turjaite: The carbonatite–melilitite connection. Annual Meeting Ottawa. Geol.Ass./Mineral. Ass. , p. A77 (Abstracts).
Keller, J., 2008. Tertiary Rhinegraben volcanism: Kaiserstuhl and Hegau. 9th International Kimberlite Conference. Field Trip Guide, p. 38.
Keller, J., Brey, G., Lorenz, V., Sachs, P., 1990. IAVCEI 1990 Pre-conference Excursion 2A: Volcanism and Petrology of the Upper Rhinegraben (Urach–Hegau–Kaiserstuhl). pp. 1–60.
Keller, J., Sigmund, J., Muller-Sigmund, H., Czirjak, A., 1997. Mantle xenoliths in Rhinegraben volcanics from the Black Forest-Vosges Dome. Terra Nova 9 (Supplement 1), 56 (Abstract).
Keller, J., Kraml, M., Henjes-Kunst, F., 2002. $^{40}Ar/^{39}Ar$ single crystal laser dating of early volcanism in the Upper Rhine Graben and tectonic implications. Schweiz. Mineral. Petrogr. Mitt. 82, 121–130.
Kendrick, M.A., Burgess, R., Harrison, D., Bjørlykke, A., 2005. Noble gas and halogen evidence for the origin of Scandinavian sandstone-hosted Pb–Zn deposits. Geochim. Cosmochim. Acta 69 (1), 109–129.
Kendrick, M.A., Kamenetsky, V.S., Phillips, D., Honda, M., 2012. Halogen systematics (Cl, Br, I) in mid-ocean ridge basalts: a Macquarie Island case study. Geochim. Cosmochim. Acta 81, 82–93.
Kendrick, M.A., Arculus, R., Burnard, P., Honda, M., 2013a. Quantifying brine assimilation by submarine magmas: examples from the Galápagos Spreading Centre and Lau Basin[J]. Geochim. Cosmochim. Acta 123, 150–165.
Kendrick, M.A., Honda, M., Pettke, T., Scambelluri, M., Phillips, D., Giuliani, A., 2013b. Subduction zone fluxes of halogens and noble gases in seafloor and forearc serpentinites. Earth Planet. Sci. Lett. 365, 86–96.
Kent, A.J., Peate, D.W., Newman, S., Stolper, E.M., Pearce, J.A., 2002. Chlorine in submarine glasses from the Lau Basin: seawater contamination and constraints on the composition of slab-derived fluids. Earth Planet. Sci. Lett. 202 (2), 361–377.
Köhler, J., Schönenberger, J., Upton, B., Markl, G., 2009. Halogen and trace-element chemistry in the Gardar Province, South Greenland: subduction-related mantle metasomatism and fluid exsolution from alkalic melts. Lithos 113 (3), 731–747.
Korotev, R.L., 1996. A self-consistent compilation of elemental concentration data for 93 geochemical reference samples. Geostand. Newslett. 20 (2), 217–245.
Kraml, M., Keller, J., Henjes-Kunst, F., 1995. New K/Ar, $^{40}Ar/^{39}Ar$ step-heating and $^{40}Ar/^{39}Ar$ laser fusion dates for the Kaiserstuhl volcanic complex (Upper Rhine Graben; Germany). Eur. J. Mineral. Beih. 7 (1), 142.
Kraml, M., Pik, R., Rahn, M., Selbekk, R., Carignan, J., Keller, J., 2006. A new multi-mineral age reference material for $^{40}Ar/^{39}Ar$, (U–Th)/He and Fission Track dating methods: the Limberg t3 tuff. Geostand. Geoanal. Res. 30, 73–86.
Krumrei, T.V., Pernicka, E., Kaliwoda, M., Markl, G., 2007. Volatiles in a peralkaline system: abiogenic hydrocarbons and F-Cl-Br systematics in the naujaite of the Ilímaussaq intrusion, South Greenland. Lithos 95 (3), 298–314.

Appendix 1

Le Roux, P.J., Shirey, S.B., Hauri, E.H., Perfit, M.R., Bender, J.F., 2006. The effects of variable sources, processes and contaminants on the composition of northern EPR MORB (8–10° N and 12–14° N): evidence from volatiles (H_2O, CO_2, S) and halogens (F, Cl). Earth Planet. Sci. Lett. 251 (3), 209–231.

Lippolt, H.J., 1983. K/Ar age determinations and the correlation of Tertiary volcanic activity in Central Europe. Geol. Jahrb. D52, 113–135.

Lippolt, H.J., Todt, W., Baranyi, I., 1973. K–Ar ages of basaltic rocks from the Urach volcanic district SW-Germany. Fortschr. Miner. 50 Beih. 3, 101–102.

Lowenstern, J.B., Bleick, H., Vazquez, J.A., Castro, J.M., Larson, P.B., 2012. Degassing of Cl, F, Li, and Be during extrusion and crystallization of the rhyolite dome at Volcán Chaitén, Chile during 2008 and 2009. Bull. Volcanol. 74 (10), 2303–2319.

Lustrino, M., Wilson, M., 2007. The circum-Mediterranean anorogenic Cenozoic igneous province. Earth Sci. Rev. 81 (1), 1–65.

Lyubetskaya, T., Korenaga, J., 2007. Chemical composition of Earth's primitive mantle and its variance: 1. Method and results. J. Geophys. Res. Solid Earth 112 (B3), 1978–2012.

Maghraoui, M.E., Joron, J.L., Etoubleau, J., Cambon, P., Treuil, M., 1999. Determination of forty four major and trace elements in GPMA magmatic rock reference materials using X-ray Fluorescence Spectrometry (XRF) and Instrumental Neutron Activation Analysis (INAA). Geostand. Newslett. 23 (1), 59–68.

Mangler, M.F., Marks, M.A.W., Zaitzev, A.N., Eby, G.N., Markl, G., 2014. Halogen (F, Cl, and Br) at Oldoinyo Lengai volcano (Tanzania): effects of magmatic differentiation, silicate-natrocarbonatite melt separation and surface alteration of natrocarbonatite. Chem. Geol. 365, 43–53.

Marks, A.W.M., Wenzel, T., Whitehouse, M.J., Loose, M., Zack, T., Barth, M., Worgard, L., Krasz, V., Eby, G.N., Stosnach, H., Markl, G., 2012. The volatile inventory (F, Cl, Br, S, C) of magmatic apatite: an integrated analytical approach. Chem. Geol. 291, 241–255.

Markl, G., Marks, M., Schwinn, G., Sommer, H., 2001. Phase equilibrium constraints on intensive crystallization parameters of the Illimaussaq Complex, South Greenlad. J. Petrol. 42 (12), 2231–2257.

Mäussnest O., Die Eruptionspunkte des Schwäbischen Vulkans. Z. Deutsch, Gol. Ges. 125, 1974, 23–54

Metrich, N., 1990. Chlorine and fluorine in tholeiitic and alkaline lavas of Etna (Sicily). J. Volcanol. Geotherm. Res. 40 (2), 133–148.

Michael, P.J., Schilling, J.G., 1989. Chlorine in mid-ocean ridge magmas: evidence for assimilation of seawater-influenced components. Geochim. Cosmochim. Acta 53 (12), 3131–3143.

Michel, A., Villemant, B., 2003. Determination of halogens (F, Cl, Br, I), sulfur and water in seventeen geological reference materials. Geostand. Newslett. 27 (2), 163–171.

Misra, N.L., Singh Mudher, K.D., 2002. Total reflection X-ray fluorescence: a technique for trace element analysis in materials. Prog. Cryst. Growth Charact. Mater. 45 (1), 65–74.

Muramatsu, Y., Wedepohl, K.H., 1979. Chlorine in Tertiary basalts from the Hessian Depression in NW Germany. Contrib. Mineral. Petrol. 70 (4), 357–366.

Newsom, H.E., 1995. Composition of the solar system, planets, meteorites, and major terrestrial reservoirs. Glob. Earth Phys. 159–189.

Noble, D.C., Smith, V.C., Peck, L.C., 1967. Loss of halogens from crystallized and glassy silicic volcanic rocks. Geochim. Cosmochim. Acta 31 (2), 215–223.

Ozaki, H., Ebihara, M., 2007. Determination of trace halogens in rock samples by radiochemical neutron activation analysis coupled with the k0-standardization method. Anal. Chim. Chim. Acta Acta 583 (2), 384–391.

Pan, Y., Dong, P., 2003. Bromine in scapolite-group minerals and sodalite: XRF microprobe analysis, exchange experiments, and application to skarn deposits. Can. Mineral. 41 (2), 529–540.

Peterman, Z.E., Cloke, P.L., 2002. Geochemistry of rock units at the potential repository level, Yucca Mountain, Nevada. Appl. Geochem. 17 (6), 683–698.

Pyle, D.M., Mather, T.A., 2009. Halogens in igneous processes and their fluxes to the atmosphere and oceans from volcanic activity: a review. Chem. Geol. 263 (1), 110–121.

Saal, A.E., Hauri, E.H., Langmuir, C.H., Perfit, M.R., 2002. Vapour undersaturation in primitive mid-ocean-ridge basalt and the volatile content of Earth's upper mantle. Nature 419, 451–455.

Salters, V.J., Stracke, A., 2004. Composition of the depleted mantle. Geochem. Geophys. Geosyst. 5 (5).

Schilling, J.G., Unni, C.K., Bender, M.L., 1978. Origin of chlorine and bromine in the oceans. Nature 273, 631–636.

Schilling, J.G., Bergeron, M.B., Evans, R., Smith, J.V., 1980. Halogens in the Mantle beneath the North Atlantic. Philos. Trans. R. Soc. A Math. Phys. Eng. Sci. 297, 147–178.

Schleicher, H., Keller, J., Kramm, U., 1990. Isotope studies on alkaline volcanics and carbonatites from the Kaiserstuhl, Federal Republic of Germany. Lithos 26, 21–35.

Schleicher, H., Baumann, A., Keller, J., 1991. Pb isotopic systematics of alkaline volcanic rocks and carbonatites from the Kaiserstuhl, upper Rhine rift valley, FRG. Chem. Geol. 93, 231–243.

Shimizu, K., Itai, T., Kusakabe, M., 2006. Ion chromatographic determination of fluorine and chlorine in silicate rocks following alkaline fusion. Geostand. Geoanal. Res. 30 (2), 121–129.

Shinonaga, T., Ebihara, M., Nakahara, H., Tomura, K., Heumann, K.G., 1994. Cl, Br and I in igneous standard rocks. Chem. Geol. 115 (3), 213–225.

Signorelli, S., Carroll, M.R., 2000. Solubility and fluid-melt partitioning of Cl in hydrous phonolitic melts. Geochim. Cosmochim. Acta 64 (16), 2851–2862.

Smith, J.V., 1981. Halogen and phosphorus storage in the earth. Nature 289, 762–765.

Sommerauer, J., Katz-Lehnert, K., 1985. A new partial substitution mechanism of CO_3^{2-}/CO_3OH_3- and SiO_4^{4-} for the PO_4^{3-} group in hydroxyapatite from the Kaiserstuhl alkaline complex (SW-Germany). Contrib. Mineral. Petrol. 91, 360–368.

Stecher, O., 1998. Fluorine geochemistry in volcanic rock series: examples from Iceland and Jan Mayen. Geochim. Cosmochim. Acta 62 (18), 3117–3130.

Sumino, H., Burgess, R., Mizukami, T., Wallis, S.R., Holland, G., Ballentine, C.J., 2010. Seawater-derived noble gases and halogens preserved in exhumed mantle wedge peridotite. Earth Planet. Sci. Lett. 294 (1), 163–172.

Ulianov, A., Müntener, O., Ulmer, P., Pettke, T., 2007. Entrained macrocryst minerals as a key to the source region of olivine nephelinites: Humberg, Kaiserstuhl, Germany. J. Petrol. 48 (6), 1079–1118.

Wang, L.X., Marks, M.A.W., Wenzel, T., von der Handt, A., Keller, J., Teiber, H., Markl, G., 2014. Apatites from the Kaiserstuhl Volcanic Complex, Germany: new constraints on the relationship between carbonatite and associated silicate rocks. Eur. J. Mineral. http://dx.doi.org/10.1127/0935-1221/2014/0026-2377 (in press).

Watson, E.B., 1980. Apatite and phosphorus in mantle source regions: an experimental study of apatite/melt equilibria at pressures to 25 kbar. Earth Planet. Sci. Lett. 51 (2), 322–335.

Webster, J.D., Kinzler, R.J., Mathez, E.A., 1999. Chloride and water solubility in basalt and andesite melts and implications for magmatic degassing. Geochim. Cosmochim. Acta 63 (5), 729–738.

Wedepohl, K.H., Gohn, E., Hartmann, G., 1994. Cenozoic alkali basaltic magmas of western Germany and their products of differentiation. Contrib. Mineral. Petrol. 115 (3), 253–278.

Wilson, M., Downes, H., 1991. Tertiary–Quaternary extension-related alkaline magmatism in Western and Central Europe. J. Petrol. 32 (4), 811–849.

Wilson, M., Downes, H., 2006. Tertiary-Quaternary intra-plate magmatism in Europe and its relationship to mantle dynamics. In: Gee, D.G., Stephenson, R. (Eds.), European lithosphere dynamics. Geological Society of London, London, pp. 147–166.

Wimmenauer, W., 1962. Beiträge zur Petrographie des Kaiserstuhls. Teil IV: Die Gesteine der phonolithischen Familie. Teil V: Die subvulkanischen Breccien. Neues Jb. Mineral. Abh. 98, 367–415.

Wimmenauer, W., 1966. The eruptive rocks and carbonatites of the Kaiserstuhl, Germany. Carbonatites, Wiley, London pp. 183–204.

Wimmenauer, W., 1974. The alkaline province of central Europe and France. In: Sørensen, H. (Ed.), The Alkaline Rocks. John Wiley & Sons Ltd., London, pp. 238–271.

Wimmenauer, W., 2003. Geologische Karte von Baden-Württemberg 1:25.000 Erläuterungen zum Blatt Kaiserstuhl, Landesamt für Geologie, Rohstoffe und Bergbau Baden-Württemberg, Freiburg i. Br., 47-130.

Appendix 2

Apatites from the Kaiserstuhl Volcanic Complex, Germany: new constraints on the relationship between carbonatite and associated silicate rocks

Authors

Lian-Xun Wang, Michael A.W. Marks, Thomas Wenzel, Anette von der Handt, Jörg Keller, Holger Teiber, Gregor Markl

Status

Published in *EUROPEAN JOURNAL OF MINERALOGY* (2014), v. 26, p.397-414

Editor

Reto Gieré

Reviewer

Anton R. Chakhmouradian and Tahar Hammouda

Contributions of the candidate

Scientific ideas	50%
Data acquisition	100%
Analysis and interpretation	60%
Preparation of manuscript	60%

Apatites from the Kaiserstuhl Volcanic Complex, Germany: new constraints on the relationship between carbonatite and associated silicate rocks

LIAN-XUN WANG[1,3*], MICHAEL A.W. MARKS[1], THOMAS WENZEL[1], ANETTE von der HANDT[2], JÖRG KELLER[2], HOLGER TEIBER[1], GREGOR MARKL[1]

1 = Universität Tübingen, Mathematisch-Naturwissenschaftliche Fakultät, FB Geowissenschaften, 72074 Tübingen, Germany

* Corresponding author, e-mail: lian.x.wang@gmail.com

2 = Albert-Ludwigs-Universität Freiburg, Institut für Geowissenschaften - Mineralogie-Geochemie, 79104 Freiburg, Germany

3 = Faculty of Earth Sciences, China University of Geosciences, Wuhan 430074, China

* = corresponding author. Tel: +49 (0) 7071-29 730 77. Fax: +49(0)7071-29 3060. Email: lian.x.wang@gmail.com;

Abstract: Apatites from carbonatites, related alkaline silicate rocks, a carbonate-bearing melilititic dyke rock (bergalite), and a diatreme breccia (containing both carbonate and silicate fragments) of the Miocene Kaiserstuhl Volcanic Complex, SW Germany, are used to reconstruct the petrogenetic relationship among these rocks. Apatites from carbonatites reach higher Sr and Nb contents but are generally lower in Fe, Mn, Th, U, Si, S, Cl and Br compared to apatites from associated silicate rocks, whilst Na, REE and F contents are overlapping. Apatites from bergalite show a systematic and discontinuous core-rim zonation, with the core being compositionally

similar to apatites from silicate rocks and the rim corresponding to carbonatitic apatites. These observations imply that the bergalite apatites nucleated in a silicate melt and continued to crystallize from an evolving CO_2-enriched melt probably with carbonatitic affinity. Apatites from a diatreme breccia comprise three populations: (1) similar to the apatites from silicate rocks, (2) similar to the carbonatitic apatites, and (3) resembling apatite population (1) partially replaced by apatite (2). We infer that apatite (1) was derived from silicate-rock fragments and apatite (2) crystallized from a later intruding carbonatitic melt, which metasomatized the silicate-rock fragments and caused the replacement textures as observed in apatite population (3). We conclude that apatites from the Kaiserstuhl complex preserve important information on the petrogenetic relationship between carbonatitic and silicate melts. The carbonatitic melts at the Kaiserstuhl complex are probably the products of protracted fractionation of a CO_2-rich nephelinitic melt.

Key-words: apatite, carbonatite, bergalite, Kaiserstuhl, replacement, zoning texture.

1. Introduction

From the approximately 500 carbonatite occurrences worldwide, more than 75% are associated with alkaline silicate rocks, ultramafic lamprophyres or kimberlites (*e.g.* Woolley & Kjarsgaard, 2008) and, in many cases, carbonatites postdate the silicate rocks (*e.g.*, Keller *et al.*, 1990; Bailey, 1993; Bell et al., 1999; Woolley, 2003, 2008; Halama *et al.*, 2005). Despite nearly a century of research on carbonatites, their origin and relationships to associated silicate rocks is not completely understood yet (Bell *et al.*, 1999; Gittins & Harmer, 2003). Experimental work showed that carbonatites can be generated by (1) liquid immiscibility of carbonatite and silicate melts (*e.g.*, Koster van Groos & Wyllie, 1966; Freestone & Hamilton, 1980; Brooker & Kjarsgaard, 2011); (2) partial melting of carbonate-bearing mantle peridotite (*e.g.*, Wallace & Green, 1988; Dalton & Presnall, 1998; Ghosh *et al.*, 2009); and (3) fractional crystallization of a carbonate-rich alkaline silicate magma (Watkinson & Wyllie, 1971; Lee & Wyllie, 1994). In some localities, unusual transitional rocks (cf. carbonate-rich/bearing silicate rocks), such as bergalites, turjaites and okaites, are found temporally and spatially close to the carbonatite and

associated silicate rocks (Eby, 1975; Keller *et al.*, 1990; Keller, 1991, 1997; Bell *et al.*, 1996). These rocks may provide important clues for the petrogenetic link between carbonatite and associated silicate rocks (Keller *et al.*, 1990; Keller, 1991, 1997; Chakhmouradian & Zaitsev, 2004; Moore *et al.*, 2009).

Apatite is a good indicator for magma evolution (Seifert *et al.*, 2000; Piccoli & Candela, 2002; Zhang *et al.*, 2012) and occurs in a wide range of magmatic systems such as mafic rocks (*e.g.*, Brown & Packett, 1977; Binder & Troll, 1989; Tribuzio *et al.*, 1999), granitic rocks (*e.g.*, Watson, 1980; Sha & Chappell, 1999; Marks *et al.*, 2012) and syenitic rocks (*e.g.*, Liferovich & Mitchell, 2006; Rønsbo, 2008). In particular, carbonatite (*e.g.*, Bühn *et al.*, 2001; Brassinnes *et al.*, 2005; Chen & Simonetti, 2012) and related rocks (Eby, 1975; Keller *et al.*, 1990; Bell *et al.*, 1996; Moore *et al.*, 2009) contain appreciable amounts of apatite. Experimental studies imply that many trace elements (*e.g.* Sr, rare earth elements [REE], Th, U) exhibit distinct partitioning behavior in carbonatitic and silicate melt systems (Klemme & Dalpé, 2003; Prowatke & Klemme, 2006; Hammouda *et al.*, 2010). Thus, chemical differences between apatites from carbonatites and from associated silicate rocks are expected, and detailed investigations of apatite from the transitional dyke rocks might help to decipher the petrogenetic relationships between the two rock types.

The Kaiserstuhl Volcanic Complex (KVC) comprises a series of alkaline silicate rocks, associated with carbonatites as well as transitional dyke rocks (bergalites) and polygenic diatreme breccias (mixtures of carbonatite and silicate-rock fragments, *e.g.*, Keller, 1984, Schleicher *et al.*, 1990; Wimmenauer 2003). In these rocks, apatite is a common accessory mineral. Hence, in the present work we studied the apatites from various rocks of KVC with the aim to (1) constrain the chemical variations of these apatites; (2) shed more light on the petrogenetic relationship between carbonatite and associated silicate rocks; and (3) investigate the abundance and variability of volatile elements (F, Cl, Br, S) in apatites from alkaline silicate rocks and carbonatite.

2. Geological setting and sample description

The KVC is located in the southern part of Upper Rhine Graben (Fig. 1a) and is part of extensive Cenozoic volcanism in Central Europe (Keller *et al.*, 1990; Wilson & Downes, 1991, 2006; Riley *et al.*, 1999; Wimmenauer, 2003). Ages of the Kaiserstuhl rocks range between 18 and 13 Ma (Lippolt *et al.*, 1963; Baranyi *et al.*, 1976; Kraml *et al.*, 1995, 2006; Keller, 2002). The KVC is a sequence of early intrusion and extrusion of alkaline silicate rocks followed by late formation of carbonatites (Keller *et al.*, 1990, 2008; Wimmenauer, 2003).

The silicate rocks are dominated by tephrites, essexites and phonolites (Fig.1b). Sub-dominant rock types include olivine-melilitites, olivine-nephelinites, limburgites (olivine + augite + glassy groundmass), hauynophyres, syenites, shonkinite porphyries, and mondhaldeites (Wimmenauer, 2003; Keller, 2008). Shonkinite porphyry and mondhaldeite are fractionated dyke rocks from the tephritic magma. Carbonatites consist of sövite intrusions (Badberg and Orberg), alvikitic dykes and rare extrusive carbonatites (Keller, 1981, 2001; Hubberten *et al.*, 1988). These are spatially and temporally associated with (1) magmatic diatreme breccias, some of which are polygenic mixtures consisting of mafic cumulates, carbonatite and silicate rock fragments, fill pipe structures in the sövite bodies (Baranyi, 1977; Katz & Keller, 1981; Hubberten *et al.*, 1988; Keller *et al.*, 1990; Sigmund, 1996), and (2) bergalite dyke rocks (Hubberten *et al.*, 1988; Schleicher *et al.*, 1990; Keller, 1991, 1997), which are carbonate-bearing, silica-undersaturated rocks with a mineral assemblage of melilite + sodalite + perovskite + biotite ± nepheline + apatite + magnetite + calcite (Keller, 2001, 2008).

In this study we investigate apatite separates from twelve KVC rocks, including four sövitic carbonatites from surface outcrops and drill cores, one diatreme breccia, one bergalite, one essexite, one mondhaldeite, one shonkinite porphyry, and three phonolitic rocks (Table 1a). Details on the petrography, mineralogy and geochemistry of these samples are given in Hubberten *et al.* (1988), Keller *et al.* (1990) and Schleicher *et al.* (1990). Apatite separates were produced by using standard heavy liquid methods and were subsequently mounted in epoxy, polished and carbon coated for further cathodoluminescence studies (CL), electron microprobe analysis (EMPA), secondary ion mass spectrometry (SIMS), and total reflection X-ray fluorescence analysis (TXRF).

3. Analytical methods

3.1. Electron microprobe analysis

Major and minor element compositions of apatites were determined using a JEOL 8900 electron microprobe operated in wavelength-dispersive mode at Tübingen University. A beam current of 10 nA and an acceleration voltage of 15 kV were used in connection with a defocused beam diameter of 10 µm. Durango apatite was used as the standard for Ca, P and F. Other standards included albite for Na, diopside for Si, hematite for Fe, rhodonite for Mn, barite for S, tugtupite for Cl, La-glass (REE16G) for La, Ce-glass (REE16G) for Ce, and synthetic GaAs and $SrTiO_3$ for As and Sr, respectively. Counting times were 16 s for the Ca peak; 30 s for P, F, Na, Si, S and Sr peaks; and 60 s for Fe, Mn, As, La, Ce and Cl peaks, resulting in detection limits that are very similar to those reported by Marks *et al.* (2012). Data reduction was performed using the internal ZAF matrix correction software of JEOL (Armstrong, 1991).

Cathodoluminescence imaging, a powerful tool to reveal internal textures of minerals (*e.g.*, Götze *et al.*, 2013), was used prior to EMPA to document the internal structures in apatite crystals. According to Stormer *et al.* (1993) and Goldoff *et al.* (2012), long-time exposure under an electron beam might cause F and Cl diffusion depending on the orientation of the apatite crystal. To monitor these effects, we performed two tests. In the first test we analyzed apatite grains of sample M2 by EMPA along profiles parallel to the *c*- and *a*-axes of a crystal. Subsequently, these grains were exposed for around 3 minutes to the low-intensity (10 nA) CL-imaging tool integrated into the electron microprobe. The same grains were then reanalyzed with the analysis points set close to the previous ones. For the second test the sample holder was re-polished and carbon coated again. Additional apatite grains were analyzed and subsequently these grains were exposed for around 3 minutes to the high-intensity electron gun of a CL microscope (12-15 mA). These grains were then re-analyzed close to the previous points with the electron microprobe. The results from these two tests are shown in Fig. 2. Low-intensity CL did not cause statistically significant diffusion effects for F and Cl. In contrast, the high-intensity CL enhanced F diffusion. Thus, we conclude that the F and Cl diffusion effects are related to the intensity of the electron beam, and the use of a low (<10 nA) beam current for the CL study should not affect the quality of F and Cl analyses.

3.2. Secondary-ion mass spectrometry

Trace elements were analyzed using an upgraded CAMECA ims-3f ion microprobe at the Max-Planck-Institute for Chemistry in Mainz. The primary beam consisted of negative oxygen ions at a nominal accelerating potential of 12.5 kV and a beam current of 20 nA, resulting in a sputtering surface of 15-20 µm. Positive secondary ions of ^{16}O, ^{23}Na, ^{30}Si, ^{44}Ca, ^{88}Sr, ^{89}Y, ^{90}Zr, ^{93}Nb, ^{139}La, ^{140}Ce, ^{141}Pr, ^{146}Nd, ^{147}Sm, ^{153}Eu, ^{157}Gd, ^{163}Dy, $^{16}7Er$, ^{174}Yb, ^{232}Th, ^{238}U were extracted in that order, using an acceleration potential of 4.5 kV with a 25 eV energy window and fully open entrance and exit slits. Ions were counted in a peak jumping mode and ratioed to ^{44}Ca to quantify element abundances. Each measurement consisted of a six-cycle routine. At the beginning of each measurement, the energy distribution of ^{16}O and subsequent peak centers for ^{44}Ca, ^{88}Sr, ^{140}Ce and ^{232}Th were determined by scanning the peak in 20 steps across a 1.5 per mille wide B-field and the neighboring masses adjusted to these new peak centers. Measurement times were 30 s for Nb, Er, Yb; 20 s for Sm, Eu, Gd, Dy, U; 8 s for Y and Nd, 5 s for Ba, La, Ce, Pr, Th and 1 s for all other elements. Ion yields in phosphates are comparable to those from silicate glasses (Sano *et al.*, 2002) and sensitivity factors were determined with MPI-DING reference glasses KL2-G, ML3B (Jochum *et al.*, 2006) and NIST 610 (Jochum & Stoll, 2008). Energy filtering of molecular ion species was achieved with an offset of -80 eV. In apatite, the only molecular ions in the mass range of the REE that are not suppressed by energy filtering are monoxides and fluorides. However, the only substantial fluoride interference in the apatites was found at mass 159 where $^{140}Ce^{19}F$ interferes with Tb whereas hydride, hydroxide, and chloride peaks were found to be insignificant (Crozaz & Zinner, 1985; Zinner & Crozaz, 1986). Accordingly, Tb was not analyzed and oxide interferences on Eu, Gd, Dy, Er and Yb were corrected offline. Here, the general light-REE-enriched apatite pattern produces significant interferences where BaO^+ interferes with $^{153}Eu^+$, $^{141}PrO^+$ with $^{157}Gd^+$; $^{147}SmO^+$ with $^{163}Dy^+$; $^{151}EuO^+$ with $^{167}Er^+$; and both $^{158}GdO^+$ and $^{158}DyO^+$ with $^{174}Yb^+$. The MO^+ to M^+ ratios used for the correction are 0.057, 0.165, 0.127, 0.058, 0.049, 0.145 and 0.127, respectively. The largest uncertainties are introduced by the correction of GdO and DyO interferences on Yb.

3.3. Total reflection X-ray fluorescence analysis

These analyses were performed using a S2 PICOFOX TXRF (Bruker AXS) at Universität Tübingen. Hand-picked apatite separates were milled to a fine-grained powder (< 15 µm). Around 1 mg apatite powder was dispensed in 1 ml Triton (1 vol.%) as solvent in an Eppendorf tube; 10 µl of a 10 mg/l Se solution was added as an internal standard. These suspensions were then homogenized for about 2 minutes, and aliquots of these suspensions were pipetted onto quartz glass sample discs and dried on a hot plate at 70°C. The dried samples where then analyzed for 1000 s (live time) using a Mo X-ray tube with an operating voltage of 50 kV and a beam current of 600 µA. The spectra were fitted with the Spectra 6.2 software (Bruker Nano GmbH). Further technical details can be found in Marks *et al.* (2012). TXRF is barely used to analyze solid materials (minerals and rocks) and available analytical approaches are limited (*e.g.*, García-Heras *et al.*, 1997; Misra *et al.*, 2002; Marks *et al.*, 2012). Here, we compare the results and uncertainties of apatite compositions analyzed by EPMA, SIMS and TXRF. Our data show good consistency between the three methods (see supplementary material), demonstrating that TXRF is reliable in quantifying REE.

4. Results

4.1. CL imaging

The observed variations in CL intensity and color (Fig. 3) are generally related to the contents of luminescence activator elements, *e.g.* REE, Mn and Eu (Mariano, 1988; Koberski 1995; Mitchell *et al.*, 1997; Waychunas, 2002; Dempster *et al.*, 2003). To better illustrate the different apatite types from various KVC rocks, we use the abbreviations listed in Table 1b.

4.1.1. Apatite from silicate rocks and carbonatites

Apatites from silicate rocks (S.Ap) generally show complex zonations, either oscillatory or patchy (Fig. 3a-c), which, however, do not reflect any detectable systematic compositional variation. Apatites from carbonatites (C.Ap) appear brighter than those from silicate rocks and occasionally contain micro-holes and calcite inclusions (Fig. 3d-e). Sample KB3, which has an

unusual orbicular texture in hand-specimen, shows varying CL intensities in apatite separates, and at least two types of apatite (brightly luminescent and dull) can be distinguished (Fig. 3f).

4.1.2. Apatite from bergalite

Most apatite grains from bergalite show regular zoning with a gray inner core, darker outer core, and a bright rim (Fig. 3g-h). The boundaries between these zones are generally abrupt and often display euhedral outlines. In rare cases, the core appears to be partially resorbed (rounded shape; Fig. 3h). Apparently unzoned grains show a similar CL brightness as the cores (Fig. 3g) and have similar chemical compositions (see below). We assume that this is an effect of different orientations of the crystals in the sample mount.

4.1.3. Apatite from diatreme breccia

Apatites from a diatreme breccia comprise three different populations (Fig. 3i): (1) grains with lower CL brightness (D.Ap); (2) higher-brightness grains with occasional micro-holes and calcite inclusions (B.Ap, Fig. 3j); and (3) grains with replacement textures (R.Ap), resembling apatite population (1) partially replaced by apatite (2) preferentially around the margins of crystals and along cracks (Fig. 3k-l).

4.2. Compositional variation

4.2.1. Comparison of C.Ap and S.Ap

Strontium is generally higher in C.Ap than in S.Ap (Fig. 4a; Table 2). Iron and Mn are low in C.Ap (mostly < 0.005 apfu) with more than 50% of values below the respective detection limits (360 ppm for Fe, 220 ppm for Mn), whereas they are higher in S.Ap (mostly > 0.005 apfu, Fig. 4a). The C.Ap and S.Ap datasets generally overlap in their REE and Na contents (Fig. 4b and 4e), with apatites from sövite KB3 showing a REE variation (from 0.06 to 0.15 apfu) that is distinct from other C.Ap (Table 2). Thorium in C.Ap is commonly lower than 10 ppm with some cases below the detection limit of 0.4 ppm (Table 3, Fig. 4f). Uranium in C.Ap is always below the detection limit (0.04 ppm). In contrast, the S.Ap has much higher Th (40 to 200 ppm) and U (6 to 72 ppm) contents (Fig. 4f). Silicon and S contents are generally lower in C.Ap than in S.Ap

(Fig. 4c), reaching 0.17 apfu Si and 0.09 apfu S in S.Ap. An exception, again, is sövite KB3, with Si contents as high as 0.27 apfu. Arsenic is higher in C.Ap (23-47 ppm) than in S.Ap (<10 ppm; Table 3). Niobium in C.Ap is always higher than 2 ppm, compared to < 1ppm in S.Ap (Fig. 4f).

Variation in F is very similar in C.Ap and S.Ap (Fig. 4d), whereas Cl is significantly lower in C.Ap (<0.01 apfu) than in S.Ap (0.02-0.2 apfu). In both groups, F and Cl are negatively correlated to each other (Fig. 4d). Bromine is always below the detection limit of TXRF in C.Ap (around 0.5 ppm), but generally between 1 and 3 ppm in S.Ap with an exceptionally high Br content of 12 ppm in apatites from a phonolitic dyke (Table 4).

4.2.2. Apatite from bergalite

The CL zonation in bergalite apatites (Fig. 3i-k) correlates with compositional differences (Fig. 5; Table 2). The inner cores are characterized by low Sr and REE and intermediate Na contents (Fig. 5; Table 2). The rims are highest in Sr and lowest in Na. The outer cores generally overlap with the inner cores in terms of Sr, REE and Na. Silicon contents increase from inner to outer core and decrease towards the rims (Fig. 5). Sulfur concentrations in the inner cores show a large variation and overlap considerably with those in the outer cores. The rims, however, are notably poorer in S (Table 2). The average F content in the inner cores (0.35 apfu) is slightly lower than in the outer cores (0.47 apfu; Fig. 5). The highest values were found in the rims (0.75 apfu). The contents of Cl and calculated OH are lower in the rims than in the cores (Table 2).

4.2.3. Apatite from diatreme breccia

The B.Ap grains show large variation in many elements and commonly overlap with the data for D.Ap (Fig. 6). Fluorine and Cl contents in both groups exhibit significant differences. R.Ap.rel always shows the same compositional range as defined by D.Ap, whereas R.Ap.sec is compositionally similar to B.Ap.

5. Discussion

5.1. Interpretation of the compositional differences between C.Ap and S.Ap

Chemical variation of magmatic apatites depends on apatite–melt partitioning coefficients, melt composition, charge-balance constraints for multi-element substitutions, and possibly other factors (*e.g.*, Peng *et al.*, 1997; Sha & Chappell, 1999; Harlov *et al.*, 2002). In the following, we evaluate the influences of these factors on the chemical differences between C.Ap and S.Ap.

5.1.1. Apatite–melt partition coefficients and host melt compositions

According to experimental work (Klemme & Dalpé, 2003; Prowatke & Klemme, 2006; Hammouda *et al.*, 2010), apatite in the carbonatitic system has lower $D^{apatite\text{-}melt}$ values for Sr, La and Ce and higher values for Nb in comparison with those from the silicate-melt system (Supplementary Table; Klemme & Dalpé, 2003; Prowatke & Klemme, 2006; Hammouda *et al.*, 2010). Indeed, C.Ap from the Kaiserstuhl has higher Nb concentrations than S.Ap (Table 3), implying that partition coefficients play an important role. However, the Sr, La and Ce concentrations in C.Ap are not lower than those in S.Ap, although they have lower $D^{apatite\text{-}melt}$ values in C.Ap (Table 2). We attribute this to the effect of melt composition, since carbonatitic melts are usually enriched in Sr and REE compared to silicate melts (Hubberten *et al.*, 1988; Keller *et al.*, 1990; Martin *et al.*, 2013). For instance, according to Keller *et al.* (1990 and unpublished), carbonatites from the KVC contain up to 16000 ppm Sr, whereas the silicate rocks contain < 1000 ppm.

5.1.2. Substitution mechanisms

A positive correlation between S and Si for C.Ap and S.Ap (Fig. 7a) indicates that sulfur is mainly incorporated according to the substitution

$$Si^{4+} + S^{6+} = 2P^{5+}$$

(Pan & Fleet, 2002). However, the high Si contents in apatite from sövite KB3 cannot be explained this way. Apatites from this sample also show the highest La + Ce contents, which clearly correlate with Si (Fig. 7b), pointing to the importance of the substitution

$$REE^{3+} + Si^{4+} = Ca^{2+} + P^{5+},$$

as proposed for apatites from other localities (*e.g.*, Comodi *et al.*, 1999; Harlov *et al.*, 2002, 2005). The combination of these two substitutions (Fig. 7c) demonstrates that both mechanisms

can explain the variation observed in C.Ap and S.Ap. However, for sample KB3, a significant deviation from the 1:1 line exists. This is probably because only La + Ce were analyzed by EPMA, thereby underestimating the total REE. Alternatively, other substitution mechanisms may play a role for apatites from this sample. The substitution mechanism $REE^{3+} + Na^{+} = 2\ Ca^{2+}$ (Harlov *et al.*, 2002, 2005), however, does not play a major role since Na does not correlate with La + Ce (Fig. 4b) and apatites from KB3 are not exceptionally Na-rich (Table 2).

5.2. Interpretation of the zoned apatites from bergalite

Zoning patterns in apatite may be related to a variety of processes such as fractional crystallization, magma mixing, magmatic degassing, diffusion, disequilibrium crystallization, partial dissolution, and recrystallisation (*e.g.*, Jolliff *et al.*, 1989; Brenan, 1994; Sha *et al.*, 1999; Tepper & Kuehner, 1999; Chakhmouradian *et al.*, 2008; Rønsbo, 2008; Boyce & Hervig, 2008; 2009). The zoning textures found in the bergalite apatites (Fig. 5) display discontinuous concentration changes in both volatile (F, Cl and S) and non-volatile elements (*e.g.*, Sr and Si). Therefore, it seems unlikely that magma degassing can fully explain these zonations.

Clear compositional differences between inner and outer cores are only observed for Si (Fig. 5). The difference may be caused by fractionation of the parental melt combined with changing trace element substitution mechanisms in apatite. However, the observed CL textures and chemical profiles show abrupt changes (Fig. 3g-h) and rounded shapes and embayments in some cores (Fig. 3g-h). This can be explained by the stirring of magmas during ascent in high-level magma bodies. Such stirring could result in partial thermal and chemical changes of the magma and lead to disequilibrium crystallization of apatite.

The chemical differences between core and rim probably rather reflect the evolving magma composition during bergalite crystallization. The rims of the bergalite apatites are very similar to those of C.Ap (*e.g.*, relatively high CL brightness, low Si, Cl and S, but high Sr contents; Fig. 8), whereas the cores are chemically similar to S.Ap. To further evaluate the compositional similarity, we calculated Sr concentrations of the related parental melts from the apatite compositions. We assume that the cores crystallized from a melilite nephelinite melt, whereas the rims crystallized from a late-stage melt with carbonatitic affinity. The D_{Sr} partition

coefficients used here are 5.1 for apatite/phonolite, 1.56 for apatite/tephrite and 0.53 for apatite/carbonatite (Prowatke & Klemme, 2006; Hammouda *et al.*, 2010). A comparison of the modeling result with the whole-rock Sr contents (Keller, unpublished data) shows that the calculated Sr concentrations are in agreement with, or close to, those from whole-rock data (Fig. 9). Moreover, it also supports the hypothesis that the cores of the bergalite apatites correspond to S.Ap., whereas the rims correspond to C.Ap.

The overgrowth of C.Ap-like rims on S.Ap-like cores in the apatite crystals from bergalite can be explained by the following processes: (1) fractional crystallization of a melilite nephelinite magma; and (2) mixing of two independent magmas, a silicate and a carbonatitic one. These two magmas will either mix to form a homogeneous intermediate product, or remain immiscible. Watkinson & Wyllie (1971) produced calcite + cancrinite + melilite at 1 kbar using a carbonated nepheline-rich liquid at *ca*. 600 ° C, indicating that carbonatite can be generated by fractional crystallization of a carbonated nephelinite magma. Accordingly, it was assumed that the bergalite melt fractionated from a parental CO_2-rich olivine melilite nephelinite mantle-derived magma (Keller *et al.*, 1990, 2008). This fractionation caused the enrichment of CO_2, Sr, and REE in the evolved melt (Keller, 1991, 1997). The residual melt from which the C.Ap-like rims crystallized would, in this case, have carbonatitic affinity. Dempster *et al.* (2003) demonstrated that discontinuously zoned apatite can monitor changing permeability in granites, in which apatite cores grew early in the magma chamber, whereas rims record late-stage crystallization within more isolated interstitial melt pockets in a highly solidified and compacted crystal mush. Similarly, C.Ap-like rims may represent the late-stage crystallization from carbonate-rich melt pockets.

Mixing of carbonatitic and melilititic magmas could theoretically yield an intermediate product such as bergalite. However, the Sr contents in the rims do not support this assumption, because they generally plot outside the interval defined by the two assumed end-members, C.Ap and S.Ap (Fig. 8). Moore *et al.* (2009) interpreted the genesis of silicocarbonatite dykes by mingling between carbonatitic and silicate magmas, involving liquid immiscibility. If we assume a carbonatitic melt was injected into a melilititic melt with immiscibility during the late stage, it is still not clear whether core-rim zoned apatite or replaced apatite (as observed in diatreme breccias; see below) will form during this mingling process.

In summary, the zoning textures in bergalitic apatites imply that they initially nucleated in a silicate melt and later developed a rim while in equilibrium with a carbonatitic melt. We favour hypothesis (1) to explain the observed apatite textures.

5.3. Interpretation of the replacement textures in apatite from diatreme breccias

Mineral replacement reactions are generally related to dissolution-reprecipitation processes resulting from chemical weathering, leaching, alteration, metamorphism or metasomatism (Putnis, 2002; Engvik, *et al.*, 2009). Replacement of chlorapatite by hydroxy-fluorapatite during metasomatism in metagabbro has been described by Harlov *et al.* (2002) and Engvik *et al.* (2009) and has been experimentally reproduced under alkaline hydrothermal conditions (Yanagisawa *et al.*, 1999; Harlov *et al.*, 2002). However, the replacement of hydroxyapatite by fluorapatite, as documented experimentally by Rendón-Angeles *et al.* (2000), has so far not been reported for natural apatites. In the present study, the replacement textures found in apatites from the diatreme breccia reveal hydroxy-fluorapatite replaced by fluorine-hydroxyapatite (Figs. 3i-l and 7). The R.Ap.sec represents a late-stage fluid/melt re-equilibration product. Compositional and CL similarities between R.Ap.rel and S.Ap indicate that the former represent relict grains of early-formed apatites crystallized from a silicate melt. In contrast, R.Ap.sec is similar to C.Ap, implying formation from a carbonatitic melt. These observations suggest that a carbonatitic magma captured silicate-rock fragments and rapidly rose to the surface to form the diatreme breccias. During this process, metasomatism of the silicate xenoliths by the carbonatitic melt caused the replacement textures observed in some of the apatites.

5.4. Abundances and variability of volatile elements (F, Cl, Br, S) in apatite

Apatites from the KVC are mostly fluorine-hydroxyapatite or hydroxy-fluorapatite (Fig. 10). Their Cl contents are quite low, especially in the C.Ap (Fig. 11a). This agrees well with previous studies where apatites from carbonatite complexes were reported as Cl-poor with mostly less than 0.1 wt% Cl (*e.g.*, Eby, 1975; Hogarth, 1989; Seifert *et al.*, 2000; Patiño Douce *et al.*, 2011). The low Cl content was explained by Cl partitioning into an aqueous fluid phase, which

generally coexisted with the carbonatitic melt (Gittins, 1989; Seifert *et al.*, 2000). Bromine contents generally correlate with Cl: in Cl-poor C.Ap Br is below the detection limit but reaches around 2.5 ppm in relatively Cl-rich S.Ap. This is consistent with previously found positive correlations between Cl and Br (O'Reilly & Griffin, 2000; Marks *et al.*, 2012;), implying Cl and Br behave similarly during incorporation by apatite.

Sommerauer & Katz-Lehnert (1989) determined carbon concentrations in some apatites from Kaiserstuhl using coulometric titration and Fourier-transformed infrared (FTIR) spectroscopy, revealing up to 3.9 wt% CO_2 in carbonatitic apatites and up to 0.9 wt% in apatites from the silicate rock. However, the calcite inclusions in C.Ap observed in the present work and the strong zoning in apatite from the bergalite samples make the interpretation of Sommerauer & Katz-Lehnert (1989) problematic, because their work was performed on bulk powder samples.

Sulfur is incorporated in apatite as sulfate (Pan & Fleet, 2002), and most natural apatites contain <0.5 wt% SO_3 (Broderick *et al.*, 2007), although concentrations of up to 2 wt % have been reported (Imai et al, 1993; Streck & Dilles, 1998; Broderick *et al.*, 2007; Parat *et al.*, 2011). The S.Ap from KVC are rich in SO_3 (0.74–1.11 wt%), indicating that the KVC silicate magma was enriched in S and crystallized under relatively oxidizing conditions (Imai et al, 1993; Peng *et al.*, 1997; Parat *et al.*, 2002). In contrast, C.Ap is relatively poor in SO_3 (0.02-0.5 wt%). These low contents of both SO_3 and Cl (Fig. 11b) probably reflect the relative depletion of carbonatitic magma in both elements. It is unlikely to represent a Cl and S loss during degassing, because when nephelinitic magma fractionated to carbonatitic magma, non-volatile elements (*e.g.*, Si) vary with Cl and S as well (see the compositional variation in core-rim zoned apatite from bergalite in Fig. 5).

6. Conclusions

Textural and chemical variations of apatites from the KVC provide important information for the genesis of their host rocks: Apatites from bergalite allow for the reconstruction of the genetic relations between carbonatites and associated alkaline silicate rocks. Their textural and compositional core-rim zonation implies that these apatites initially crystallized from a silicate melt and further developed in a melt with carbonatitic affinity. This carbonatitic melt is likely a

product of prolonged fractional crystallization of an initial CO_2-rich melilite nephelinite melt. On the other hand, apatites from silicate rock fragments found in a diatreme breccia were subsequently metasomatized by late-injected carbonatitic melt, as shown by their replacement textures. Overall, our study shows that apatite is an equally sensitive monitor for primary magmatic processes (*e.g.*, fractional crystallization) and secondary processes, such as metasomatic overprint.

Acknowledgements: Dr. M. Rahn and Prof. H. Schleicher are gratefully thanked for kindly providing some of the investigated apatite separates and for insightful discussions. Prof. Ch. Ma is thanked for the helpful suggestions and comments. We also thank B. Walter for assistance with apatite separation and M. Mangler for discussions about the TXRF method. The China Scholarship Council (CSC) is thanked for granting scholarship (2010641006) to the first author. H. Teiber is supported by the Deutsche Forschungsgemeinschaft (grant MA 2563/3-1), which is gratefully acknowledged. We appreciate the detailed reviews of A. Chakhmouradian and T. Hammouda as well as the editorial handling of R. Gieré.

References

Armstrong, J.T. (1991): Quantitative elemental analysis of individual microparticles with electron beam instruments. *in* "Electron Probe Quantitation". K.F.J. Heinrich & D.E. Newbury ed., Plenum, New York, 261-315.

Bailey, D.K. (1993): Carbonate magmas. *J. Geol. Soc.*, **50**, 637-651.

Baranyi, I. (1977): Petrography and geochemistry of the subvolcanic breccias of the Kaiserstuhl volcano (SW-Germany). *Neues Jahrbuch für Mineralogie Abhandlungen*, **128**, 254-284.

Baranyi, I., Lippolt, H.J., Todt, W. (1976): K-Ar Altersbestimmungen an tertiären Vulkaniten des Oberrheingraben-Gebietes: II Die Alterstraverse vom Hegau nach Lothringen. *Oberrheinische Geologische Abhandlungen,* **25**, 41-62.

Bell, K. & Simonetti, A. (1996): Carbonatite magmatism and plume activity: implications from the Nd, Pb and Sr isotope systematics of Oldoinyo Lengai. *J. Petrol.*, **37(6)**, 1321-1339.

Bell, K., Kjarsgaard, B.A., Simonetti, A. (1999): Carbonatites – into the twenty-first century. *J. Petrol.*, **39**, 1839-1845.

Binder, G. & Troll, G. (1989): Coupled anion substitution in natural carbon-bearing apatites. *Contrib. Mineral. Petrol.*, **101**, 394-401.

Boyce, J.W. & Hervig, R. (2008): Magmatic degassing histories from apatite volatile stratigraphy. *Geology*, **36**, 63-66.

—, — (2009): Apatite as a monitor of late-stage magmatic processes at Volcán Irazú, Costa Rica. *Contrib. Mineral. Petrol.*, **157**, 135-145.

Brassinnes, S., Balaganskaya, E., Demaiffe, D. (2005): Magmatic evolution of the differentiated ultramafic, alkaline and carbonatite intrusion of Vuoriyarvi (Kola Peninsula, Russia). A LA-ICP-MS study of apatite. *Lithos*, **85**, 76-92.

Brenan, J. (1994): Kinetics of fluorine, chlorine and hydroxyl exchange in fluorapatite. *Chem. Geol.*, **110**, 195-210.

Broderick, C.A., Streck, M.J., Halter, W.E. (2007): Sulfur-rich apatites in silicic, calc-alkaline magmas: inherited or not? American Geophysical Union, Fall Meeting, abstract #V11B-0592.

Brooker, R.A. & Kjarsgaard, B.A. (2011): Silicate-Carbonate liquid immiscibility and phase relations in the system SiO_2-Na_2O-Al_2O_3-CaO-CO_2 at 0.1-2.5 GPa with application to carbonatite genesis. *J. Petrol.*, **52**, 1281-1305.

Brown, G.M. & Peckett, A. (1977): Fluorapatites from Skaergaard intrusion, East Greenland. *Mineral. Mag.*, **41**, 227-232.

Bühn, B., Wall, F., Le Bas, M.J. (2001): Rare-earth element systematic of carbonatitic fluorapatites, and their significance for carbonatite magma evolution. *Contrib. Mineral. Petrol.*, **141**, 572-591.

Chakhmouradian, A.R. & Zaitsev, A.N. (2004): Afrikanda: an association of ultramafic, alkaline and alkali-silica rich carbonatitic rocks from mantle-derived melts. *in* "Phoscorites and Carbonatites from Mantle to Mine: the Key Example of the Kola Alkaline Province", F.Wall & A.N. Zaitsev, ed., Mineralogical Society of Great Britain & Ireland, 247-291.

Chakhmouradian, A.R., Mumin, A.H., Demény, A., Elliott, B. (2008): Postorogenic carbonatites at Eden Lake, Trans-Hudson Orogen (northern Manitoba, Canada): Geological setting, mineralogy and geochemistry. *Lithos*, **103**, 503-526.

Chen, W. & Simonetti, A. (2013): In-situ determination of major and trace elements in calcite and apatite, and U-Pb ages of apatite from the Oka carbonatite complex: Insights into a complex crystallization history. *Chem. Geol.,* 353, 151-172. doi:10.1016/j.chemgeo.2012.04.02.

Chu, M.F., Wang, K.L., Griffin, W.L., Chung, S.L., O'Reilly, S.Y., Pearson, N.J., Iizuka, Y. (2009): Apatite composition: tracing petrogenetic processes in Transhimalayan granitoids. *J. Petrol.,* **50**, 1829-1855.

Crozaz, G. & Zinner, E. (1985): Ion probe determinations of the rare earth concentrations of individual meteoritic phosphate grains. *Earth. Planet. Sci. Lett.,* **73(1)**, 41-52.

Dalton, J.A. & Presnall, D.C. (1998): The continuum of primary carbonatitic-kimberlitic melt compositions in quilibrium with lherzolite: Data from the system CaO-MgO-Al_2O_3-SiO_2-CO_2 at 6 GPa. *J. Petrol.,* **39**, 1953-1964.

Dempster, T.J., Jolivet, M., Tubrett, M.N., Braithwaite, C.J.R. (2003): Magmatic zoning in apatite: a monitor of porosity and permeability change in granites. *Contrib. Mineral. Petrol.,* **145**, 568-577.

Eby, G.N. (1975): Abundance and distribution of the rare-earth elements and yttrium in the rocks and minerals of the Oka carbonatite complex. *Geochim. Cosmochim. Acta,* **39**, 597-620.

Engvik, A.K., Golla-Schindler, U., Berndt, J., Austrheim, H., Putnis, A. (2009): Intragranular replacement of chlorapatite by hydroxy-fluor-apatite during metasomatism. *Lithos*, **112**, 236-246.

Freestone, I.C. & Hamilton, D.L. (1980): The role of liquid immiscibility in the genesis of carbonatites - An experimental study. *Contrib. Mineral. Petrol.,* **73**, 105-117.

García-Heras, M., Fernandez-Ruiz, R., Tornero, J. D. (1997): Analysis of archaeological ceramics by TXRF and contrasted with NAA. *J. Archaeol. Sci.,* **24**, 10003-11014.

Ghosh, S., Ohtani, E., Litasov, K.D., Terasaki, H. (2009): Solidus of carbonated peridotite from 10 to 20 GPa and origin of magnesiocarbonatite melt in the Earth's deep mantle. *Chem. Geol.,* **262**, 17-28.

Gittins, J. (1989): The origin and evolution of carbonatite magmas. *in* "Carbonatites: Genesis and Evolution", K. Bell ed., Unwin Hyman, London, 580-600.

Gittins, J. & Harmer, R.E. (2003): Myth and reality in the carbonatite–silicate rock "association". *Period. Mineral.,* **72**, 19-26.

Goldoff, B., Webster, J. D., Harlov, D. E. (2012): Characterization of fluor-chlorapatites by electron probe microanalysis with a focus on time-dependent intensity variation of halogens. *Am. Mineral.*, **97(7),** 1103-1115.

Götze, J., Schertl, H.P., Neuser, R.D., Kempe, U., Hanchar, J.M. (2013): Optical microscope-cathodoluminescence (OM-CL) imaging as a powerful tool to reveal internal textures of minerals. *Miner. Petrol.*, **107**, 373-392.

Halama, R., Vennemann, T., Siebel, W., Markl, G. (2005): The Grønnedal-Ika carbonatite-syenite complex, south Greenland: carbonatite formation by liquid immiscibility. *J. Petrol.*, **46**, 191-217.

Hammouda, T., Chantel, J., Devidal, J.L. (2010): Apatite solubility in carbonatitic liquids and trace element partitioning between apatite and carbonatite at high pressure. G*eochim. Cosmochim. Acta*, **74**, 7220-7235.

Harlov, D. E., Förster, H. J., Nijland, T. G. (2002): Fluid-induced nucleation of (Y+ REE)-phosphate minerals within apatite: nature and experiment. Part I. Chlorapatite. *Am. Mineral.*, **87(2-3)**, 245-261.

Harlov, D. E., Wirth, R., Förster, H. J. (2005): An experimental study of dissolution–reprecipitation in fluorapatite: fluid infiltration and the formation of monazite. *Contrib. Mineral. Petrol.*, **150(3)**, 268-286.

Hogarth, D.D. (1989): Pyrochlore, apatite and amphibole: distinctive minerals in carbonatite. *in* "Carbonatites: Genesis and Evolution", K. Bell ed., Unwin Hyman, London, 105-148.

Hubberten, H.W., Katz-Lehnert, K., Keller, J. (1988): Carbon and oxygen isotope investigations in carbonatites and related rocks from the Kaiserstuhl, Germany. *Chem. Geol.*, **70**, 257-274.

Imai, A., Listanco, E.L., Fujii, T. (1993): Petrologic and sulfur isotopic significance of highly oxidized and sulfur-rich magma of Mt. Pinatubo, Philippines. *Geology*, **21(8)**, 699-702.

Jochum, K.P. & Stoll, B. (2008): Reference materials for elemental and isotopic analyses by LA-(MC)-ICP-MS: successes and outstanding needs. *in* "Laser Ablation ICP-MS in the Earth Sciences: Current Practices and Outstanding Issues", P. Sylvester, ed., Mineralogical Association of Canada, **29**, 147-168.

Jochum, K.P., Stoll, B., Herwig, K., Willbold, M., Hofmann, A.W., Amini, M., Vannucci, R. (2006): MPI-DING reference glasses for in situ microanalysis: New reference values for element concentrations and isotope ratios. *Geochem. Geophys. Geosys.*, **7**. doi: 10.1029/2005GC001060.

Jolliff, B.L., Papike, J.J., Shearer, C.K., Shimizu, N. (1989): Inter-and intra-crystal REE variations in apatite from the Bob Ingersoll pegmatite, Black Hills, South Dakota. *Geochim. Cosmochim. Acta*, **53(2)**, 429-441.

Katz, K. & Keller, J. (1981): Comb-layering in carbonatite dykes. *Nature*, **294**, 350-352.

Keller, J. (1981): Carbonatitic volcanism in the Kaiserstuhl alkaline complex: Evidence for highly fluid carbonatitic melts at the earth's surface. *J. Volcanol. Geotherm. Res.*, **9**,423-431.

— (1984): Der jungtertiäre Vulkanismus Südwestdeutschlands: Exkursionen im Kaiserstuhl und Hegau. *Fortschr. Mineral.*, **62**, Bh. 2, 2-35.
— (1991): Petrogenetic carbonatite-melilitite relationships in the Kaiserstuhl complex, Upper Rhinegraben. 5th international Kimberlite Conference Araxa, Brasil. Extended Abstracts, 217-218.

— (1997): Bergalite-Okaite-Turjaite: The carbonatite-melilitite connection. Geol.Ass./Mineral. Ass. Annual Meeting Ottawa. Abstracts, A77.

— (2001): ESF EUROCARB Kaiserstuhl Carbonatite Workshop, Breisach 6.-8.4 Excursion Guide: 29 p.

— (2008): Tertiary Rhinegraben volcanism: Kaiserstuhl and Hegau. 9th International Kimberlite Conference in Frankfurt /Main, Germany. August 2008. Field Trip Guide,38 p.

Keller, J., Brey, G., Lorenz, V., Sachs, P. (1990): IAVCEI 1990 Pre-conference Excursion 2A: Volcanism and Petrology of the Upper Rhinegraben (Urach-Hegau-Kaiserstuhl). 1-60.

Keller, J., Kraml, M., Henjes-Kunst, F. (2002): $^{40}Ar/^{39}Ar$ single crystal laser dating of early volcanism in the Upper Rhine Graben and tectonic implications. *Schweiz. Mineral. Petrogr. Mitt.*, **82**, 121-130.

Klemme, S. & Dalpé, C. (2003): Trace-element partitioning between apatite and carbonatite melt. *Am. Mineral.*, **88**, 639-646.

Koberski, U. & Keller, J. (1995): Cathodoluminescence observations of natrocarbonatites and related peralkaline nephelinites at Oldoinyo Lengai. *Carbonatite Volcanism*, **4**, 87-99.

Koster van Groos, A.F. & Wyllie, P.J. (1966): Liquid immiscibility in the system Na_2O-Al_2O_3-SiO_2-CO_2 at pressures to 1 kilobar. *Am. J. Sci.*, **264**, 234-255.

Kraml, M., Keller, J., Henjes-Kunst, F. (1995): New K/Ar, $^{40}Ar/^{39}Ar$ step-heating and $^{40}Ar/^{39}Ar$ laser fusion dates for the Kaiserstuhl volcanic complex (Upper Rhine Graben; Germany). *Eur. J. Mineral.*, **7**, 142.

Kraml, M., Pik, R., Rahn, M., Selbekk, R., Carignan, J., Keller, J. (2006): A new multi-mineral age reference material for $^{40}Ar/^{39}Ar$, (U-Th)/He and Fission Track dating methods: The Limberg t3 tuff. *Geostand. Geoanal. Res.*, **30**, 73-86.

Lee, W.J. & Wyllie, P.J. (1994): Experimental data bearing on liquid immiscibility, crystal fractionation, and the origin of calciocarbonatites and natrocarbonatites. *Int. Geol. Rev.*, **36**, 797-819.

Liferovich, R.P. & Mitchell, R.H. (2006): Apatite-group minerals from nepheline syenite, Pilansberg alkaline complex, South Africa. *Mineral. Mag.*, **70(5)**, 463-484.

Lippolt, H.J., Gentner, W., Wimmenauer, W. (1963): Altersbestimmungen nach der Kalium-Argon Methode an tertiären Eruptivgesteinen Südwestdeutschlands. *Jahreshefte des Geologischen Landesamts Baden-Württemberg*, **6**, 507-538.

Mariano, A.N. (1988): Some further geological applications of cathodoluminescence. *in* "Cathodoluminescence of Geological Materials" D.J. Marshall, ed., Unwin Hyman, London, 94-123.

Marks, A.W.M., Wenzel, T., Whitehouse, M.J., Loose, M., Zack, T., Barth, M., Worgard, L., Krasz, V., Eby, G.N., Stosnach, H., Markl, G. (2012): The volatile inventory (F, Cl, Br, S, C) of magmatic apatite: an integrated analytical approach. *Chem. Geol.,* **291**, 241-255.

Martin, L.H.J., Schmidt, M.W., Mattson, H.B., Guenther, D. (2013): Element partitioning between immiscible carbonatite and silicate melts for dry and H_2O-bearing systems at 1-3 GPa. *J. Petrol.*, **54**, 2301-2338.

Misra, N. L. & Singh Mudher, K. D. (2002): Total reflection X-ray fluorescence: a technique for trace element analysis in materials. *Progress in crystal growth and characterization of materials*, **45(1)**, 65-74.

Mitchell, R.H., Xiong, J., Mariano, A.N., Fleet, M.E. (1997): Rare-earth element-activated cathodoluminescence in apatite. *Can. Mineral.,* **35**, 979-998.

Moore, K.R., Wall, F., Divaev, F.K., Savatenkov, V.M. (2009): Mingling of carbonate and silicate magmas under turbulent flow conditions: Evidence from rock textures and mineral chemistry in sub-volcanic dykes, Chagatai, Uzbekistan. *Lithos*, **110 (1)**, 65-82.

O'Reilly, S. & Griffin, W.L. (2000): Apatite in the mantle: implication for metasomatic processes and high heat production in Phanerozoic mantle. *Lithos*, **53**, 217-232.

Pan, Y. & Fleet, M.E. (2002): Compositions of the apatite-group minerals: Substitution mechanisms and controlling factors. *Rev. Mineral. Geochem.,* **48(1)**, 13-49.

Parat, F., Holtz, F., Streck, M.J. (2011): Sulfur-bearing magmatic accessory minerals. *Rev. Mineral. Geochem.,* **73(1)**, 285-314.

Patiño Douce, A.E., Roden, M.F., Chaumba, J., Fleisher, C., Yogodzinski, G. (2011): Compositional variability of terrestrial mantle apatites, thermodynamic modeling of apatite volatile contents, and the halogen and water budgets of planetary mantles. *Chem. Geol.*, **288**, 14-31.

Peng, G., Luhr, J.F., McGee, J.J. (1997): Factors controlling sulfur concentrations in volcanic apatite. *Am. Mineral.,* **82**, 1210-1224.

Piccoli, P.M. & Candela, P.A. (2002): Apatite in Igneous Systems. *Rev. Mineral. Geochem.,* **48**, 255-292.

Prowatke, S. & Klemme, S. (2006): Trace element partitioning between apatite and silicate melt. *Geochim. Cosmochim. Acta,* **70**, 4513-4527.

Putnis, A. (2002): Mineral replacement reactions: from macroscopic observations to microscopic mechanisms. *Mineral. Mag.,* **66(5)**, 689-708.

Rendón-Angeles, J.C., Yanagisawa, K., Ishizawa, N., Oishi, S. (2000): Topotaxial conversion of chlorapatite and hydroxyapatite to fluorapatite by hydrothermal ion exchange. *Chem. Mater.*, **12(8)**, 2143-2150.

Riley, T.R., Bailey, D.K., Harmer, R.E., Liebsch, H., Lloyd, F.E., Palmer, M.R. (1999): Isotopic and geochemical investigation of a carbonatite-syenite-phonolite diatreme, West Eifel (Germany). *Mineral. Mag.*, **63 (5)**, 615-631.

Rønsbo, J.G. (2008): Apatite in the Ilímaussaq alkaline complex: Occurrence, zonation and compositional variation. *Lithos*, **106**, 71-82.

Sano, Y., Terada, K., Fukuoka, T. (2002): High mass resolution ion microprobe analysis of rare earth elements in silicate glass, apatite and zircon: lack of matrix dependency. *Chem. Geol.*, **184**, 217-230.

Schleicher, H., Keller, J., Kramm, U. (1990): Isotope studies on alkaline volcanics and carbonatites from the Kaiserstuhl, Federal Republic of Germany. *Lithos*, **26**, 21-35.

Seifert, W., Kämpf, H., Wasternack, J. (2000): Compositional variation in apatite, phlogopite and other accessory minerals of the ultramafic Delitzsch complex, Germany: implication for cooling history of carbonatites. *Lithos*, **53**, 81-100.

Sha, L.K. & Chappell, B.W. (1999): Apatite chemical composition, determined by electron microprobe and laser-ablation inductively coupled plasma mass spectrometry, as a probe into granite petrogenesis. *Geochim. Cosmochim. Acta*, **63**, 3861-3881.

Sigmund, J. (1996): Diatrembreccien, Mantelxenolithe und Karbonatite in der Kernbohrung KB2 im Kaiserstuhl. PhD thesis Universität Freiburg (unpublished).

Sommerauer, J. & Katz-Lehnert, K. (1985): A new partial substitution mechanism of CO_3^{2-} /$CO_3OH_3^-$ and SiO_4^{4-} for the PO_4^{3-} group in hydroxyapatite from the Kaiserstuhl alkaline complex (SW-Germany). *Contrib. Mineral. Petrol.*, **91**, 360-368.

Stormer Jr, J.C., Pierson, M.L., Tacker, R.C. (1993): Variation of F and Cl X-ray intensity due to anisotropic diffusion in apatite. *Am. Mineral.*, **78**, 641-648.

Streck, M.J. (2008): Mineral textures and zoning as evidence for open system processes. *Rev. Mineral. Geochem.*, **69**, 595-622.

Streck, M.J. & Dilles, J.H. (1998): Sulfur evolution of oxidized arc magmas as recorded in apatite from a porphyry copper batholiths. *Geology*, **26**, 523-526.

Sun, S.S. & McDonough, W.F. (1989): Chemical and isotopic systematic of oceanic basalt: implications for mantle composition and processes. *Geol. Soc. London, Special Publications*, **42**, 313-345.

Tepper, J.H. & Kuehner, S.M. (1999): Complex zoning in apatite from the Idaho Batholith: a record of magma mixing and intracrystalline trace element diffusion. *Am. Mineral.*, **84(4)**, 581-595.

Tribuzio, R., Tiepolo, M., Vannucci, R., Bottazzi, P. (1999): Trace element distribution within olivine-bearing gabbros from the Northern Apennine ophiolites (Italy): Evidence for post-cumulus crystallization in MOR-type gabbroic rocks. *Contrib. Mineral. Petrol.,* **134**, 123-133.

Wallace, M. & Green, D.H. (1988): An experimental determination of primary carbonatite magma composition. *Nature*, **355**, 343-346.

Watkinson, D.H. & Wyllie, P.J. (1971): Experimental study of the composition join $NaAlSiO_4$-$CaCO_3$-H_2O and the genesis of alkali rock-carbonatite complexes. *J. Petrol.,* **12**, 357-378.

Watson, E.B. (1980): Apatite and phosphorus in mantle source regions: An experimental study of apatite/melt equilibria at pressures to 25 kbar. *Earth. Planet. Sci. Lett.,* **51**, 322-335.

Waychunas, G.A. (2002): Grazing-incidence X-ray absorption and emission spectroscopy. *Rev. Mineral. Geochem.,* **49 (1)**, 267-315.

Wilson, M. & Downes, H. (1991): Tertiary-Quaternary extension-related alkaline magmatism in western and central Europe. *J. Petrol.,* **32**, 811-849.

—, — (2006): Tertiary-Quaternary intraplate magmatism in Europe and its relationship to mantle dynamics. *in* "European Lithosphere Dynamics" D.G. Gee, & R. Stephenson, ed., Geological Society of London, London, 147-166.

Wimmenauer, W. (2003): Kaiserstuhl. Geologische Karte von Baden-Württemberg 1:25.000 mit Erläuterungen. 280 p. Landesamt für Geologie etc. Baden-Württemberg (LGRB) Freiburg.

Woolley, A.R. (2003): Igneous silicate rocks associated with carbonatites: their diversity, relative abundances and implications for carbonatite genesis. *Period. Mineral.,* **72**, 9-17.

Woolley, A.R. & Kjarsgaard, B.A. (2008): Paragenetic types of carbonatites as indicated by the diversity and relative abundances of associated silicate rocks: Evidence from a global database. *Can. Mineral.,* **46**, 741-752.

Yanagisawa, K., Rendon-Angeles, J.C., Ishizawa, N., Oishi, S. (1999): Topotaxial replacement of chlorapatite by hydroxyapatite during hydrothermal ion exchange. *Am. Mineral.,* **84**, 1861-1869.

Zhang, C., Holtz, F., Ma, C., Wolff, P.E., Li, X. (2012): Tracing the evolution and distribution of F and Cl in plutonic systems from volatile-bearing minerals: a case study from the Liujiawa pluton (Dabie orogen, China). *Contrib. Mineral. Petrol.,* **164**, 859-879.

Zinner, E. & Crozaz, G. (1986): A method for the quantitative measurement of rare earth elements in the ion microprobe. *Int. J. Mass Spectrom. Ion Process.,* **69**, 17-38.

Figure Captions:

Fig. 1: Simplified geological map of the Rhine Graben district (a), and the Kaiserstuhl Volcanic Complex (b).

Fig. 2: Comparison of F and Cl contents in apatites from sample M2 before and after EMPA integrated Low intensity CL (LE CL, 10 nA; a & b) and external High intensity CL (HE CL, 12-15 mA; c & d).

Fig. 3: Cathodoluminescence and topographic images of apatites from the Kaiserstuhl Volcanic Complex. (a) Patchy zoning in apatite from essexite (Pulverbuck). (b) Core-rim zoning texture in apatite from phonolite dome M15. (c) Complex zoned apatite crystals from phonolite tuff M2. (d) Calcite inclusions and holes in apatite from sövite KB3. (e) Patchy zoned apatite from sövite at Badloch. (f) Overview of apatites from sövite KB3, showing populations with high and low CL brightness, respectively. (g) Apatites from bergalite, mostly consisting of core-mantle-rim zoned crystals. A few unzoned apatites are similar in CL brightness to the core of the zoned crystals. (h) Core-mantle-rim zoned apatite crystal from bergalite with relatively broad rim. (i) Three groups of breccia apatites: B.Ap = bright apatites; D.Ap = dark apatites; and a third group, partly replaced crystals (R.Ap). (j) Bright crystals from breccias contain micro-holes and calcite inclusions as found in sövite samples (Figs. 3d&f). (k) & (l) Partially replaced dark grains. The replacement occurs preferably around the rim and along cracks in the crystals. In several images (a, b, c, e, g, h, i and l) of this Figure, analysis spots are visible.

Fig. 4: Comparison of the chemical composition of carbonatitic apatites (C.Ap) and apatites from associated silicate rocks (S.Ap) based on EMPA (a - d) and SIMS (e & f) data, respectively. Sövite KB3 has a special orbicular texture in hand specimen (Keller et al., 1990). It is a somewhat exotic sample of the C.Ap group regarding its Si and REE contents (Figs. 6 & 8; Table 2) and is not shown here. d.l. = detection limit. Data below the detection limit are not shown. Chondrite-normalization after Sun and McDonough (1989).

Fig. 5: Chemical variations (EMPA data) between different zones in apatites from bergalite.

Fig. 6: Chemical variations (EMPA data) of different apatite populations from a diatreme breccia. B.Ap. apatites showing bright CL intensity; D.Ap, apatites showing dark CL intensity; R.Ap.sec, secondary bright replacement of the apatites; R.Ap.rel, relics of the replaced apatites.

Fig. 7: Correlations between REE (La + Ce) and S with Si contents of apatite samples from the Kaiserstuhl Volcanic Complex.

Fig. 8: CL characteristics and compositional variations of apatites from the KVC. The rims of the bergalite apatites and B.Ap and R.Ap.sec from breccias, show compositional similarities with C. Ap. In contrast, the cores of bergalite apatites and D.Ap and R.Ap.rel are similar to S.Ap..

Fig. 9: Calculated Sr contents of carbonatite and silicate melts based on their apatite compositions (EMPA results). Partition coefficients (D_{Sr}) between apatite and silicate melt are from Prowatke & Klemme (2006), those between apatite and carbonatite melt are from Hammouda et al. (2010). Whole rock data for silicate rocks are from Keller (unpublished), those for sövites from Keller et al. (1990). The parental melt in which the apatite core from bergalite formed is assumed to be of silicate composition, whereas the rim is thought to have crystallized from a carbonatitic melt.

Fig. 10: Triangular plot of the halogen and hydroxyl contents in apatite from the KVC. (a) C.Ap and S.Ap, (b) bergalite, (c) diatreme breccia.

Fig. 11: Volatile systematics of apatites from the KVC, illustrating the intermediate composition of apatites from the bergalite.

Fig. 1

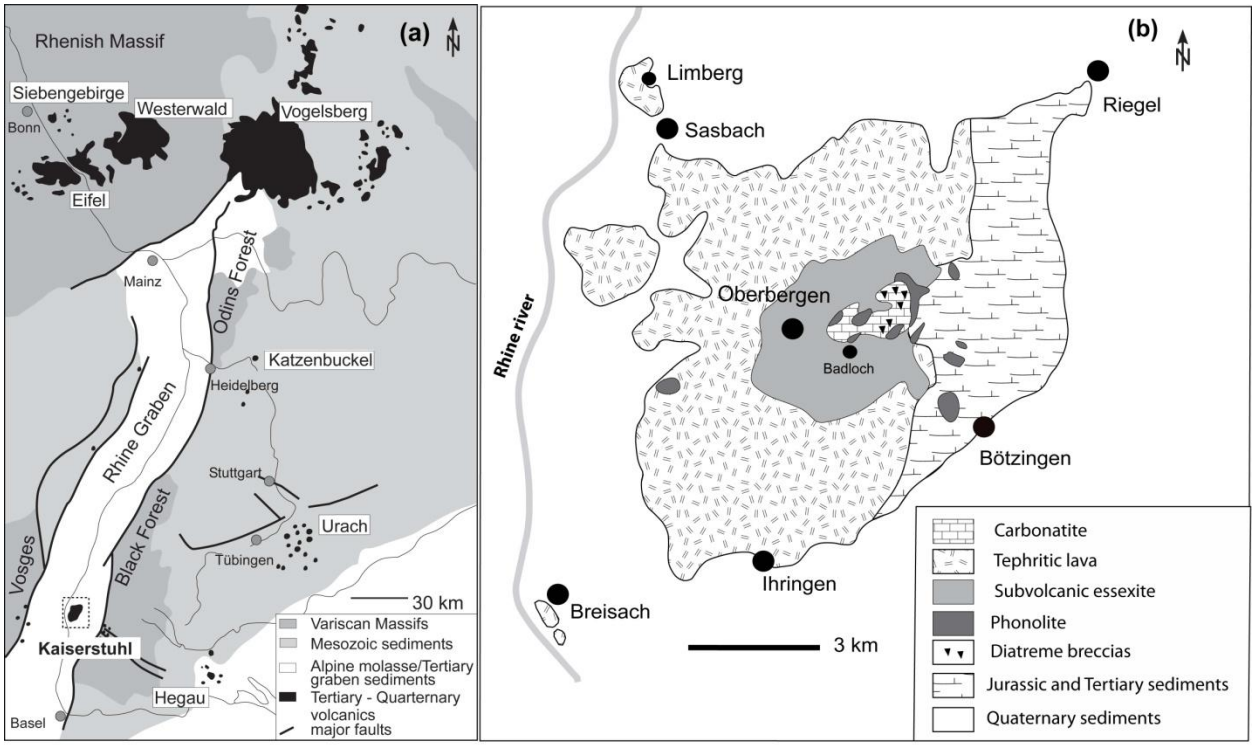
(a)
N
Rhenish Massif
Siebengebirge
Bonn
Westerwald
Vogelsberg
Eifel
Mainz
Odins Forest
Katzenbuckel
Heidelberg
Rhine Graben
Black Forest
Vosges
Stuttgart
Urach
Tübingen
Kaiserstuhl
Hegau
Basel
30 km
Variscan Massifs
Mesozoic sediments
Alpine molasse/Tertiary graben sediments
Tertiary - Quarternary volcanics
major faults
(b)
N
Limberg
Sasbach
Riegel
Oberbergen
Badloch
Rhine river
Bötzingen
Ihringen
Breisach
3 km
Carbonatite
Tephritic lava
Subvolcanic essexite
Phonolite
Diatreme breccias
Jurassic and Tertiary sediments
Quaternary sediments

Fig. 2

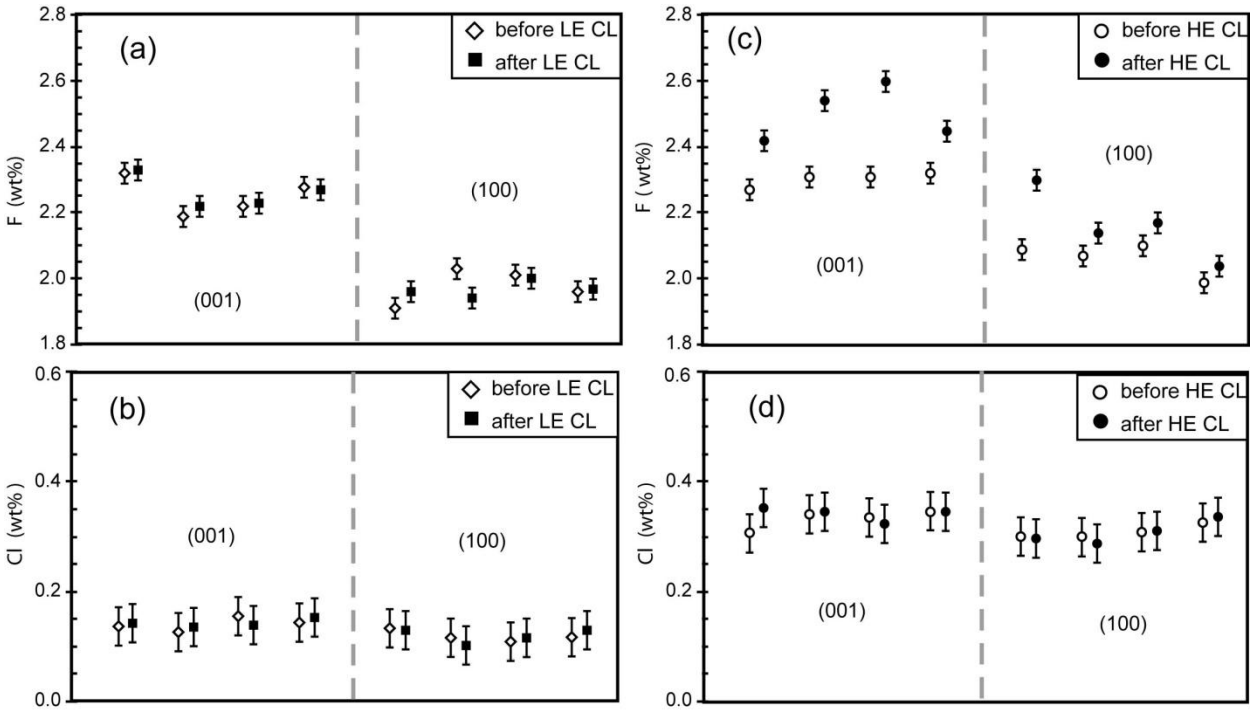
(a)
before LE CL
after LE CL
F (wt%)
(001)
(100)
(b)
Cl (wt%)
(c)
before HE CL
after HE CL
(d)

Fig. 3

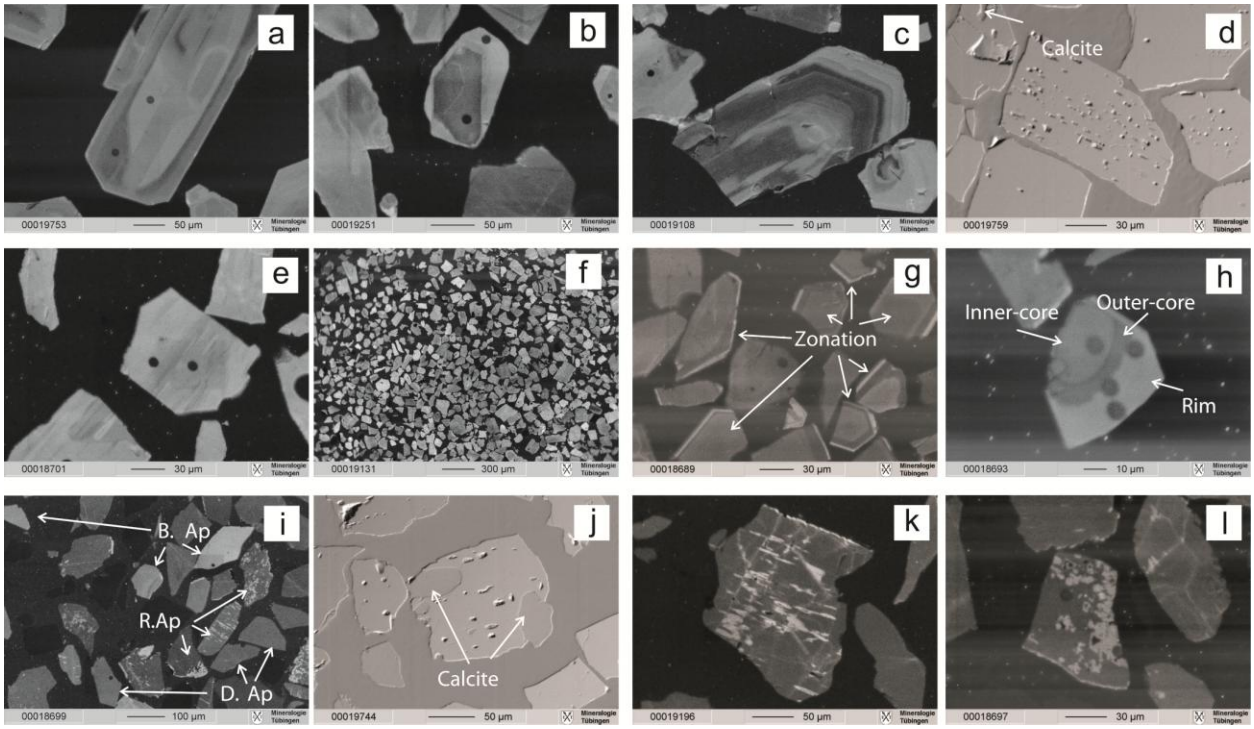
a
b
c
d
Calcite
e
f
g
Zonation
h
Inner-core
Outer-core
Rim
i
B. Ap
R.Ap
D. Ap
j
Calcite
k
l

Fig. 4

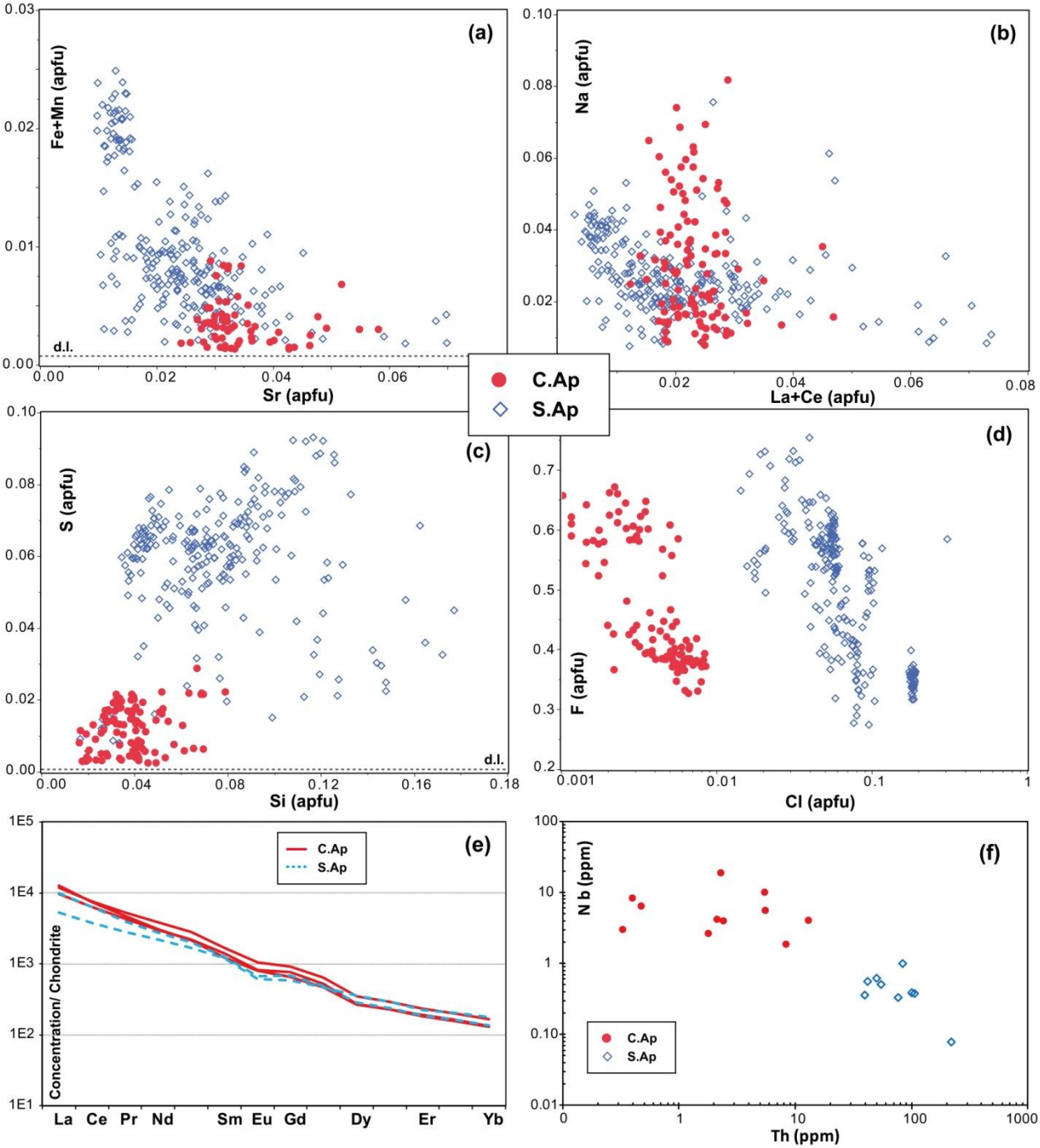
(a)
Fe+Mn (apfu)
Sr (apfu)
d.l.
(b)
Na (apfu)
La+Ce (apfu)
C.Ap
S.Ap
(c)
S (apfu)
Si (apfu)
d.l.
(d)
F (apfu)
Cl (apfu)
(e)
C.Ap
S.Ap
Concentration/ Chondrite
La Ce Pr Nd Sm Eu Gd Dy Er Yb
(f)
N b (ppm)
Th (ppm)
C.Ap
S.Ap

Fig. 5

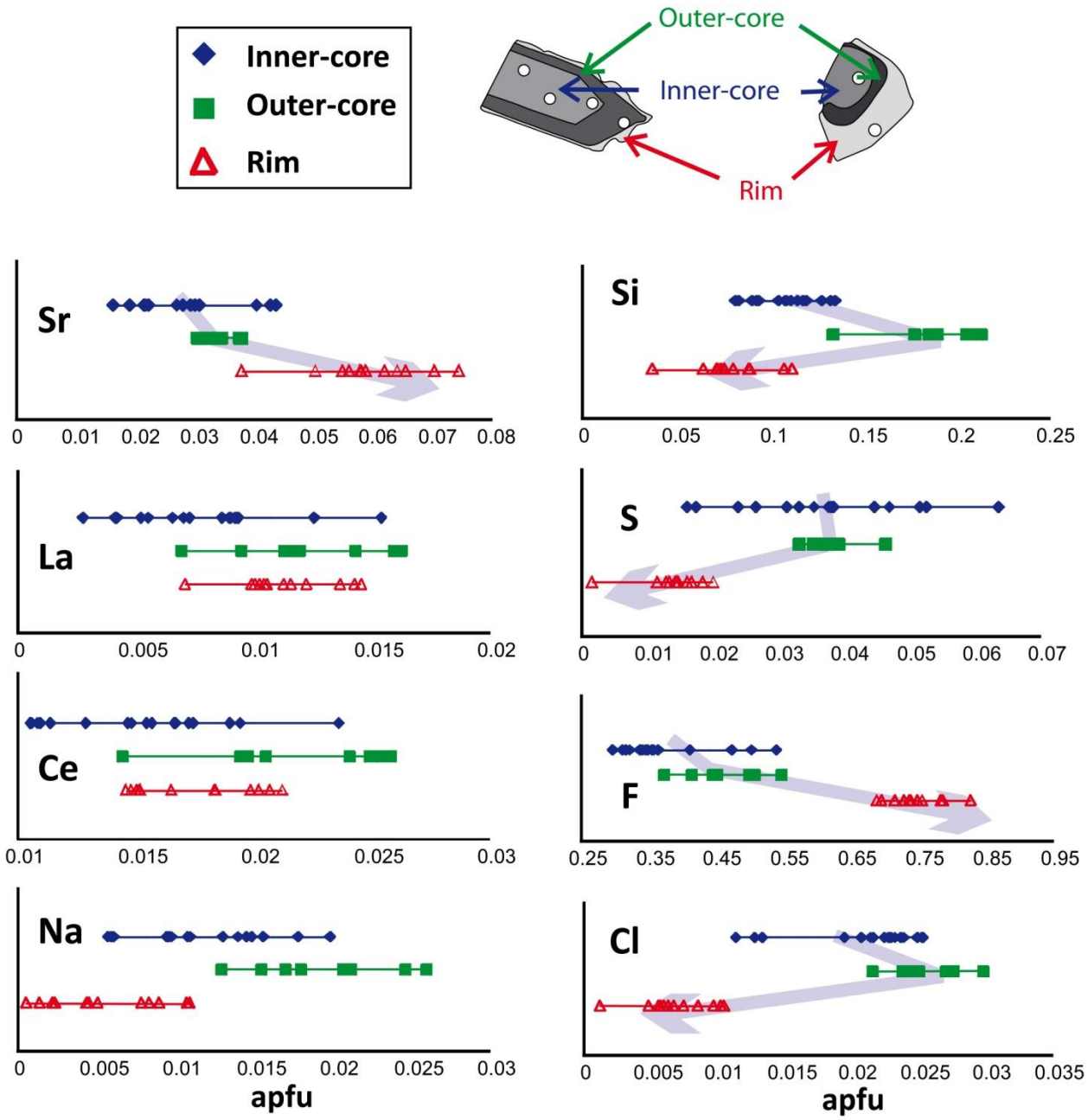
Inner-core
Outer-core
Rim
Outer-core
Inner-core
Rim
Sr
0 0.01 0.02 0.03 0.04 0.05 0.06 0.07 0.08
Si
0 0.05 0.1 0.15 0.2 0.25
La
0 0.005 0.01 0.015 0.02
S
0 0.01 0.02 0.03 0.04 0.05 0.06 0.07
Ce
0.01 0.015 0.02 0.025 0.03
F
0.25 0.35 0.45 0.55 0.65 0.75 0.85 0.95
Na
0 0.005 0.01 0.015 0.02 0.025 0.03
apfu
Cl
0 0.005 0.01 0.015 0.02 0.025 0.03 0.035
apfu

Fig. 6

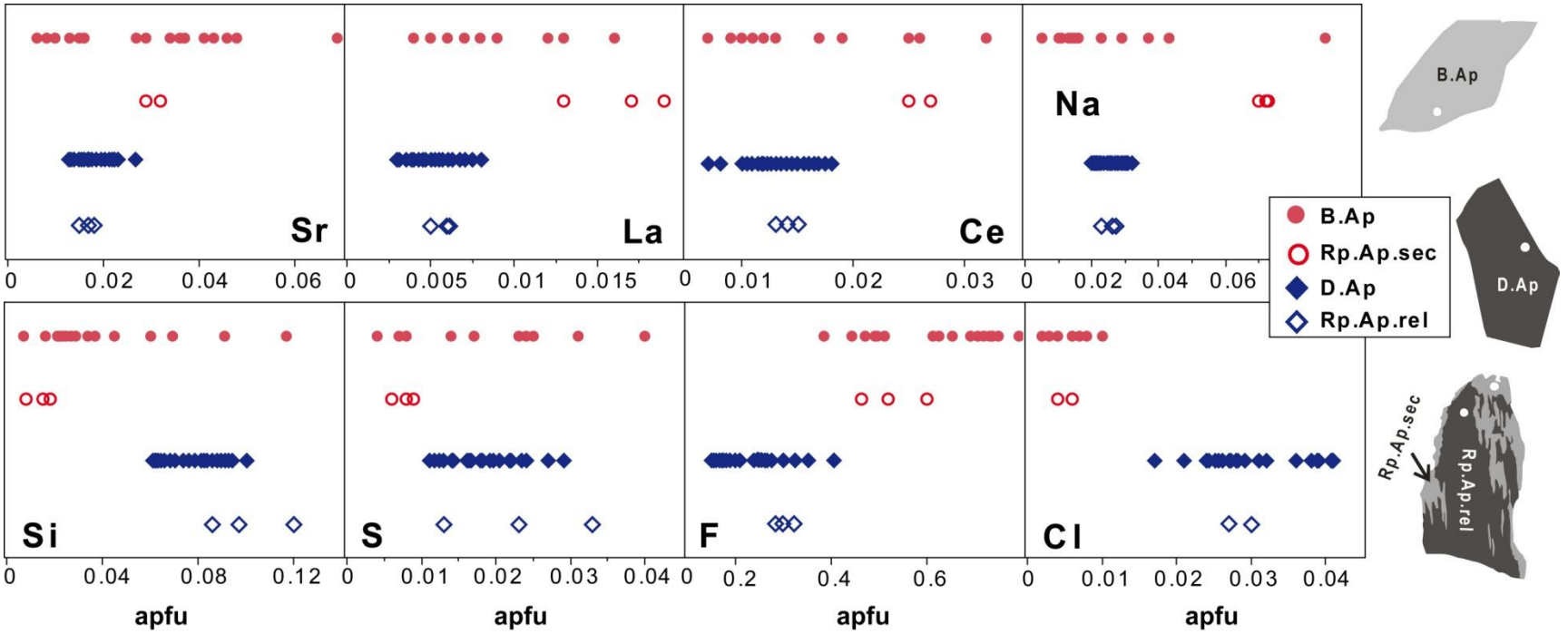
Sr
La
Ce
Na
Si
S
F
Cl
0 0.02 0.04 0.06
0 0.005 0.01 0.015
0 0.01 0.02 0.03
0 0.02 0.04 0.06
0 0.04 0.08 0.12
0 0.01 0.02 0.03 0.04
0 0.2 0.4 0.6
0 0.01 0.02 0.03 0.04
apfu
apfu
apfu
apfu
B.Ap
Rp.Ap.sec
D.Ap
Rp.Ap.rel
B.Ap
D.Ap
Rp.Ap.sec
Rp.Ap.rel

Fig. 7

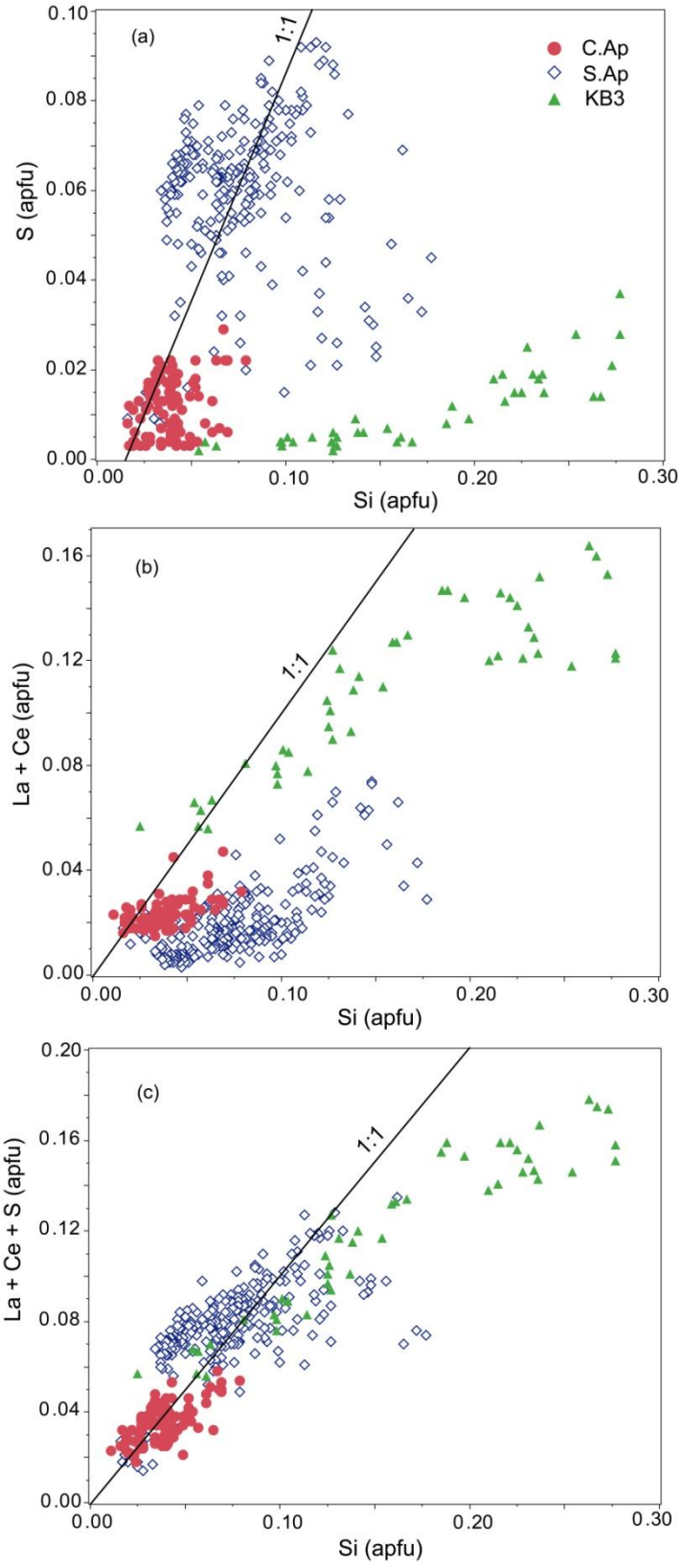
(a)
1:1
C.Ap
S.Ap
KB3
S (apfu)
Si (apfu)
0.00
0.02
0.04
0.06
0.08
0.10
0.00
0.10
0.20
0.30
(b)
1:1
La + Ce (apfu)
Si (apfu)
0.00
0.04
0.08
0.12
0.16
0.00
0.10
0.20
0.30
(c)
1:1
La + Ce + S (apfu)
Si (apfu)
0.00
0.04
0.08
0.12
0.16
0.20
0.00
0.10
0.20
0.30

Fig. 8

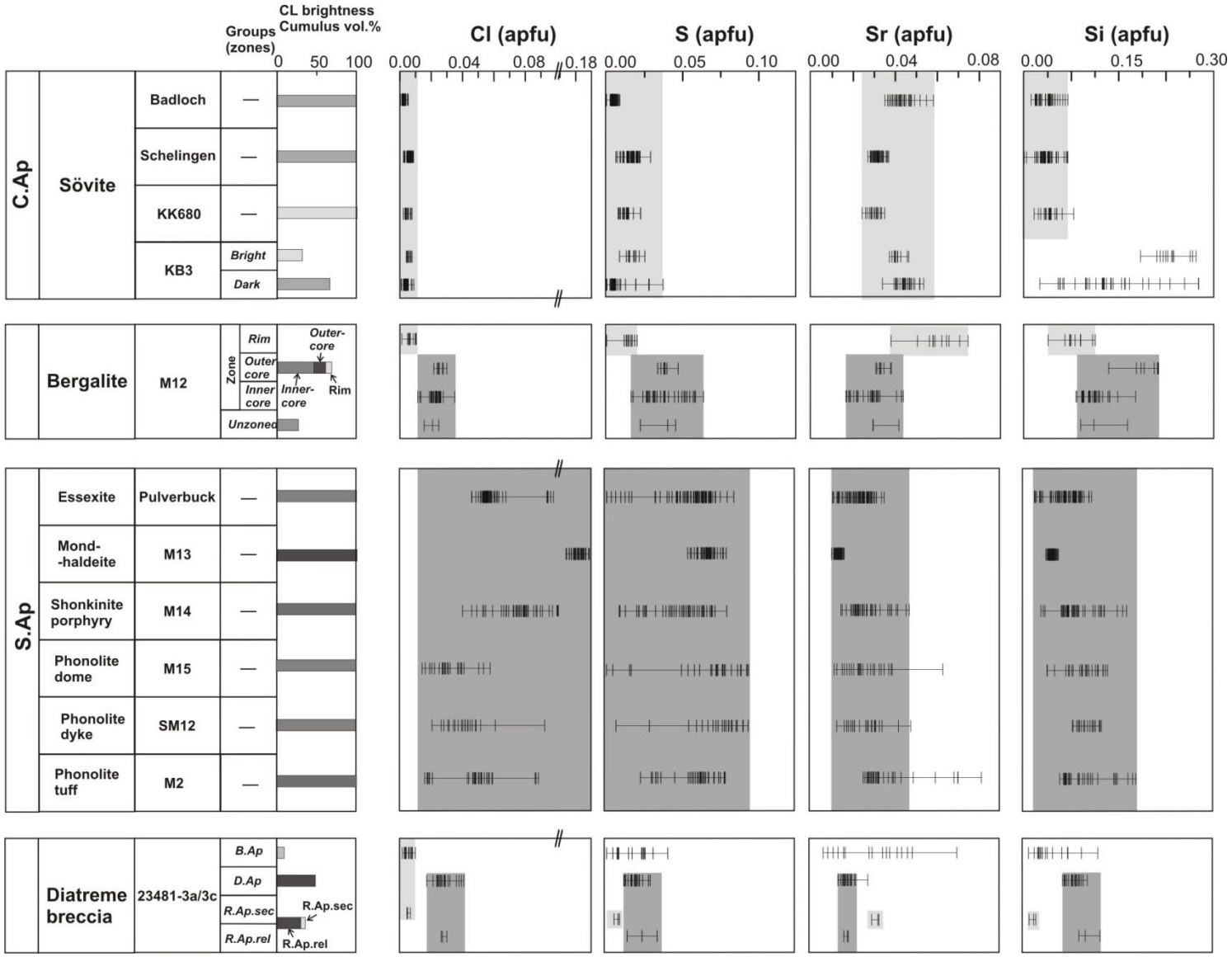
Groups (zones)
CL brightness Cumulus vol.%
0
50
100
Cl (apfu)
0.00
0.04
0.08
0.18
S (apfu)
0.00
0.05
0.10
Sr (apfu)
0.00
0.04
0.08
Si (apfu)
0.00
0.15
0.30
C.Ap
Sövite
Badloch
Schelingen
KK680
KB3
Bright
Dark
Bergalite
M12
Zone
Rim
Outer core
Inner core
Unzoned
Outer-core
Inner-core
Rim
S.Ap
Essexite
Pulverbuck
Mond--haldeite
M13
Shonkinite porphyry
M14
Phonolite dome
M15
Phonolite dyke
SM12
Phonolite tuff
M2
Diatreme breccia
23481-3a/3c
B.Ap
D.Ap
R.Ap.sec
R.Ap.rel

Fig. 9

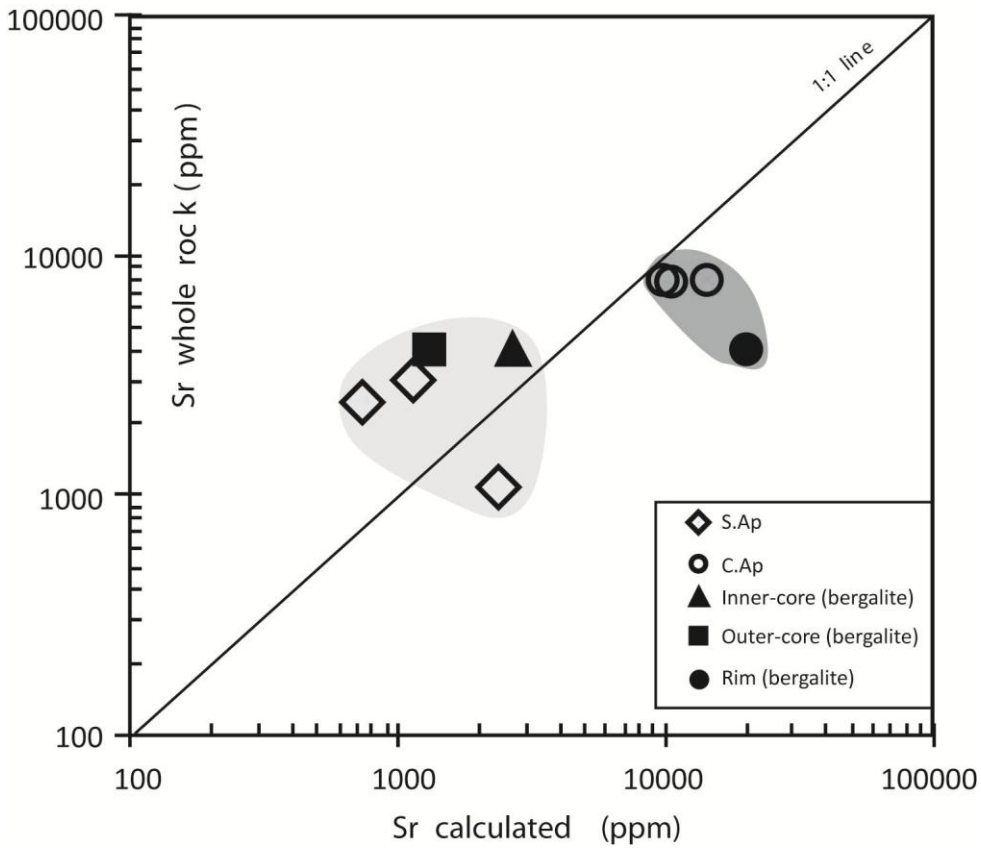
100000
10000
1000
100
Sr whole roc k (ppm)
1:1 line
S.Ap
C.Ap
Inner-core (bergalite)
Outer-core (bergalite)
Rim (bergalite)
100
1000
10000
100000
Sr calculated (ppm)

Fig. 10

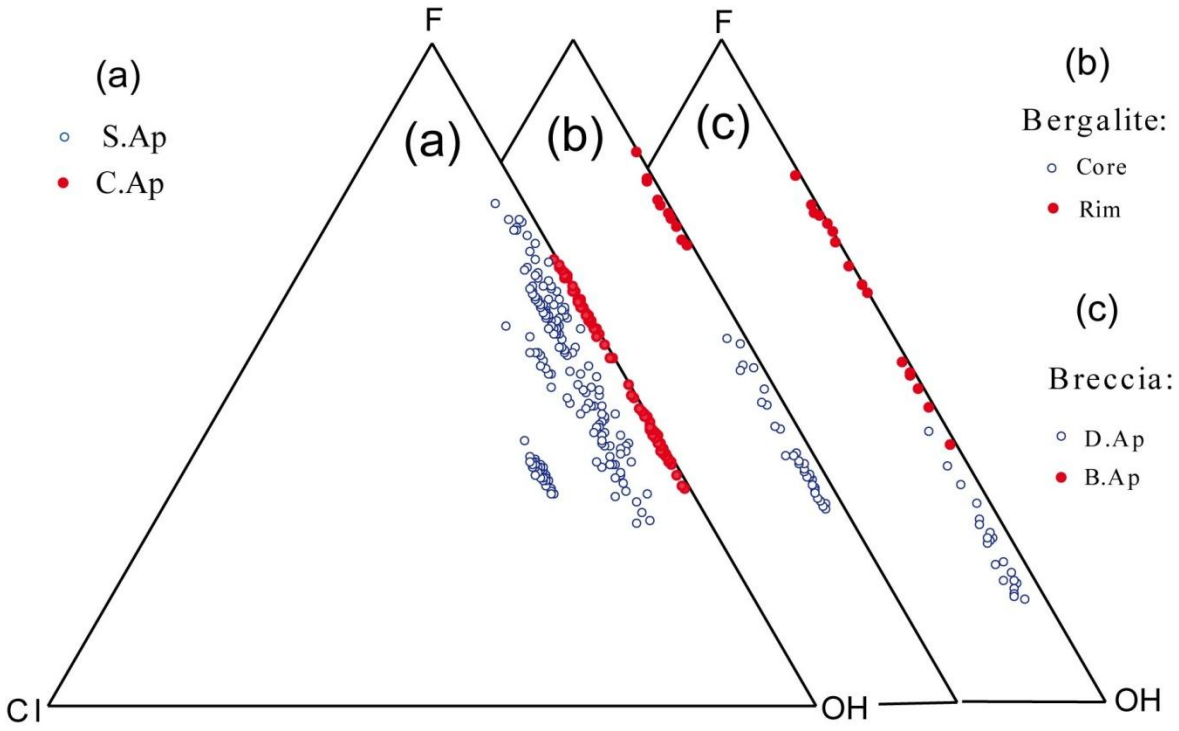

Fig. 11

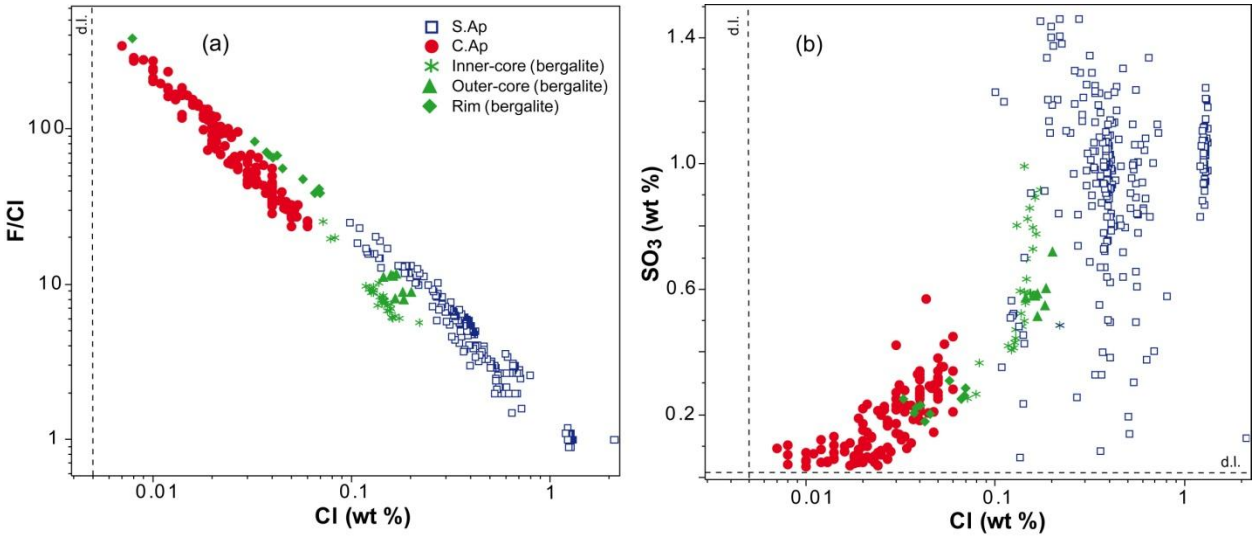
(a)
S.Ap
C.Ap
Inner-core (bergalite)
Outer-core (bergalite)
Rim (bergalite)
d.l.
F/Cl
100
10
1
0.01
0.1
1
Cl (wt %)
(b)
d.l.
SO3 (wt %)
1.4
1.0
0.6
0.2
0.01
0.1
1
Cl (wt %)

Table 1: (a) Investigated apatite samples of this study and (b) abbreviations for the various apatite types. All samples were analyzed by EPMA, some samples were additionally analyzed by SIMS (in italics) and by TXRF (in bold)

(a)	Rock type	Sample	Locality
C.Ap	Sövite	*Badloch*	Badberg
	Sövite	*KK680*	Orberg
	Sövite	***Schelingen***	Schelingen
	Sövite	**KB3**	Badberg
S.Ap	Essexite	***Pulverbuck***	Pulverbuck
	Mondhaldeite	**M13**	Ihringen
	Shonkinite porphyry	**M14**	Horberig
	Phonolite dome	***M15***	Bötzingen
	Phonolite dyke	**SM 12**	Bötzingen
	Phonolite tuff	**M2**	Limberg
	Bergalite	**M12**	Bötzingen
	Diatreme Breccia	23481-3a/3c	Vogtsburg

(b)	Illustration of the abbreviations
C.Ap	apatite from sövitic carbonatites
S.Ap	apatite from alkaline silicate rocks
D.Ap	lower CL brightness apatites from diatreme breccia
B.Ap	higher CL brightness apatites from diatreme breccia
R.Ap	replaced apatites from diatreme breccia
R.Ap.rel	relict part of the R.Ap
R.Ap.sec	secondary replaced areas of the R.Ap

Table 2: Average EMPA data (wt%) for apatites from different rocks of the Kaiserstuhl Volcanic Complex.

	C.Ap					Apatites from Bergalite			
	Badloch	KK680	Schelingen	KB3		M12			
	___	___	___	*L.B.CL*	*H.B.CL*	*I.Core*	*O.Core*	*Rim*	*Unzone*
	n=39	n=20	n=50	n=12	n=16	n=30	n=8	n=11	n=3
SiO_2	0.43(16)	0.49(16)	0.43(16)	2.66(28)	1.07(40)	1.29(23)	2.22(29)	0.95(23)	1.42(36)
La_2O_3	0.28(8)	0.29(8)	0.24(5)	1.65(18)	0.90(20)	0.25(10)	0.38(9)	0.36(7)	0.26(15)
Ce_2O_3	0.48(12)	0.53(14)	0.47(8)	2.75(29)	1.62(36)	0.47(12)	0.69(12)	0.55(8)	0.51(18)
FeO	0.05(2)	0.04(1)	0.06(2)	0.06(3)	0.06(3)	0.07(2)	0.09(4)	0.04(1)	0.05(2)
MnO	0.03(1)	0.03(1)	0.04(1)	b.d.l.	b.d.l.	0.03(1)	b.d.l.	0.02(1)	0.02(1)
CaO	54.05(44)	55.17(64)	54.12(38)	51.77(33)	53.04(76)	54.23(49)	53.8(35)	53.53(46)	54.12(53)
Na_2O	0.09(2)	0.17(5)	0.27(9)	0.10(2)	0.16(6)	0.08(4)	0.12(3)	0.05(1)	0.09(2)
SrO	0.88(10)	0.61(6)	0.64(5)	0.80(5)	0.94(7)	0.55(14)	0.68(5)	1.2(19)	0.68(11)
P_2O_5	40.59(48)	40.25(34)	40.31(62)	36.26(40)	39.47(68)	39.18(53)	37.02(49)	39.79(59)	39.04(62)
As_2O_5	b.d.l.	b.d.l.	b.d.l.	b.d.l.	b.d.l.	b.d.l.	b.d.l.	b.d.l.	b.d.l.
SO_3	0.08(3)	0.21(6)	0.26(7)	0.25(6)	0.07(2)	0.61(20)	0.59(6)	0.24(4)	0.56(16)
Cl	0.02(1)	0.03(1)	0.04(1)	0.04(1)	0.02(1)	0.15(3)	0.17(2)	0.05(2)	0.14(3)
F	2.24(13)	1.54(8)	1.47(17)	1.65(13)	2.49(15)	1.31(21)	1.71(20)	2.75(14)	1.33(13)
Total	99.22	99.36	98.35	97.99	99.84	98.22	97.46	99.52	98.22
Formula based on 8 oxygen atoms									
Ca	4.94	4.98	4.94	4.86	4.88	4.95	4.97	4.92	4.95
Sr	0.04	0.03	0.03	0.04	0.05	0.03	0.03	0.06	0.03
Fe	0.00	0.00	0.00	0.00	0.00	0.00	0.01	0.00	0.00
Mn	0.00	0.00	0.00	0.00	0.00	0.00	0.00	0.00	0.00
La	0.01	0.01	0.01	0.05	0.03	0.01	0.01	0.01	0.01
Ce	0.02	0.02	0.01	0.09	0.05	0.01	0.02	0.02	0.02
Na	0.02	0.03	0.04	0.02	0.03	0.01	0.02	0.01	0.02
Sum A	5.03	5.07	5.04	5.06	5.04	5.02	5.07	5.02	5.02
P	2.93	2.87	2.90	2.69	2.87	2.83	2.70	2.89	2.82
Si	0.04	0.04	0.04	0.23	0.09	0.11	0.19	0.08	0.12
As	0.00	0.00	0.00	0.00	0.00	0.00	0.00	0.00	0.00
S	0.00	0.01	0.02	0.02	0.00	0.04	0.04	0.02	0.04
Sum B	2.97	2.93	2.96	2.94	2.96	2.98	2.93	2.98	2.98
Cl	0.00	0.00	0.01	0.01	0.00	0.02	0.03	0.01	0.02
F	0.60	0.41	0.40	0.46	0.68	0.35	0.47	0.75	0.36
OH (cal.)	0.39	0.59	0.60	0.54	0.32	0.62	0.51	0.25	0.62

(to be continued)

b.d.l. = below detection limit. Formula calculations are based on a total of eight cations in the A and X sites. OH was calculated assuming stoichiometry, i.e. F+Cl+OH = 1 in the Z site. L.B.CL = Low brightness in CL image; H.B.CL = High brightness in CL image.

Table 2 Continued

	S.Ap						Apatites from Breccia			
	M13	M14	Pulverbuck	M15	SM12	M2	23481-3a/3c			
	___ n=44	___ n=43	___ n=75	___ n=26	___ n=21	___ n=33	*B.Ap* n=16	*D.Ap* n=21	*R.Ap.sec* n=3	*R.Ap.rep* n=3
SiO_2	0.52(6)	0.99(35)	0.77(26)	1.01(41)	1.13(30)	1.12(41)	0.51(34)	0.92(12)	0.16(5)	1.19(17)
La_2O_3	0.13(2)	0.30(20)	0.24(9)	0.28(18)	0.24(14)	0.31(19)	0.29(12)	0.18(4)	0.51(8)	0.19(1)
Ce_2O_3	0.19(4)	0.57(34)	0.46(13)	0.46(29)	0.46(23)	0.59(32)	0.51(23)	0.41(9)	0.82(4)	0.45(3)
FeO	0.23(3)	0.10(4)	0.08(3)	0.08(4)	0.07(3)	0.07(4)	0.07(5)	0.08(3)	0.06(3)	0.07(1)
MnO	0.06(2)	0.04(1)	0.04(1)	0.03(2)	0.04(1)	0.04(2)	0.04(1)	0.04(2)	0.03(2)	0.04(2)
CaO	54.57(38)	54.28(64)	54.49(43)	54.68(65)	54.93(43)	54.33(64)	54.55(79)	54.25(41)	53.27(66)	54.58(32)
Na_2O	0.24(2)	0.17(8)	0.14(5)	0.16(4)	0.15(5)	0.12(3)	0.15(13)	0.16(2)	0.43(1)	0.16(1)
SrO	0.26(3)	0.55(15)	0.45(12)	0.53(21)	0.54(17)	0.76(29)	0.61(34)	0.35(6)	0.62(4)	0.34(2)
P_2O_5	40.12(32)	39.23(85)	39.85(80)	39.07(99)	38.92(65)	39.25(76)	40.76(88)	39.57(46)	40.62(30)	39.33(47)
As_2O_5	b.d.l.	b.d.l.	b.d.l.	b.d.l.	b.d.l.	b.d.l.	b.d.l.	b.d.l.	b.d.l.	b.d.l.
SO_3	1.03(9)	0.74(29)	0.86(26)	1.06(37)	1.11(32)	0.91(25)	0.28(16)	0.29(7)	0.12(2)	0.36(13)
Cl	1.27(3)	0.56(26)	0.43(10)	0.24(12)	0.29(10)	0.32(13)	0.04(2)	0.20(4)	0.03(1)	0.19(1)
F	1.31(6)	1.48(25)	2.08(21)	2.29(38)	2.15(32)	2.08(10)	2.30(48)	0.87(25)	1.95(20)	1.12(6)
Total	99.93	99.01	99.89	99.89	100.03	99.90	100.11	97.32	98.62	98.02
Formula based on 8 oxygen atoms										
Ca	4.94	4.95	4.95	4.96	4.97	4.94	4.94	4.97	4.88	4.97
Sr	0.01	0.03	0.02	0.03	0.03	0.04	0.03	0.02	0.03	0.02
Fe	0.02	0.01	0.01	0.01	0.01	0.01	0.01	0.01	0.00	0.00
Mn	0.00	0.00	0.00	0.00	0.00	0.00	0.00	0.00	0.00	0.00
La	0.00	0.01	0.01	0.01	0.01	0.01	0.01	0.01	0.02	0.01
Ce	0.01	0.02	0.01	0.01	0.01	0.02	0.02	0.01	0.03	0.01
Na	0.04	0.03	0.02	0.03	0.02	0.02	0.02	0.03	0.07	0.03
Sum A	5.02	5.04	5.02	5.05	5.05	5.03	5.02	5.04	5.04	5.04
P	2.87	2.83	2.86	2.80	2.78	2.82	2.92	2.86	2.94	2.83
Si	0.04	0.08	0.06	0.09	0.10	0.10	0.04	0.08	0.01	0.10
As	0.00	0.00	0.00	0.00	0.00	0.00	0.00	0.00	0.00	0.00
S	0.07	0.05	0.05	0.07	0.07	0.06	0.02	0.02	0.01	0.02
Sum B	2.98	2.96	2.98	2.95	2.95	2.97	2.98	2.96	2.96	2.96
Cl	0.18	0.08	0.06	0.03	0.04	0.05	0.01	0.03	0.00	0.03
F	0.35	0.40	0.56	0.61	0.57	0.56	0.61	0.24	0.53	0.30
OH (cal.)	0.47	0.52	0.38	0.35	0.38	0.40	0.38	0.74	0.47	0.67

Table 3: Average SIMS data (ppm) for apatites from different rocks of the Kaiserstuhl Volcanic Complex.

	C.Ap						S.Ap			
	Schelingen (6)		KK680 (4)		Badloch (4)		Pulverbuck (5)		M15 (5)	
	mean	S.D.	mean	S.D.	mean	S.D.	mean	S.D.	mean	S.D.
Na	1514	592	1400	953	794	266	1027	91	856	239
Sr	6611	436	6567	237	9147	271	5463	684	5333	713
Y	292	70	339	17	310	24	343	84	372	220
Zr	4	2	6	3	3	1	10	2	10	5
Nb	5.2	3.7	9.1	6.6	5.0	0.7	0.4	0.1	0.6	0.3
Ba	86	86	104	55	77	3	48	6	41	16
La	2325	690	2809	226	2991	98	2343	805	1260	791
Ce	3858	1139	4692	341	4518	166	3858	1141	2338	1397
Pr	410	119	508	32	447	16	377	102	266	149
Nd	1425	382	1816	98	1434	54	1300	297	1027	538
Sm	214	54	261	14	188	9	195	35	183	68
Eu	48	12	60	3	46	3	39	7	35	18
Gd	157	38	189	8	135	10	141	30	122	44
Dy	69	17	89	7	68	5	73	16	90	46
Er	30	7	39	3	32	3	31	7	37	22
Yb	22	6	28	2	23	3	23	7	31	21
Th	0.4	0.3	2.9	1.4	5.1	4.8	75	25	79	74
U	b.d.l.	—	b.d.l.	—	b.d.l.	—	11	3	23	25

Table 4: TXRF data (ppm) for apatites from different rocks of the Kaiserstuhl Volcanic Complex.

				Sr	Br	La	Ce	Nd	Gd	Y	As
C.Ap	KB3	MIN	n=6	7062	b.d.l.	11642	19021	4951	129	431	23
		MAX		8976		14759	24227	6244	159	548	38
		MEAN		8102		13585	22256	5740	145	499	30
		1σ		634		1067	1799	443	9	42	6
	Schelingen	MIN	n=12	4253	b.d.l.	1625	3099	656	41	254	32
		MAX		6616		2651	5001	1228	65	348	47
		MEAN		5146		2022	3850	875	52	294	38
		1σ		633		270	487	162	7	27	5
Bergalite	M12	MIN	n=12	4939	1.1	1977	3465	876	56	362	b.d.l.
		MAX		6913	1.7	2576	4508	1305	92	467	
		MEAN		5739	1.4	2254	3953	1108	73	418	
		1σ		558	0.2	163	268	112	10	35	
S.AP	M13	MIN	n=12	2012	1.5	529	1135	487	11	190	b.d.l.
		MAX		2576	4.2	719	1652	629	11	250	
		MEAN		2319	2.5	635	1374	565	11	224	
		1σ		191	0.8	57	145	48	0	20	
	Pulverbuck	MIN	n=12	4070	1.1	2329	3821	1132	85	396	1
		MAX		5314	1.6	2933	4868	1425	122	522	4
		MEAN		4660	1.3	2590	4231	1295	101	453	2
		1σ		349	0.2	169	300	91	11	35	1
	M14	MIN	n=6	4079	0.7	1890	3825	1335	60	389	1
		MAX		5772	2.3	2523	5140	1866	106	561	2
		MEAN		4744	1.4	2169	4365	1532	84	462	2
		1σ		642	0.6	255	509	189	16	62	1
	M15	MIN	n=18	4586	0.7	1833	3333	1125	94	310	4
		MAX		6037	3.7	3451	6266	1862	119	424	10
		MEAN		5423	1.9	2766	4894	1504	109	369	7
		1σ		367	0.8	468	784	185	7	27	2
	SM12	MIN	n=6	4314	9.7	937	2811	1116	96	342	1
		MAX		5187	14.1	1448	4158	1473	115	411	3
		MEAN		4776	12.2	1212	3586	1313	104	376	2
		1σ		272	1.3	175	465	118	6	24	0
	M2	MIN	n=12	6233	0.8	2163	4947	1412	65	240	2
		MAX		9070	2.9	3858	6786	2115	101	370	9
		MEAN		7601	1.8	3139	5719	1711	85	295	5
		1σ		852	0.9	431	566	209	11	36	2

Appendix 3

Halogen partitioning between coexisting minerals from alkaline-peralkaline rocks: a case study of the Tamazeght Complex, Morocco

Authors

Lian-Xun Wang, Michael A.W. Marks, Thomas Wenzel, Gregor Markl

Status

Prepared for submission

Editor

-

Reviewer

-

Contributions of the candidate

Scientific ideas	50%
Data acquisition	100%
Analysis and interpretation	70%
Preparation of manuscript	70%

Halogen partitioning between coexisting minerals from alkaline-peralkaline rocks: a case study of the Tamazeght complex, Morocco

Lian-Xun Wang[a*] Michael A.W. Marks[a] Thomas Wenzel[a] Gregor Markl[a]

a = FB Geowissenschaften, Mathematisch-Naturwissenschaftliche Fakultät, Universität Tübingen, 72074 Tübingen, Germany

* = corresponding author. Tel: +49 (0) 7071-29 730 77. Fax: +49(0)7071-29 3060. Email: lian.x.wang@gmail.com;

Abstract: The partitioning of F and Cl between common halogen-bearing minerals (apatite, biotite, amphibole and titanite) from a large variety of alkaline-peralkaline rocks in Tamazeght complex, Morocco was investigated in detail. The partitioning coefficients, for example, of F in apatite-biotite pair, are expressed as

$$K_{D,F}^{Ap/Bt} = \left(\frac{X_F}{X_{OH}}\right)^{Ap} \Big/ \left(\frac{X_F}{X_{OH}}\right)^{Bt}$$

in the present study. Our data indicate $K_{D,F}^{Bt/Am}$, $K_{D,Cl}^{Bt/Am}$ and $K_{D,F}^{Ap/Ttn}$ values are fairly constant at 1.1, 0.3 and 99, respectively. However, the K_D values of F and Cl for other coexisting mineral pairs (e.g., $K_{D,F}^{Ap/Bt}$, $K_{D,Cl}^{Ap/Bt}$, $K_{D,F}^{Ap/Am}$, $K_{D,Cl}^{Ap/Am}$, $K_{D,F}^{Bt/Ttn}$ and $K_{D,F}^{Am/Ttn}$) are highly variable and controlled by the crystal chemistry of mineral, halogen contents and prevailing temperature of melt. The generally observed and preferred partitioning sequence for F is apatite ≫ biotite, amphibole, titanite, whereas for Cl it is apatite > amphibole > biotite. In addition to these common halogen-bearing minerals, sodalite, fluorite and eudialyte are further observed stable phases in some studied rock types. Based on our data, F contents in apatite, titanite, biotite and amphibole generally increase with the presence of fluorite. Conversely, with the presence of

sodalite and eudialyte, the Cl contents of these common halogen-bearing minerals obviously decrease. These observations are attributed to the extremely strong partitioning preference of Cl to sodalite and eudialyte with respect to others.

Keywords: Halogens; Partitioning; Coexisting minerals; Phase stability; Alkaline rocks; Tamazeght complex

1. Introduction

Halogens play essential roles in many geological processes, e.g., they assist metal transporting and depositing during mineralization, influence phase stabilities and solidus temperature during partial melting, and cause environment impact during degassing of eruptive volcanoes (see the recent reviews of Aiuppa et al., 2009; Pyle and Mather, 2009). As a result, they recently received considerable attention (e.g., Webster et al., 2009; Zhang et al., 2012; Kenderick et al. 2012; 2013; 2014; Giehl et al., 2014; Mangler et al., 2014; Marks et al., 2014; Teiber et al., 2014; Wang et al., 2014).

Halogens are significant constitutes in common hydrous minerals, such as amphibole, biotite, apatite and titanite, where they usually replace hydroxyl and oxygen. The F and Cl abundances in these minerals and their partitioning between mineral, melt, and fluid have been investigated in numerous studies (e.g., Munoz, 1984; Volfinger et al., 1985; Zhu and Sverjensky, 1992; Brenan, 1993; Edgar and Pizzolato, 1995; Icenhower and London, 1997; Mathez and Webster, 2005; Chevychelov et al., 2008; Webster, 2009). However, few works focus on F and Cl partitioning between coexisting minerals (e.g., apatite and biotite), and demonstrate that the partitioning coefficients of F and Cl between apatite and biotite depend on temperature, pressure and major element compositions of biotite (Ekström, 1972; Munoz, 1984; Zhu and Sverjensky, 1992). Halogen partitioning in other coexisting mineral pairs (e.g., apatite-amphibole, amphibole-biotite, and titanite-apatite/biotite/amphibole) have been even rarely studied (e.g., Ekström, 1972; Markl et al., 1998).

Alkaline-peralkaline melts have high solubilities of F and Cl (Carroll, 2005; Giehl et al., 2014), and in addition to the common halogen-bearing minerals mentioned above, they may crystallize

sodalite, eudialyte and fluorite upon cooling, potentially retaining halogens during crystallization (e.g., Giehl et al., 2014; Wang et al., 2014). The distribution of halogens in these minerals is much less known.

The Tamazeght complex is a well-studied alkaline-peralkaline complex, involving a large variety of alkaline silicate rocks from alkaline pyroxenite to syenite (e.g., Bouabdli et al., 1988; Kchit, 1990; Bernard-Griffiths et al., 1991; Salvi et al., 2000; Marks et al., 2008; 2009; Schilling et al., 2009; Bouabdellah et al., 2010). Apatite and titanite occur in all rock types, while biotite, amphibole, sodalite, fluorite and eudialyte are present in some units. This allows for a detailed investigation of halogen partitioning between coexisting minerals and their influencing factors.

The present study aims to determine halogen partitioning coefficients between coexisting minerals in alkaline to peralkaline rocks, and relate them to mineral chemistry, equilibrium temperature and other possible factors.

2. Geological background

The Tamazeght (also known as Tamazert) complex is located in the northern margin of the High Altlas Mountain Range of Morocco (**Fig. 1**). It intruded into Liassic to Cretaceous limestones within a Mesozoic graben-like structure that formed as a result of the continental collision between Africa and Europe and and the opening of Atlantic Ocean (Tisserant et al., 1976; Laville and Harmand, 1982). The Tamazeght complex is a multiphase plutonic to sub-volcanic complex with an outcrop area of around 70 km^2 and an intrusive depth of less than 3 km (Salvi et al., 2000). Chronology studies imply that the complex was emplaced between 44 to 35 Ma (Tisserant et al., 1976; Klein and Harmand, 1985; Marks et al., 2008; Wu et al., 2010).

The complex consists of a wide range of silica-undersaturated alkaline-peralkaline rocks and carbonatites as well as subsequent dyke swarms (**Fig. 1**). The alkaline rocks include ultramafic pyroxenite (also known as jacupirangite and in some places change to foidolite with abundant nepheline; Kchit, 1990), glimmerite, shonkinite, gabbro, monzonite, monzosyenite (or plagisyenite; Kchit, 1990), nepheline syenite and malignite. Based on petrography, mineral chemisty and petrology (Marks et al., 2008, 2009), these rocks are classified into several rock

groups, namely the ultramafic, shonkinitic, monzonitic and syenitic group (**Table 1**). Petrogenesis of these rocks are assumed as products of variable degrees of fractional crystallization by a common parental magma with nephelinitic or monchiquitic composition, which was originated by low-degree partial melting of a carbonated amphibole-Iherzolite mantle source (Bouabdli et al., 1988; Kchit, 1990). However, Marks et al., (2008; 2009) proposed that the large variety of lithologies in the Tamazeght complex results from successive melting of compositionally heterogeneous mantle source region followed by different amounts of fractional crystallization processes.

3. Sample description

For this study, 15 representative samples were chosen from major rock units in Tamazeght Complex (**Fig. 1**). The halogen-bearing mineral assemblages of these samples are given in **Table 1** and the geochemical and petrographic characteristics of these rocks are briefly summarized below. More details on the petrography and petrology of these rocks can be found in Marks et al. (2008, 2009) and Schilling et al. (2009).

Ultramafic rocks

Ultramafic rocks (pyroxenites and glimmerites) contain the lowest SiO_2 contents and the highest MgO contents and fall into the foidolite field of the TAS diagram (**Figs. 2a**). These rocks are free of feldspar and amphibole and are dominated by clinopyroxene and biotite, respectively, with variable amounts of garnet + Fe-Ti oxides + nepheline ± titanite/perovskite ±calcite ± olivine. The halogen-bearing minerals observed include various amounts of biotite, minor titanite and abundant apatite (**Table 1; Figs. 3a and b**). In these rocks apatites either coexist with titanite and/or biotite (**Fig. 3a**), or present as cumulus phase (**Fig. 3b**).

Shonkinitic rocks

Shonkinites generally fall into foid gabbro field of the TAS diagram (**Figs. 2a and b**). Petrographically, they are similar to pyroxenites, except for the presence of amphibole and alkali feldspar. The halogen-bearing minerals (apatite, amphibole, biotite and titanite) all reach

appreciable amounts and generally coexist with each other (**Table 1; Fig. 3c**) in these rocks.

Monzonitic rocks

The monzonitic unit consists of gabbros, monzonites and foid monzosyenites. Their SiO_2 and MgO contents are variable, partly overlapping with that of the shonkinites, but reaching relatively high SiO_2 and alkali alkali ($Na_2O + K_2O$) and low MgO contents (**Fig. 2**). These rocks are characterized by the presence of plagioclase and the absence of garnet, with variable amounts of clinopyroxene, Fe-Ti oxides, alkaline feldspar, nepheline, amphibole, biotite, titanite and apatite. Coexisting of halogen-bearing minerals is common in these rocks (**Figs. 3d and e**). In one sample (TMZ 157) sodalite also occurs (**Fig. 3f; Table 1**).

Syenitic rocks

The syenitic rocks include nepheline syenites, miaskitic malignites and agpaitic malignites. They are the most evolved rocks of the complex, showing very high alkali ($Na_2O + K_2O$) and low MgO contents (**Fig. 2**). These rocks are generally rich in alkaline feldspar and nepheline with variable amounts of clinopyroxene + titanite ± amphibole ± biotite and are further characterized by the presence of sodalite and fluorite (**Table 1; Figs. 3g-i**). Malignites are free of amphibole and biotite and contain only rare apatite and titanite, which generally occur as inclusions in clinopyroxene (**Fig. 3i**). Additional eudialyte is present in the agpaitic malignite (TMZ 238).

3. Analytical techniques

Electron Microprobe analyses (EMPA)

All mineral analyses were performed using a JEOL 8900 electron microprobe operated in wavelength-dispersive mode (WDS) at the Fachbereich Geowissenschaften, Universität Tübingen, Germany. For apatite analyses, we used an acceleration voltage of 15 kV, a beam current of 10 nA, and a defocused beam diameter of 10 μm. Using these conditions, we observed a constant count rate for F and Cl during peak counting time. Therefore diffusion of F and Cl potentially caused by long-time exposure under the electron beam (Stormer et al., 1993) is largely avoided using our condition. Also, we re-analyzed the Durango apatite periodically during each analytical session to assure consistence and quality of our data. For mica, amphibole

and titanite, an acceleration voltage of 15 kV, a beam current of 20 nA, and a defocused beam diameter of 2 μm was applied. Details on the WDS analyses configuration used (e.g., standard materials and counting time) are given in **Supplementary Table 1.** Processing of the raw data was carried out with the internal ϕρZ correction method of JEOL (Armstrong, 1991).

Total Reflection X-ray Fluorescence (TXRF)

The Br concentrations of halogen-bearing minerals have been determined using a S2 PICOFOX TXRF (Bruker AXS) at the Fachbereich Geowissenschaften, Universität Tübingen, Germany. Mineral purification was performed by magnetic and density separations followed by hand picking under ultraviolet (for sodalite) and natural light (for other minerals). Hand-picked minerals were then washed and dried to exclude any possible contaminations during separation. Subsequently, 2 to 5 mg mineral separates were powered and dispensed in 1 ml Triton (1 vol. %), with 10 μl of 10 mg/l Se solution added as internal standard. After homogenization, 10 μl aliquots of the suspension were immediately pipette onto quartz-glass discs and dried using a heating plate. The dried sample cakes were then analyzed for 1000 s (live time) using a Mo X-ray tube with an operating voltage of 50 kV and a beam current of 600 μA. Handling of the data was performed using Spectra program 6.2.0.0.(Bruker AXS Microanalysis GmbH) with K, Ca, P, Fe and Ti pile-up corrections. The detection limits and standard deviations for Br were 0.4 μg/g and around 0.2 μg/g, respectively.

4. Halogen results

Apatite

In all investigated samples, apatites are fluorapatite with X_F (= molar F/(F+Cl+OH)) > 0.5. The Cl contents vary from below detection limit (around 40 μg/g) to around 0.36 wt% (average value; **Table 2**). Within single apatite crystals no significant compositional zonation was observed and no systematic variations of F and Cl contents related to their textural position (along grain boundaries, or as inclusion in other halogen-bearing or –free minerals) were detected.

Halogen contents in apatite (**Table 2** and expressed as log (X_F/X_{OH}) and log (X_{Cl}/X_{OH}), respectively in **Fig. 4** and all following figures) show considerable variation among the various rock groups. Apatites from syenitic rocks contain the highest amounts of F (3.0-3.4 wt%, average values), whereas those from shonkinites are relatively F-poor (2.3-2.6 wt%). The F contents of apatites from ultramafic rocks show a relatively small variation in F (2.8 to 2.9 wt%), whereas those from monzonitic rocks are highly variable, with relatively lower F contents (2.5-2.7 wt%) in apatites from gabbro and higher F contents (2.7-3.2 wt%) in apatites from monzonites to monzosyenites.

The average Cl contents are lowest for apatite from syenitic rocks (mostly below detection limit of about 40 μg/g) and slightly higher in ultramafic (90-120 μg/g) and shonkinitic rocks (470-560 μg/g). The Cl contents of apatite from the monzonitic groups are highly variable with average values between 90 and 3650 μg/g (**Table 2; Fig. 4b**). A rough negative correlation between Cl and Sr contents of apatite from monzonitic rocks can be observed (**Fig. 5a**) but not between F and Sr contents (**Fig. 5b**).

Biotite and amphibole

Similar as for apatite, F contents in biotite are relatively high in ultramafic rocks (1.1-2.0 wt %), but low in shonkinitic rocks (partly below detection limit). Those from monzonitic rocks are intermediate and highly variable (0.2-1.8 wt % F) and the highest F contents are found in biotite from a syenitic rock (TMZ221; 2.6 wt %; **Table 2; Fig. 4c**). However, a syenitic sample (TMZ 165) contains very F-poor biotite (mostly below detection limit). The Cl contents in biotites are much lower than that of F and show a similar trend as for apatite (although less pronounced) with low Cl contents in biotites from ultramafic, shonkinitic and syenitic rocks (average contents of less than 140 μg/g) and variable and higher values in those from monzonitic (100-1500 μg/g) samples (**Table 2; Figs.4c and d**). The F contents in amphibole are similar to, but on average slightly lower than that of biotite from the same sample, whereas average Cl contents are always higher (**Table 2; Figs. 4c and d**). Within the monzonitic group, F contents of amphiboles are higher in samples, which do not contain additional biotite than in amphibole- and biotite-bearing samples. Similarly, the F content of biotite in the amphibole-free sample is higher than those containing additional amphibole. The average Br contents in biotites and amphiboles vary from

below detection limit (around 0.4 µg/g) to 2.1 µg/g with no clear differences between the two minerals and no correlations are observed in the Br variation in amphibole and biotite.

A positive correlation between Log (X_F/X_{OH}) and X_{Mg} (= molar Mg/(Mg+Fe+Mn+Ti+Al^{VI})) is observed in most investigated biotites of particular in the ultramafic rocks (**Fig. 5c**). This increase of Log (X_F/X_{OH}) with X_{Mg} in biotites from alkaline rocks is just opposite to the observation for biotites from calc-alkaline granitoids and diorites (Teiber et al., 2014). In contrast, no similar correlation was observed between Log (X_{Cl}/X_{OH}) and X_{Mg} in biotite and between Log (X_F/X_{OH}) and X_{Mg} in amphibole (**Figs. 5d and e**). According to Teiber et al. (2014) and Zhang et al. (2012), positive correlations between Log (X_{Cl}/X_{OH}) and X_{Mg} or Log (X_{Cl}/X_{OH}) and (Al^{IV}+Fe+K) are frequently developed in amphiboles from calc-alkaline granitoids and diorites, however, they are not observed in this work (e.g., **Fig. 5f**).

Titanite

In titanite, average F contents are lowest (0.03 wt %, average value) for an ultramafic sample (**Table 2**), increase via shonkinitic (0.18-0.34 wt %) and monzonitic rocks (0.25-0.41 wt %) and reach their highest values in titanites from syenitic rocks (0.46-0.75 wt %). This is a rather systematic as observed for apatite, biotite and amphibole except for the very low F contents found in titanite from the ultramafic samples (**Fig. 4**; **Table 2**).

A clear positive correlation exists between X_{Al}^{Ttn} and X_F^{Ttn} for ultramafic, shonkinitic and monzonitic rocks, but not for syenitic samples (**Fig. 6a**). In syenitic rocks, however, the F contents in titanite correlate with Fe^{3+} contents (**Fig. 6b**) and the combination of Al and Fe^{3+} show a good correlation with F for almost all titanites (**Fig. 6c**).

Sodalite and eudialyte

Sodalite from a monzosyenite is slightly higher in Cl contents (6.7 wt %) than that from syenitic rocks (6.1-6.4 wt %), in agreement with Cl systematics of apatite and amphibole from these rocks (**Table 2**). Sodalite from Sample TMZ 238 contains about 76 µg/g Br. Eudialyte from the same sample contains 1.2 wt % Cl and 6.6 µg/g Br.

5. Discussion

5.1. Partitioning of F and Cl between apatite, biotite, amphibole and titanite

Consistent with recent studies on halogen-bearing minerals from calc-alkaline plutonic rocks (e.g., Zhang et al., 2012; Teiber et al., 2014), our data from alkaline to peralkaline rocks show that F contents generally decrease from apatite, through biotite, to amphibole (**Table 2**) and in a given sample, F-rich apatite is normally associated with F-rich biotite and F-rich amphibole (**Figs. 4a and c**). However, one outliner (TMZ 165) shows relatively high F in apatite but relatively low F in biotite (**Fig. 4C**). The F content in titanite is significantly lower than that in apatite but undistinguishable with biotite and amphibole (**Table 2**) and in general F-rich titanite coexisted with F-rich apatite, biotite and amphibole except one ultramafic sample, TMZ 23(**Figs. 4a, c and e**).

The variation of Cl is more complex partly due to its low concentration in these minerals of this study (**Table 2**). In shonkinitic and monzonitic samples, the Cl content in apatite is generally higher than that in coexisting biotite and amphibole. However, it is not clear in ultramafic and syenitic samples (**Table 2**). But it is certain that the Cl content in amphibole is always higher than that in coexisting biotite (**Table 2; Fig. 4d**). In many but not all samples, Cl-rich apatite is normally associated with Cl-rich biotite and/or Cl-rich amphibole as well as relatively Cl-rich sodalite (**Table 2; Figs. 4b and d**).

These observations imply that for most of our samples equilibrium partitioning of F and Cl between the above-mentioned mineral phases can be assumed. Some outliners and inconsistent observations might indicate the influence factors (e.g., mineral crystal chemistry, temperature, melt composition, etc.) on the partitioning of F and Cl between coexisting minerals

Partitioning of F and Cl between apatite and biotite

Numerous experimental, theoretical and field-based studies reveal that the F and Cl concentrations in biotite are generally correlated with the Mg or Fe concentrations of biotite (usually depicted as X_{Mg} or X_{Fe}), as there are strong reciprocal effects between octahedral (Mg, Fe, Al^{VI}, etc.) and hydroxyl (OH, F, Cl) occupancy in biotite. This is the so-called “Fe-F and Mg-Cl avoidance rules” in biotite (Ekström, 1972; Munoz and Ludington, 1974; Munoz, 1984;

Volfinger et al., 1985; Zhu and Sverjensky, 1992; London, 1997; Icehower and London, 1997; Teiber et al., 2014). In this study, a positive linear correlation also exists between log $(X_F/X_{OH})^{Bt}$ and X_{Mg}^{Bt} except only few outliners (**Fig. 5c**), which is in good agreement with the "avoidance rules".

As stated by Zhu and Sverjensky (1992), the partitioning of F between apatite and biotite could be expressed using the Henderson-Kracek partitioning coefficient: $K_{D,F}^{Ap/Bt} = (\frac{X_F}{X_{OH}})^{Ap} / (\frac{X_F}{X_{OH}})^{Bt}$. Calculation of the $K_{D,F}^{Ap/Bt}$ values based on the data for coexisting apatite and biotite of this study shows large variations with ln $K_{D,F}^{Ap/Bt}$ ranging from 2 to 7 (concentrated in 2-5; **Fig. 7**). This confirms the strong favor of F to apatite with respect to biotite. Plots of ln $K_{D,F}^{Ap/Bt}$ against X_{Mg}^{Bt} shows a negative correlation (**Fig. 7a**), indicating that the partitioning coefficients of F between apatite and biotite are strongly buffered by the Mg concentrations of biotite. Coexisting with Mg-rich biotite, the partitioning preference of F to apatite becomes much less pronounced, however, no signs imply that such preference would disappear or even change opposite to biotite based on our data (**Fig. 7a**).

Using the apatite-biotite geothermeter by Zhu and Sverjensky (1992), the equilibrium temperatures for apatite-biotite pairs from various samples are estimated (**Table 3 and supplementary table**), assuming a pressure of 1 kbar (Marks et al., 2008). Based on these data, a negative correlation between ln $K_{D,F}^{Ap/Bt}$ and temperature is observed (**Fig. 7b**), indicating that equilibrium temperature of magma is also a critical factor for partitioning of F and Cl between apatite and biotite.

Recent experimental work revealed that the F and Cl contents in apatite or biotite are positively correlated with the F and Cl in melt (Chevychelov et al., 2008; Webster et al., 2009; Doherty et al., 2014). As a result, the F contents in apatite and biotite might directly reflect the enrichment of F in their host melt. Thereby, the negative correlation between ln $K_{D,F}^{Ap/Bt}$ and X_F^{Bt} and between ln $K_{D,F}^{Ap/Bt}$ and X_F^{Ap} (**Fig. 7c and supplementary figure**) might point to that the partitioning of F between apatite and biotite also depends on the F contents of melt.

Comparatively, the Cl data are more scattered (**Figs. 7d-f**). Calculation of the $K_{D,Cl}^{Ap/Bt}$ show that ln $K_{D,Cl}^{Ap/Bt}$ mainly vary from 1 to 4, that is, Cl is also preferentially partitioned into apatite with respect to biotite, but to a less extent than F. Negative correlations between ln $K_{D,Cl}^{Ap/Bt}$ and X_{Mg}^{Bt} and between ln $K_{D,Cl}^{Ap/Bt}$ and equilibration temperature are also present, but more broadly and much less pronounced than those found in F (**Figs. 7d-f**). The data are extremely scattered in the plots of ln $K_{D,Cl}^{Ap/Bt}$ vs. X_{Cl}^{Bt} and ln $K_{D,Cl}^{Ap/Bt}$ vs. X_{Cl}^{Ap}. Zhu and Sverjensky (1992) demonstrated that the partitioning preferences of Cl to apatite reduce with increasing T and X_{Fe}^{Bt}. Athough our data pointing to a similar tendency as Zhu and Sverjensky (1992) suggested, further investigations of Cl-rich samples are definitely needed. The strongly scattered Cl data could be partly attributed to its low concentration in the minerals of this study.

Partitioning of F and Cl between apatite and amphibole

Calculation of the partitioning coefficients of F and Cl between apatite and amphibole shows that ln $K_{D,F}^{Ap/Am}$ generally range from 3 to 5 and ln $K_{D,Cl}^{Ap/Am}$ range from 0 to 3 (**Fig. 8**). This indicates both F and Cl favor apatite with respect to amphibole. In contrast to apatite-biotite pair, no correlations between ln $K_{D,F}^{Ap/Am}$ and X_{Mg}^{Am} (**Fig. 8a**) and between ln $K_{D,Cl}^{Ap/Am}$ and X_{Mg}^{Am} were observed (**Figs. 8a and d**), despite the crystal chemical effects (or "avoidance rules") for biotite are also evident in amphibole and muscovite in some studies (Ekström, 1972; Volfinger et al., 1985; Morrison, 1991; Zhu and Sverjensky, 1992; Humphreys et al., 2009). This either reflects that the Mg concentrations in amphibole do not have any significant influences on the partitioning of F and Cl between apatite and amphibole in our case, or could be interpreted by the relatively concentrated X_{Mg}^{Am} (0.3-0.55 compared with the larger range of 0.3-0.8 for X_{Mg}^{Bt}) that resulted from the lack of Mg-rich amphibole in ultramafic rocks. However, similar to the observations in coexisting apatite-biotite pair, decreasing ln $K_{D}^{Ap/Am}$ for both F and Cl are found with increasing temperature and F and Cl concentrations in apatite and amphibole and the Cl data are much more scattered than the F data (**Figs. 8 and supplementary figure**). This indicates that temperature and melt composition are important factors for the partitioning of F and Cl between apatite and amphibole.

Partitioning of F and Cl between biotite and amphibole

Based on our data ln $K_{D,F}^{Bt/Am}$ values vary between -0.5 to 0.6 (average of 0.1; $K_{D,F}^{Bt/Am} = 1.1$) and ln $K_{D,Cl}^{Bt/Am}$ vary from -1.8 to -0.5 (average of -1.2; $K_{D,Cl}^{Bt/Am} = 0.3$). These data are quite similar to previous results, for example, Ekström (1972) found $K_{D,F}^{Bt/Am}$ in coexisting biotite-amphibole pairs from different iron ores vary from 1.2 to 2, with better correlations revealing lower value (1.2) and Markl et al. (1998) observed $K_{D,F}^{Bt/Am} \approx 0.89$ and $K_{D,Cl}^{Bt/Am} \approx 0.33$ in syenitic rocks. In contrast to apatite-biotite and apatite-amphibole pairs (see above), the partitioning of F and Cl between biotite and amphibole do not vary with X_{Mg}^{Bt}, X_{Mg}^{Am}, X_F^{Bt} and X_F^{Am} (**Fig. 9**), which is probably related to their relatively similar structures.

Partitioning of F between titanite and others

The F contents in titanites correlate with their Al and Fe contents (Fig. 6), for which the coupled substitution $(Al, Fe)^{3+} + F^- = Ti^{4+} + O^{2-}$ was proposed (e.g., Hollabaugh and Foit; 1984; Markl et al., 1999; Tropper et al., 2002; Seifert and Kramer, 2003). The partitioning coefficients of F between apatite and titanite (ln $K_{D,F}^{Ap/Ttn}$) vary from 3.9 to 5.5 (average of 4.6) and are independent from $X_{Al}^{Ttn} + X_{Fe}^{Ttn}$ and X_F^{Ttn} but slightly increase with increasing X_F^{Ap} (**Figs. 10a-c**). In contrast, ln $K_{D,F}^{Bt/Ttn}$ vary largely from -2.6 to 2.4 depending on $X_{Al}^{Ttn} + X_{Fe}^{Ttn}$ and X_F^{Bt} (**Figs. 10d-f**). Likewise, ln $K_{D,F}^{Am/Ttn}$ increase from -0.6 to 1.8 with increasing $X_{Al}^{Ttn} + X_{Fe}^{Ttn}$ and X_F^{Am} (**Figs. 10g-i**).

5.2. Stability of sodalite, eudialyte and fluorite

Stability of volatile-bearing minerals could be used to constrain the enrichment of volatile in the magma. The absent of amphibole and biotite in malignite might indicate the related magmas are relatively dry with low αH_2O. This could be further confirmed by the concentrative presences of sodalite in these rocks, because sodalite is only stable at low H_2O contents in alkaline rocks (Giehl et al., 2013). Besides low-water, to stabilize sodalite, high αNaCl are also needed in the magma (Stormer and Carmichael, 1971; Sharp et al., 1989; Giel et al., 2014) which suggests high Cl contents in the origin magma of sodalite-bearing syenitic rocks. However, it is surprising that in these rocks with the presence of Cl-rich sodalite, coexisted apatite, biotite and/or amphibole

are generally Cl-poor which might point to extremely strong partitioning preference of Cl to sodalite with respect to other common halogen-bearing minerals (Stormer and Carmichael, 1971). In contrast, with the presence of fluorite in the same rock group, the coexisted apatite, titanite, biotite and/or amphibole is relatively F-rich. This indicates high F contents in the syenitic magma, because experimental work show that the stability of fluorite requires high F contents in the melt (e.g., Scaillet and Macdonard, 2004; Dplejs and Baker, 2006; Giehl et al., 2014). Thermodynamic calculation by Stormer and Carmichael (1971) pointed out that sodalite would be replaced by fluorite and nepheline if the Cl fugacity is not high enough than F fugacity in the magma. As a result, the syenitic magma should be rich in both F and Cl to stabilize the mineral assemblage of sodalite + fluorite + apatite+ titanite ± biotite ± amphibole. This prediction could be further supported by the presence of eudialyte in agpaitic malignite which also requires sufficiently high Cl concentrations of the melt (Giehl et al., 2014).

5.3. Br concentrations and Cl/Br ratios

Recent studies imply that during high-temperature magmatic processes Br shows a very similar geochemical behavior as Cl and therefore Cl/Br ratios in mantle-derived rocks, glasses and melt inclusions show a relatively narrow range (Jambon et al., 1995; Balcone-Boissard et al., 2010; Kendrick et al., 2012, 2013a, 2013b; Mangler et al., 2014; Wang et al., 2014). However, Br data for rock-forming minerals are extremely scarce (Ionov et al., 1997; O'Reilly and Griffin, 2000; Kendrick, 2012; Marks et al., 2012; Teiber et al., 2014; Wang et al., 2014) which is essential to understand the further constitutes of halogens in rocks and the causes for fairly uniform Cl/Br ratios in rocks.

Our data for sodalite, eudialyte, biotite and amphibole indicate that similar to the bulk rock data, Br concentrations in minerals are roughly correlated with their overall Cl contents, as sodalite (> 6 wt %) contains the highest Br, followed by eudialyte (> 1 wt %), with biotite and amphibole (< 0.2 wt %) having much lower Br contents (**Table 2**). However, their Cl/Br ratios are highly variable and show a much larger range compared to that defined by the mantle-derived rocks, glasses and melt inclusions (**Fig. 11**).

Based on our data, Cl/Br ratios of the biotites and amphiboles are lower than that of apatites, sodalites and eudialytes (**Fig. 11**). It is therefore unclear to us why Cl/Br ratios for bulk halogens are fairly constant particularly in alkaline rocks where the halogen-bearing mineral abundances in alkaline rocks are highly variable (e.g., Wang et al., 2014). It is also surprising that in relatively Cl-rich biotites from monzonitic samples, the Br contents are generally below detection limit, whereas Mg-rich and Cl-poor biotites from ultramafic samples are relatively high in Br contents (1.5-2 μg/g; **Table 2**). We suggest that halogen-bearing minerals may fractionate Cl from Br to different extents and therefore great care has to be taken when interpreting Cl/Br ratios in minerals in terms of magma source and/or evolution. Obviously further work on this topic is needed.

5.4. Evaluation of F and Cl in alkaline melts

Given the F and Cl compositions of minerals (e.g., apatite, biotite and amphibole), People commonly quantitatively estimate halogen abundances of their host melts with known partitioning coefficients of F and Cl between minerals and melts, equilibration temperatures and pressures (Piccoli and Candela, 1994; Mathez and Webster, 2005; Webster et al., 2009; Zhang et al., 2012). In the following calculation, the pressure of the Tamazeght magmas is assumed to be constant at 1kbar (see above) and the equilibration temperatures (**Table 3**) are estimated based on apatite-biotite thermometer (see above, Zhu and Sverjensky, 1992). The partitioning coefficients between minerals and melts, however, are hard to choose, although there were a number of investigations on halogen partitioning in mineral-fluid-melt systems (e.g., Webster, 1990; Zhu and Sverjensky, 1992; London, 1997; Icenhower and London, 1997; Mathez and Webster, 2005; Sato et al., 2005; Webster et al., 2009). To our knowledge, rare of them focused on alkaline-peralkaline magma system and it is uncertain whether the partitioning coefficients for cal-alkaline magma systems suit those in alkaline magma systems. In the following we attempted to use the known partitioning coefficients of F and Cl between apatites and calc-alkaline melts from mafic to felsic, on one hand to investigate the halogen contents in Tamazeght magmas, on the other hand to evaluate the applicability of these parameters in alkaline magma system.

Appendix 3

Calculations from apatite are performed using following equations given by Mathez and Webster (2005; equations (1) and (2)), Webster (2009; equations (3) and (4)) and Zhang et al. (2012; equation (5)).

$$W_F^m = W_F^{Ap}/3.4 \quad (1)$$

$$W_{Cl}^m = W_{Cl}^{Ap}/0.8 \quad (2)$$

$$W_F^m = \left(X_F^{Ap} - 0.12\right)/3.02 \quad (3)$$

$$W_{Cl}^f = X_{Cl}^{Ap}/0.011 \quad (4)$$

$$W_{Cl}^m = W_{Cl}^f/(4.51 \times P^{2.16}) \quad (5)$$

where W_F^m and W_F^{Ap} are concentrations (wt. %) of F in melt and apatite, W_{Cl}^f; W_{Cl}^m and W_{Cl}^m are concentrations (wt. %) of F in fluid, melt and apatite, respectively; X_F^{Ap} and X_{Cl}^{Ap} are mole fraction of F and Cl in apatite, respectively, and *P* is pressure in $kbar$. The melt compositons utilized by Mathez and Webster in the experiments (2005; at 1.99-2.05 kbar and 1066-1150˚C) are mafic silicate melts, whereas those utilized by Webster (2009; at 2kbar and 900-924˚C) are rhyodacitic melts.

Calculation from biotite are based on the work by Icenhower and London (1997) and London (1997), where they experimentally determined that the F and Cl partitioning coefficients between biotite and rhyolitic melt (2 kbar and H_2O-saturated) are correlated with Mg#. For F, the $D_F^{Bt/Melt}$ value is a function of Mg#: $D_F^{Bt/Melt}$ = 10.08 × Mg# - 1.08. For Cl, we take the $D_{Cl}^{Bt/Melt}$ values which have $Mg\#^{Bt}$ similar to our samples, that is, $D_{Cl}^{Bt/Melt}$ = 1.53 when $Mg\#^{Bt}$ > 0.65, $D_{Cl}^{Bt/Melt}$ = 1.22 when $Mg\#^{Bt}$ = 0.5-0.65, and $D_{Cl}^{Bt/Melt}$ = 2.06 when $Mg\#^{Bt}$ = 0.3-0.5. Consequently, the equations can be written as

$$W_F^m = W_F^{Bt}/(10.08 \times Mg\# - 1.08) \quad (6)$$

$$W_{Cl}^m = W_{Cl}^{Bt}/D_{Cl}^{Bt/Melt} \quad (7)$$

Calculations of Cl in melt from amphibole are performed according to the Cl-OH partitioning results between amphibole and dacitic melt (Sato et al., 2005; at 2-3 kbar and 800-850°C). The relevant equation are expressed as

$$\log(Cl/OH)_{melt} = \log (Cl/OH)_{Amp} - 3.74 + 1.5 \times Mg\# + 0.0027 \times T \quad (8)$$

in which $(Cl/OH)_{melt}$ and $(Cl/OH)_{Amp}$ are molar ratios of Cl/OH in melt and amphiboles, respectively, Mg# is molar ratio of Mg/(Mg+Fe) and T is temperature in Kelvin. However, no experimental works are found concerning the partitioning of F between amphibole and melt.

Comparison of the modeling results (**Table 3)** show that the apatite modeling by Mathez and Webster (2005) give much higher F contents, largely deviated from other modeling results, which is similar to the observation by Zhang et al. (2012) and interpreted to be invalid. However, this model reveals similar range of Cl contents as the apatite modeling by Webster (2009). The biotite modeling results according to Icenhower and London (1997) show a large variation in both F and Cl, which is mainly related with the crystallization temperature. Many previous studies implied that for halogen modeling, apatite is the most reliable candidate since it is more resistant to sub-dolidus re-equilibration than biotite and amphibole (e.g., Zhang et al., 2012; Teiber et al., 2014). Therefore we suggest that the F and Cl concentrations in melt calculated based on the apatite modeling by Webster (2009) are more accurate among the above three models.

The calculated F and Cl in melts show that F increase from shonkinitic rocks (1600-2000 μg/g), through ultramafic rocks (2000-2100 μg/g) to syenitic rocks (2300-2600 μg/g) with a large variation in monzonitic rocks (1800-2400 μg/g). These calculated F data are consistent with the variation tendencies of F in apatite, biotite and amphibole and are within the variation range of bulk F contents in the alkaline rocks from Upper Rhine Graben and Lengai (Mangler et al., 2014; Wang et al., 2014). Accordingly, calculated Cl in melts also agrees with the classification of Cl in halogen-bearing minerals and calculated Cl in sodalite-absent melts generally fit with the bulk Cl contents in the alkaline rocks from Upper Rhine Graben (Wang et al., 2014). However, the Cl contents in sodalite-bearing samples are significantly lower than those from sodalite-bearing phonolitic rocks of the Kaiserstuhl, Germany (54 μg/g vs. 1200-7600 μg/g; Wang et al., 2014). As mentioned above, this is mainly due to the extremely strong partitioning preference of Cl to

sodalite. As a result, in sodalite-bearing rocks, one needs to take more care when using apatite, biotite or amphibole to model the Cl concentrations in melts.

6. Conclusion

The F and Cl contents in apatite, biotite, amphibole and titanite from various alkaline-per alkaline rocks in Tamazeght complex (Morocco) have be determined and the partitioning behaviors between coexisting mineral pairs have been investigated. Our data indicate that (1) in coexisting apatite-biotite pair, $ln\ K_{D,F}^{Ap/Bt}$ values vary between 1 and 7 and is negatively correlated with increasing X_{Mg}^{Bt}, temperature, X_F^{Ap} and X_F^{Bt}. Accordingly, $ln\ K_{D,Cl}^{Ap/Bt}$ vary from 1 to 4 and roughly depend on X_{Mg}^{Bt} and temperature. (2) In coexisting apatite-amphibole pair, $ln\ K_{D,F}^{Ap/Am}$increase from 3 to 5 with decreasing temperature, X_F^{Ap} and X_F^{Am}, whereas $ln\ K_{D,Cl}^{Ap/Am}$ vary from 0 to 3 mainly controlled by temperature and X_{Cl}^{Am}. (3) In coexisting biotite-amphibole pair, both $ln\ K_{D,F}^{Bt/Am}$ and $ln\ K_{D,Cl}^{Bt/Am}$ are much more constant with average values of 0.1 and -1.2, respectively. (4) In coexisting titanite-apatite/biotite/amphibole, $lnK_{D,F}^{Ap/Ttn}$ values are relatively constant at 4.6, whereas $lnK_{D,F}^{Bt/Ttn}$ and $lnK_{D,F}^{Am/Ttn}$ are more variable with -2.6 to 2.4 and -0.6 to 1.8, respectively. These variations are mainly buffered by the Al^{VI} and Fe^{3+} contents in titanite and the F contents in biotite or amphibole. In summary, we conclude that the partitioning of F and Cl between biotite and amphibole and the partitioning of F between apatite and titanite are relatively constant, whereas the partitioning of F and/or Cl in coexisting apatite-biotite, apatite-amphibole and titanite-biotite/amphibole pairs are largely varied and mainly controlled by crystal-chemistry, temperature and melt compositions at constant pressure.

The stability of sodalite, fluorite and eudialyte in syenitic rocks imply that the magma is rich in F and Cl but relatively poor in water. The mineral assemblages of Cl-rich sodalite and Cl-poor apatite, biotite and/or amphibole suggest that extremely strong partitioning preference of Cl to sodalite and eudialyte exist with respect to other minerals. The Br contents in biotite, amphibole, eudialyte and sodalite reveal that Br concentrations are also positively related with Cl

concentrations in minerals. However, the Cl/Br ratios in minerals are not constant as those observed in alkaline whole rocks.

Acknowledgement

Holger Teiber and Chao Zhang are acknowledged for the insightful discussions on data acquisition and on halogen modeling, respectively. Johannes Dzatkowski, Ralf Marquardt and Likai Hao are thanked for their help with the preparation of mineral separates. The China Scholarship Council (CSC) provided scholarship grants (2010641006) for the first author which is gratefully acknowledged. We are also highly grateful to the Deutsche Forschungsgemeinschaft (grant MA 2563/3-1), which financially funded the analytical work.

References

Aiuppa, A., Baker, D.R., Webster, J.D., 2009. Halogens in volcanic systems. Chemical Geology 263(1), 1-18.

Armstrong, J.T., 1991. Quantitative elemental analysis of individual microparticles with electron beam instruments. in "Electron probe quantitation", K.F.J. Heinrich & D.E. Newbury ed. Plenum, New York, 261-315.

Balcone- Boissard, H., Villemant, B., Boudon, G., 2010. Behavior of halogens during the degassing of felsic magmas. Geochemistry, Geophysics, Geosystems 11(9), DOI: 10.1029/2010GC003028.

Bernard-Griffiths, J., Fourcade, S., Dupuy, C., 1991. Isotopic study (Sr, Nd, O and C) of lamprophyres and associated dykes from Tamazert (Morroco): crustal contamination processes and source characteristics. Earth and Planetary Science Letters 103(1), 190-199.

Bouabdellah, M., Hoernle, K., Kchit, A., Duggen, S., Hauff, F., Klügel, A., Beaudoin, G., 2010. Petrogenesis of the Eocene Tamazert continental carbonatites (Central High Atlas, Morocco): implications for a common source for the Tamazert and Canary and Cape Verde Island carbonatites. Journal of Petrology 51(8), 1655-1686.

Bouabdli, A., Dupuy, C., Dostal, J., 1988. Geochemistry of Mesozoic alkaline lamprophyres and related rocks from the Tamazert massif, High Atlas (Morocco). Lithos 22(1), 43-58.

Brenan, J.M., 1993. Partitioning of fluorine and chlorine between apatite and aqueous fluids at high pressure and temperature: implications for the F and Cl content of high P-T fluids. Earth and Planetary Science Letters 117(1), 251-263.

Carroll, M.R., 2005. Chlorine solubility in evolved alkaline magmas. Reviews in Mineralogy and Geochemistry 13, 469-493.

Chevychelov, V.Y., Botcharnikov, R.E., Holtz, F., 2008. Experimental study of fluorine and chlorine contents in mica (biotite) and their partitioning between mica, phonolite melt, and fluid. Geochemistry International 46(11), 1081-1089.

Dolejš, D., Baker, D.R., 2006. Fluorite solubility in hydrous haplogranitic melts at 100 MPa. Chemical geology 225(1), 40-60.

Edgar, A.D., Charbonneau, H.E., 1991. Fluorine-bearing phases in lamproites. Mineralogy and Petrology 44(1-2), 125-149.

Edgar, A.D., Lloyd, F.E., Vukadinovic, D., 1994. The role of fluorine in the evolution of ultrapotassic magmas. Mineralogy and Petrology 51(2-4), 173-193.

Edgar, A.D., Pizzolato, L.A., Sheen, J., 1996. Fluorine in igneous rocks and minerals with emphasis on ultrapotassic mafic and ultramafic magmas and their mantle source regions. Mineralogical Magazine 60(399), 243-258.

Edgar, A.D., Pizzolato, L.A., 1995. An experimental study of partitioning of fluorine between K-richterite, apatite, phlogopite, and melt at 20 kbar. Contributions to Mineralogy and Petrology 121(3), 247-257.

Ekström, T.K., 1972. The distribution of fluorine among some coexisting minerals. Contributions to Mineralogy and Petrology 34(3), 192-200.

Giehl, C., Marks, M.A.W., Nowak, M., 2014. An experimental study on the influence of fluorine and chlorine on phase relations in peralkaline phonolitic melts. Contributions to Mineralogy and Petrology, 2014, 167(3): 1-21.

Giehl, C., Marks, M.A.W., Nowak, M., 2013. Phase relations and liquid lines of descent of an iron-rich peralkaline phonolitic melt: an experimental study. Contributions to Mineralogy and Petrology 165(2), 283-304.

Hollabaugh, C.L., Foit, F.F., 1984. The crystal structure of an Al-rich titanite from Grisons. Switzerland. American Mineralogist, 69, 725-732.

Humphreys, M.C.S., Edmonds, M., Christopher, T., Hards, V., 2009. Chlorine variations in the magma of Soufrière Hills Volcano, Montserrat: Insights from Cl in hornblende and melt inclusions. Geochimica et Cosmochimica Acta 73(19), 5693-5708.

Icenhower, J.P., London, D., 1997. Partitioning of fluorine and chlorine between biotite and granitic melt: experimental calibration at 200 MPa H_2O. Contributions to Mineralogy and Petrology 127(1-2), 17-29.

Ionov, D.A., Griffin, W.L., O'Reilly, S.Y., 1997. Volatile-bearing minerals and lithophile trace elements in the upper mantle. Chemical Geology 141(3), 153-184.

Jambon, A., Déruelle, B., Dreibus, G., Pineau, F., 1995. Chlorine and bromine abundance in MORB: the contrasting behaviour of the Mid-Atlantic Ridge and East Pacific Rise and implications for chlorine geodynamic cycle. Chemical Geology 126(2), 101-117.

Kchit, A., 1990. Le complexe plutonique alcalin du Tamazert, Haut-Atlas de Midelt (Maroc): pétrologie et structurologie. Toulouse 3.

Kendrick, M.A., Honda, M., Pettke, T., Scambelluri, T., Phillips, D., Giuliani, A., 2013. Subduction zone fluxes of halogens and noble gases in seafloor and forearc serpentinites. Earth and Planetary Science Letters 365, 86-96.

Kendrick, M.A., Jackson, M.G., Kent, A.J.R., Hauri, E.H., Wallace, P.J., Woodhead, J., 2014. Contrasting behaviours of CO_2, S, H_2O and halogens (F, Cl, Br, and I) in enriched-mantle melts from Pitcairn and Society seamounts. Chemical Geology 370, 69-81.

Kendrick, M.A., Kamenetsky, V.S., Phillips, D., Honda, M., 2012. Halogen systematics (Cl, Br, I) in mid-ocean ridge basalts: A Macquarie Island case study. Geochimica et Cosmochimica Acta ,81, 82-93.

Kendrick, M.A., Arculus, R., Burnard, P., Honda, M., 2013. Quantifying brine assimilation by submarine magmas: Examples from the Galápagos Spreading Centre and Lau Basin. Geochimica et Cosmochimica Acta 123, 150-165.

Klein, J.L., Harmand, C., 1985. Le volcanisme de la région de Zebzate; age relations avec le complex alcalin a carbonatites du Tamazert (Haut-Atlas de Midelt, Maroc). 110e Congrès National de la Société Sav., Montpellier, Sci., Fascicule VII, 147-152.

Laville, E., Harmand, C., 1982. Evolution magmatique et tectonique du bassin intracontinental mésozoique du Haut-Atlas (Maroc): un modèle de mise en place synsédimentaire de massifs “anorogeniques” liés a des dérochements. Bulletin de la Société Géologique de France 7, 221-227.

London, D., 1997. Estimating abundances of volatile and other mobile components in evolved silicic melts through mineral–melt equilibria. Journal of Petrology 38(12), 1691-1706.

Mangler, M.F., Marks, M.A.W., Zaitzev, A.N., Eby, G.N., Markl, G., 2014. Halogen (F,Cl, and Br) at Oldoinyo Lengai volcano (Tanzania): Effects of magmatic differentiation, silicate – natrocarbonatite melt separation and surface alteration of natrocarbonatite. Chemical Geology 365, 43-53.

Markl, G., Piazolo, S., 1998. Halogen-bearing minerals in syenites and high-grade marbles of Dronning Maud Land, Antarctica: monitors of fluid compositional changes during late-magmatic fluid-rock interaction processes. Contributions to Mineralogy and Petrology 132 (3), 246-268.

Markl, G., Piazolo, S., 1999. Stability of high-Al titanite from low-pressure calcsilicates in light of fluid and host-rock composition. American Mineralogist 84, 37-47.

Marks, L., Keiding, J., Wenzel, T., Trumbull, R.B., Veksler, I., Wiedenbeck, M., Markl, G., 2014. F, Cl, and S concentrations in olivine-hosted melt inclusions from mafic dikes in NW Namibia and implications for the environmental impact of the Paraná–Etendeka Large Igneous Province. Earth and Planetary Science Letters 392, 39-49.

Marks, M.A.W., Neukirchen, F., Vennemann, T., Markl, G., 2009. Textural, chemical, and isotopic effects of late-magmatic carbonatitic fluids in the carbonatite–syenite Tamazeght complex, High Atlas Mountains, Morocco. Mineralogy and Petrology 97(1-2), 23-42.

Marks, M.A.W., Schilling, J., Coulson, I.M., Wenzel, T., Markl, G., 2008. The alkaline–peralkaline Tamazeght complex, High Atlas Mountains, Morocco: mineral chemistry and petrological constraints for derivation from a compositionally heterogeneous mantle source. Journal of Petrology 49(6), 1097-1131.

Marks, A.W.M., Wenzel, T., Whitehouse, M.J., Loose, M., Zack, T., Barth, M., Worgard, L., Krasz, V., Eby, G.N., Stosnach, H., Markl, G., 2012. The volatile inventory (F, Cl, Br, S, C) of magmatic apatite: an integrated analytical approach. Chemical Geology 291, 241-255.

Mathez, E.A., Webster, J.D., 2005. Partitioning behavior of chlorine and fluorine in the system apatite-silicate melt-fluid. Geochimica et Cosmochimica Acta 69(5), 1275-1286.

Morrison, J., 1991. Compositional constraints on the incorporation of CI into amphiboles. American Mineralogist 76, 1920-1930.

Munoz, J.L., 1984. F-OH and Cl-OH exchange in micas with applications to hydrothermal ore deposits. Reviews in Mineralogy and Geochemistry 13(1), 469-493.

Munoz, J.L., Ludington, S.D. Fluoride-hydroxyl exchange in biotite. 1974. American Journal of Science 274, 396-413.

Nedachi, M., 1980. Chlorine and fluorine contents of rock-forming minerals of the neogene granitic rocks in Kyushu, Japan. 1980. Mining Geololy Special issue 8, 39-48.

O'Reilly, S.Y., Griffin, W.L., 2000. Apatite in the mantle: implications for metasomatic processes and high heat production in Phanerozoic mantle. Lithos 53, 217-232.

Piccoli, P.M., Candela, P.A., Williams, T.J., 1999. Estimation of aqueous HCl and Cl concentrations in felsic systems. Lithos 46(3), 591-604.

Pyle, D.M., Mather, T.A., 2009. Halogens in igneous processes and their fluxes to the atmosphere and oceans from volcanic activity: A review. Chemical Geology 263(1), 110-121.

Salvi, S., Fontan, F., Monchoux, P., Williams-Jones, A.E., Moine, B., 2000. Hydrothermal mobilization of high field strength elements in alkaline igneous systems: evidence from the Tamazeght Complex (Morocco). Economic Geology 95(3), 559-576.

Sato, H., Holtz, F., Behrens, H., Botcharnikov, R., Nakada, S., 2004. Experimental petrology of the 1991–1995 Unzen dacite, Japan. Part II: Cl/OH partitioning between hornblende and melt and its implications for the origin of oscillatory zoning of hornblende phenocrysts. Journal of Petrology, 46(2), 339-354.

Scaillet, B., Macdonald, R., 2004. Fluorite stability in silicic magmas. Contributions to Mineralogy and Petrology 147(3): 319-329.

Schilling, J., Marks, M.A.W., Wenzel, T., Markl, G., 2009. Reconstruction of magmatic to subsolidus processes in an agpaitic system using eudialyte textures and composition: a case study from Tamazeght, Morocco. The Canadian Mineralogist 47(2), 351-365.

Seifert, W., Kramer, W., 2003. Accessory titanite: an important carrier of zirconium in lamprophyres. Lithos 71(1), 81-98.

Sharp, Z.D., Helffrich, G.R., Bohlen, S.R., Essene, E.J., 1989. The stability of sodalite in the system NaAlSiO4 - NaCl. Geochimica et Cosmochimica Acta 53(8), 1943-1954.

Stormer Jr, J.C., Pierson, M.L., Tacker, R.C., 1993. Variation of F and Cl X-ray intensity due to anisotropic diffusion in apatite. American Mineralogist 78, 641-648.

Stormer, J.C., Carmichael, I.S.E., 1971. The free energy of sodalite and the behavior of chloride, fluoride and sulfate in silicate magmas. American Mineralogist 56, 292-306.

Teiber, H., Marks, M.A., Wenzel, T., Siebel, W., Altherr, R., Markl, G., 2014. The distribution of halogens (F, Cl, Br) in granitoid rocks. Chemical Geology 374, 92-109.

Tisserant, D., Thuizat, R., Agard, J., 1976. Données géochronologiques sur le complexe de roches alcalines du Tamazeght (Haut Atlas de Midelt, Maroc). Bureau des Recherches Géologiques Minière Bulletin, Section 23, 279-283.

Tropper, P., Manning C.E., Essene, E.J., 2002. The substitution of Al and F in titanite at high pressure and temperature: experimental constraints on phase relations and solid solution properties. Journal of Petrology 43(10), 1787-1814.

Volfinger, M., Robert, J.L., Vielzeuf, D., Neiva, A.M.R., 1985. Structural control of the chlorine content of OH-bearing silicates (micas and amphiboles). Geochimica et Cosmochimica Acta 49(1), 37-48.

Wang, L.X., Marks, M.A.W., Keller, J., Markl, G., 2014. Halogen variations in alkaline rocks from the Upper Rhine Graben (SW Germany): Insights into F, Cl and Br behavior during magmatic processes. Chemical Geology 380, 133-144.

Wang, L.X., Marks, M.A.W., Wenzel, T., von der Handt, A., Keller, J., Teiber, H., Markl, G., 2014. Apatites from the Kaiserstuhl Volcanic Complex, Germany: new constraints on the relationship between carbonatite and associated silicate rocks. European Journal of Mineralogy 26, 397-414.

Webster, J.D., Tappen, C.M., Mandeville, C.W., 2009. Partitioning behavior of chlorine and fluorine in the system apatite–melt–fluid II: Felsic silicate systems at 200MPa. Geochimica et Cosmochimica Acta 73(3), 559-581.

Webster, J.D., 1990. Partitioning of F between H_2O and CO_2 fluids and topaz rhyolite melt. Contributions to Mineralogy and Petrology 104(4), 424-438.

Wu, F.Y., Yang, Y.H., Marks, M.A.W., Liu, Z.C., Zhou, Q., Ge, W.C., Yang, J.H., Zhao, Z.F., Mitchell, R.H., Markl, G. In situ U–Pb, Sr, Nd and Hf isotopic analysis of eudialyte by LA-(MC)-ICP-MS. Chemical Geology 273(1), 8-34.

Zhang, C., Holtz, F., Ma, C., Wolff, P.E., Li, X., 2012. Tracing the evolution and distribution of F and Cl in plutonic systems from volatile-bearing minerals: a case study from the Liujiawa pluton (Dabie orogen, China). Contributions to Mineralogy and Petrology 164(5), 859-879.

Zhu, C., Sverjensky, D.A., 1992. F-Cl-OH partitioning between biotite and apatite. Geochimica et Cosmochimica Acta 56(9), 3435-3467.

Figure captions:

Fig.1: Geological sketch map of the Tamazeght alkaline complex, where locations of the investigated samples are marked.

Fig.2: Bulk rock compositions of the alkaline-per alkaline rocks from Tamazeght complex (Data from Kchit, 1990) showing the geochemical signatures of each rock units.

Fig.3: BSE images of the representive coexisting mineral assemblages from the Tamazeght complex. Abbreviations are Ap = apatite; Bt = biotite; Am = amphibole; Ttn = titanite; SGM = Sodalite group minerals; Fl = fluorite; Cpx = clinopyroxene.

Fig.4: Fluorine and chlorine contents of apatite, biotite, amphibole and titanite from Tamazeght complex.

Fig.5: Relations of fluorine and chlorine contents with Sr contents in apatite and Mg contents in biotite and amphibole from Tamazeght complex**.**

Fig.6: Relations of fluorine contents with Al^{VI} and Fe^{3+} contents in titanite from Tamazeght complex.

Fig.7: Variation of the partitioning coefficients of F and Cl between coexisting apatite and biotite from Tamazeght complex and their relations with Mg concentrations in biotite, temperature and F and Cl contents in biotite and apatite.

Fig.8: Variation of the partitioning coefficients of F and Cl between coexisting apatite and amphibole from Tamazeght complex and their relations with Mg concentrations in amphibole, temperature and F and Cl contents in amphibole and apatite. "*" the data points reflect average temperature and F, Cl contents of each sample.

Fig.9: Variation of the partitioning coefficients of F and Cl between coexisting biotite and amphibole from Tamazeght complex and their relations with Mg concentrations in biotite and amphibole, temperature and F and Cl contents in biotite and amphibole.

Fig.10: Variation of the partitioning coefficients of F between coexisting titanite and apatite/biotite/amphibole from Tamazeght complex and their relations with Mg concentrations in

biotite/amphibole,Al^{VI} and Fe^{3+} contents of titantie, temperature and F contents in titanite and apatite/biotite/ amphibole.

Fig.11: Cl/Br ratios of the investigated minerals from Tamazeght complex and its relation with Cl contents in these minerals. "*" apatite data are from Kaisersthul alkaline complex, SW Germany (Wang et al., 2014).

Fig. 1

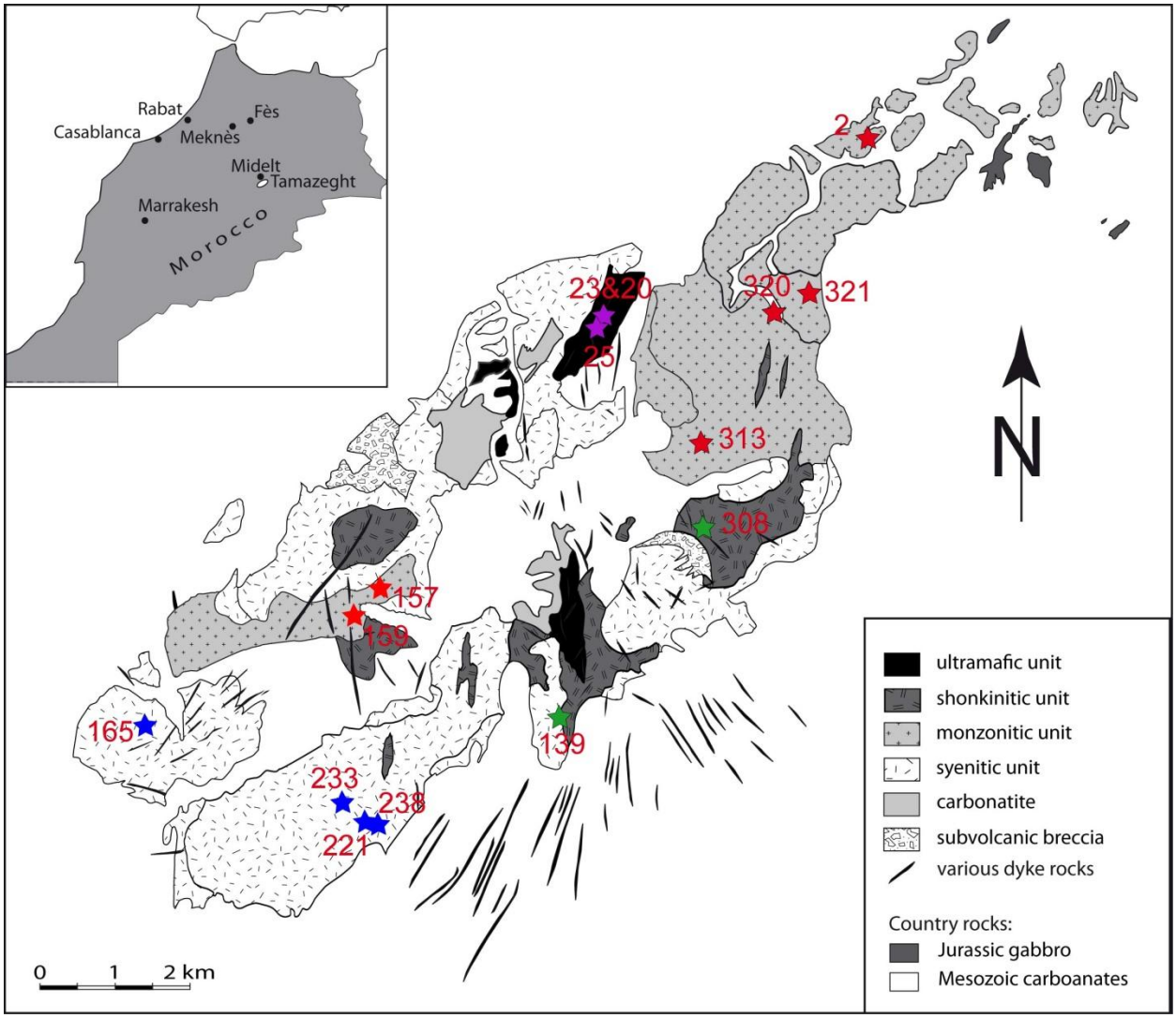
Rabat
Fès
Casablanca
Meknès
Midelt
Tamazeght
Marrakesh
Morocco
2
23&20
25
320
321
313
308
157
159
165
139
233
238
221
N
0
1
2 km
ultramafic unit
shonkinitic unit
monzonitic unit
syenitic unit
carbonatite
subvolcanic breccia
various dyke rocks
Country rocks:
Jurassic gabbro
Mesozoic carboanates

Fig. 2

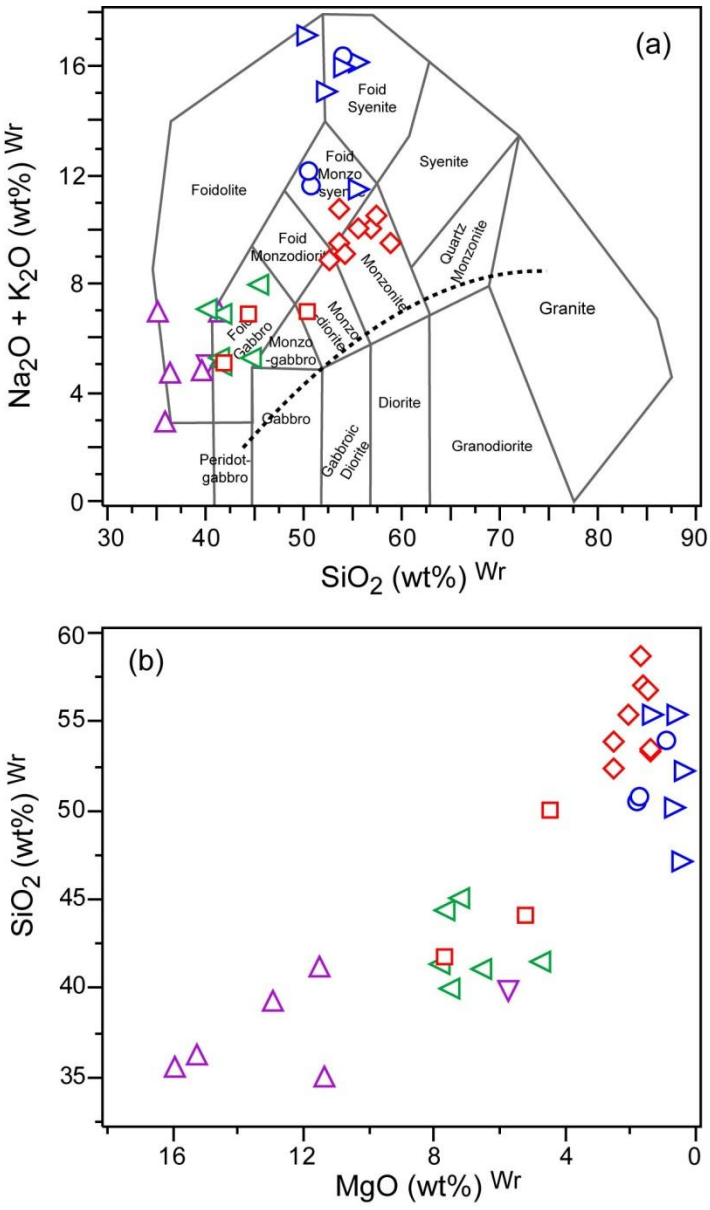
(a)
Foid Syenite
Foid Monzo syen.
Syenite
Foidolite
Foid Monzodiorite
Quartz Monzonite
Monzonite
Granite
Foid Gabbro
Monzo diorite
Monzo -gabbro
Diorite
Gabbro
Peridot-gabbro
Gabbroic Diorite
Granodiorite
$Na_2O + K_2O$ (wt%) Wr
SiO_2 (wt%) Wr
(b)
SiO_2 (wt%) Wr
MgO (wt%) Wr
Rock type
Pyroxenite
Glimerite
Shonkinite
Gabbro
Monzonite/monzosyenite
Nepheline syenite
Agpaitic malignite
Miaskitic malignite
Rock group
Ultramafic
Shonkinitic
Monzonitic
Syenitic

Fig. 3

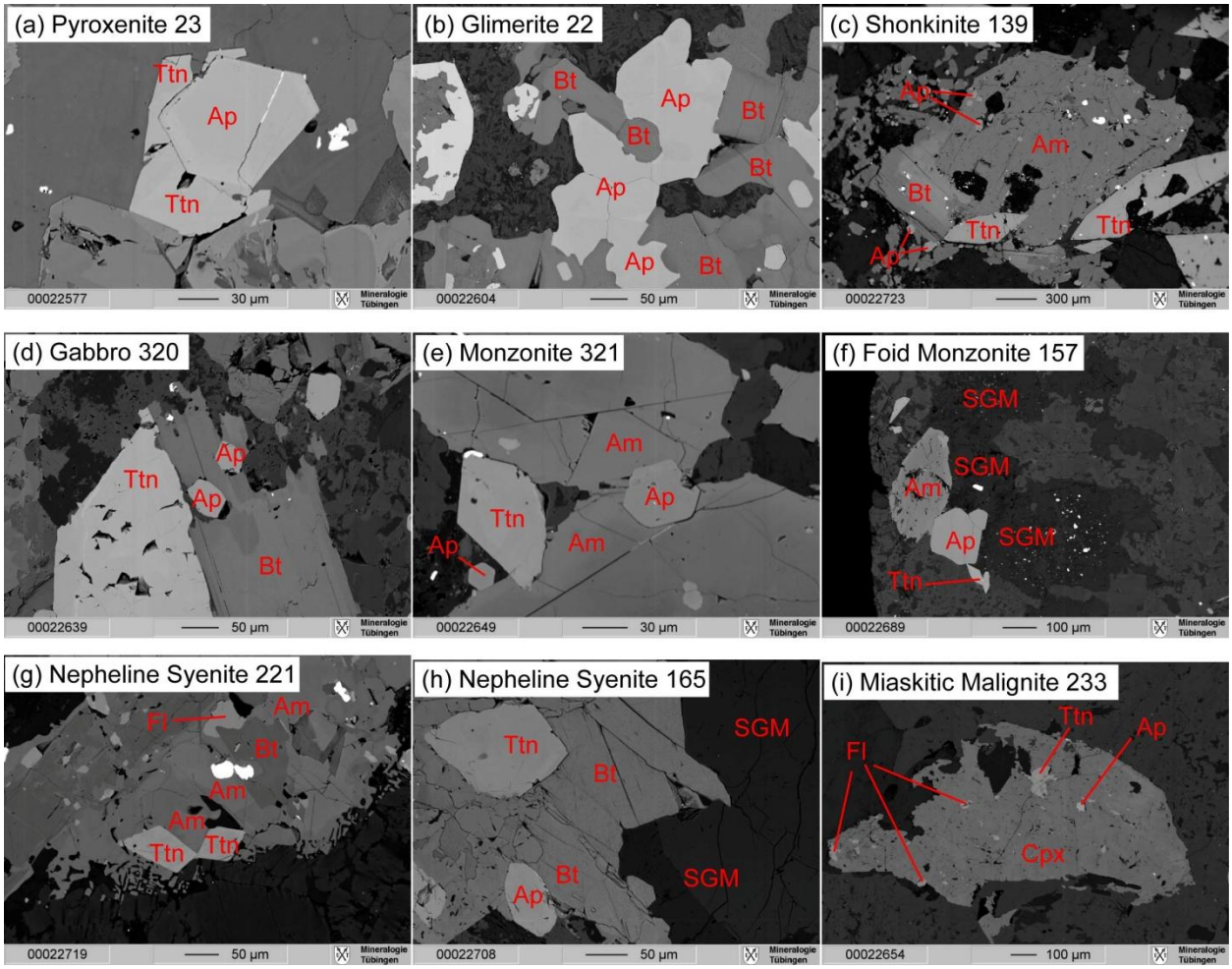
(a) Pyroxenite 23
Ttn
Ap
Ttn
00022577
30 µm
(b) Glimerite 22
Bt
Ap
Bt
Bt
Bt
Ap
Ap
Bt
00022604
50 µm
(c) Shonkinite 139
Ap
Am
Bt
Ttn
Ttn
Ap
00022723
300 µm
(d) Gabbro 320
Ap
Ttn
Ap
Bt
00022639
50 µm
(e) Monzonite 321
Am
Ap
Ttn
Ap
Am
00022649
30 µm
(f) Foid Monzonite 157
SGM
SGM
Am
Ap
SGM
Ttn
00022689
100 µm
(g) Nepheline Syenite 221
Fl
Am
Bt
Am
Am
Ttn
Ttn
00022719
50 µm
(h) Nepheline Syenite 165
Ttn
SGM
Bt
Bt
Ap
SGM
00022708
50 µm
(i) Miaskitic Malignite 233
Ttn
Ap
Fl
Cpx
00022654
100 µm

Fig. 4

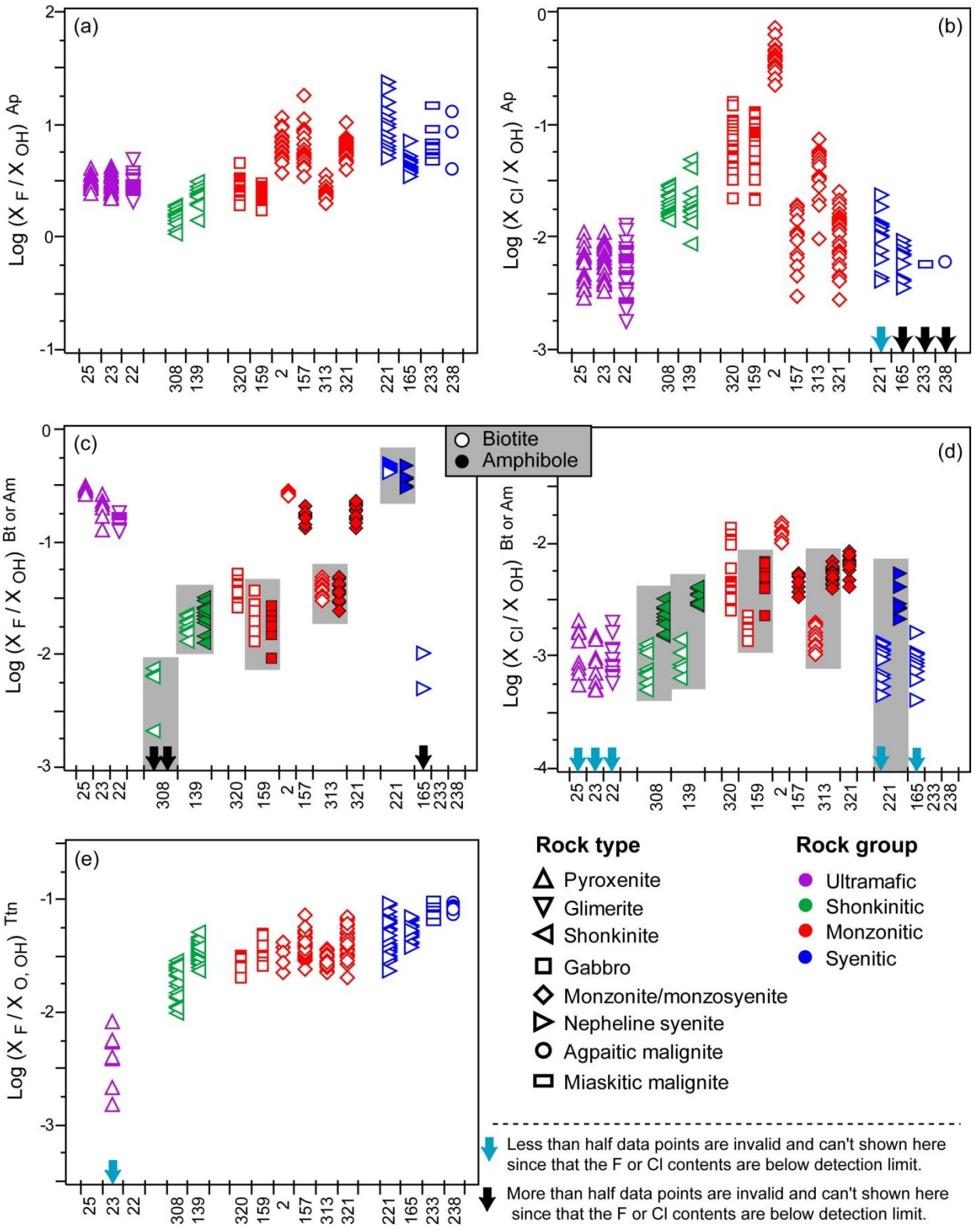
(a)
(b)
(c)
(d)
(e)
Log (X F / X OH) Ap
Log (X Cl / X OH) Ap
Log (X F / X OH) Bt or Am
Log (X Cl / X OH) Bt or Am
Log (X F / X O, OH) Ttn
Biotite
Amphibole
25 23 22 308 139 320 159 2 157 313 321 221 165 233 238
Rock type
Pyroxenite
Glimerite
Shonkinite
Gabbro
Monzonite/monzosyenite
Nepheline syenite
Agpaitic malignite
Miaskitic malignite
Rock group
Ultramafic
Shonkinitic
Monzonitic
Syenitic
Less than half data points are invalid and can't shown here since that the F or Cl contents are below detection limit.
More than half data points are invalid and can't shown here since that the F or Cl contents are below detection limit.

Fig. 5

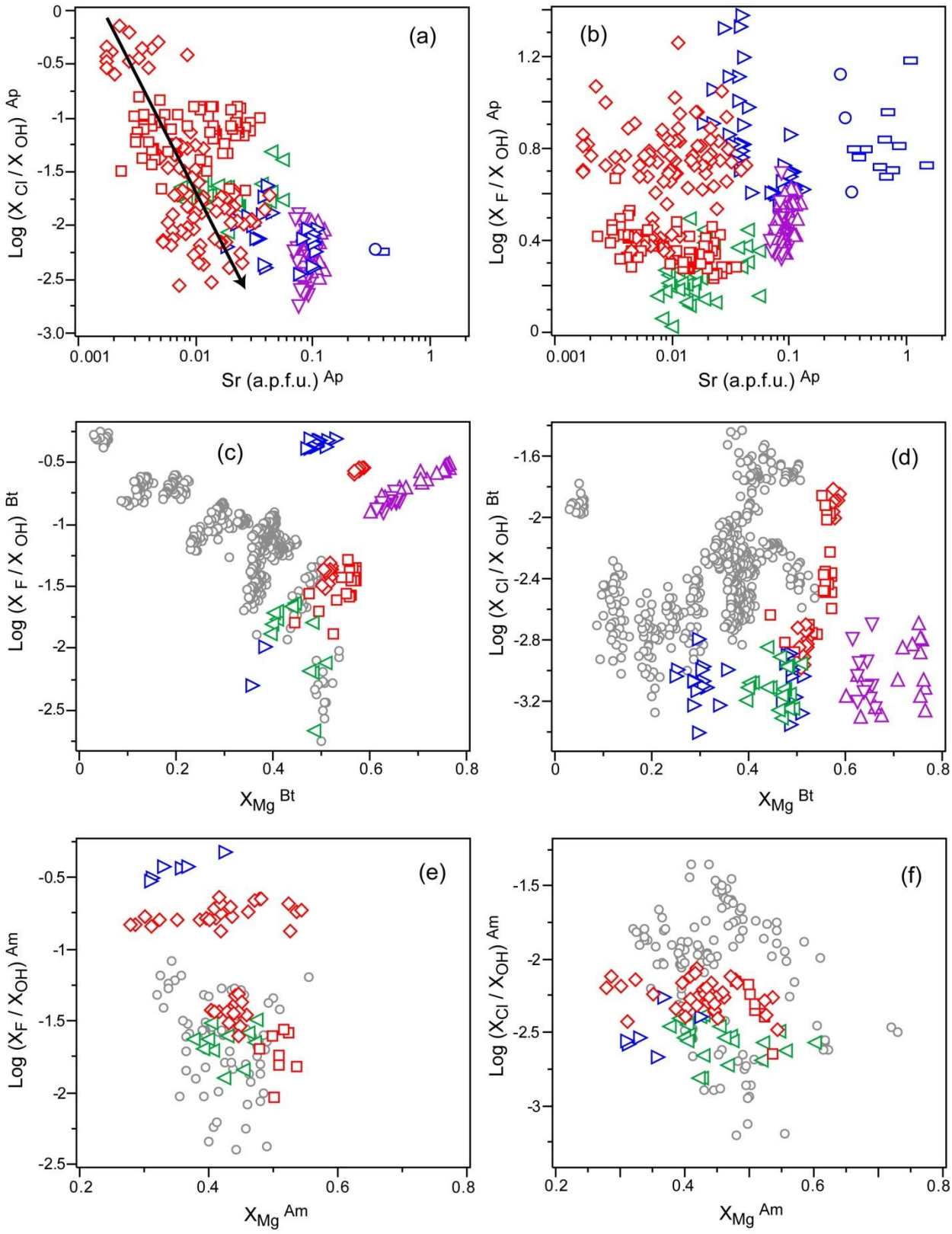
(a)
Log (X Cl / X OH) Ap
Sr (a.p.f.u.) Ap
(b)
Log (X F / X OH) Ap
Sr (a.p.f.u.) Ap
(c)
Log (X F / X OH) Bt
X Mg Bt
(d)
Log (X Cl / X OH) Bt
X Mg Bt
(e)
Log (X F / X OH) Am
X Mg Am
(f)
Log (X Cl / X OH) Am
X Mg Am

Fig. 6

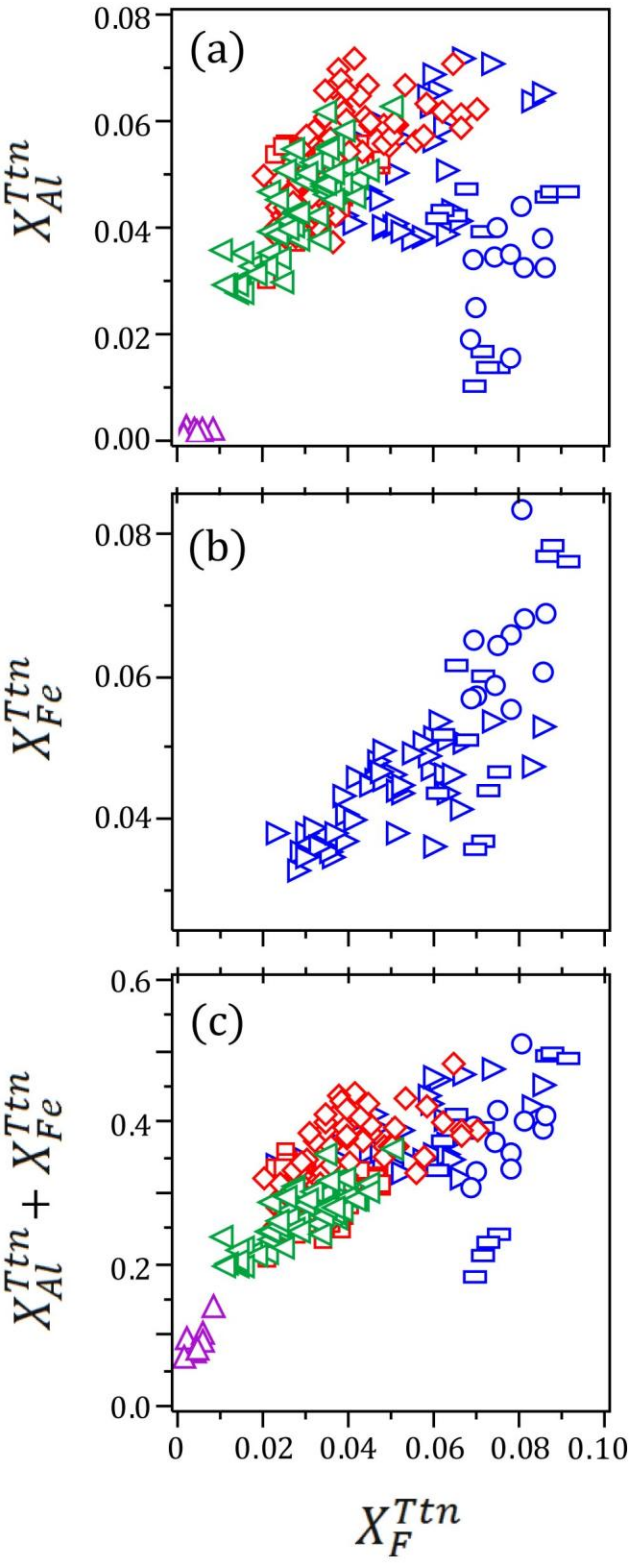
(a)
(b)
(c)
X_{Al}^{Ttn}
X_{Fe}^{Ttn}
$X_{Al}^{Ttn} + X_{Fe}^{Ttn}$
X_{F}^{Ttn}
0.08
0.06
0.04
0.02
0.00
0.6
0.4
0.2
0.0
0
0.02
0.04
0.06
0.08
0.10

Fig. 7

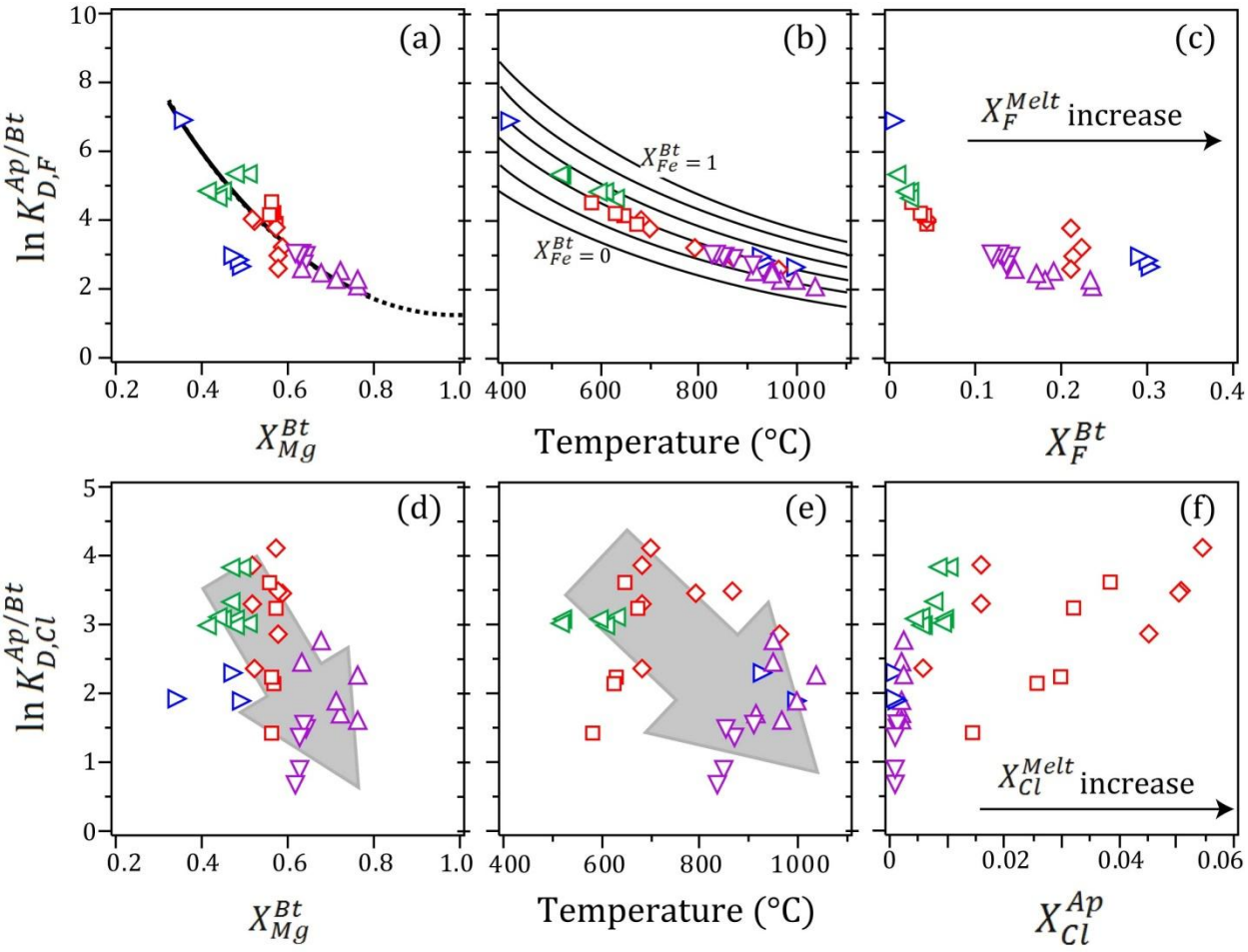
(a)
(b)
(c)
(d)
(e)
(f)
$\ln K_{D,F}^{Ap/Bt}$
$\ln K_{D,Cl}^{Ap/Bt}$
X_{Mg}^{Bt}
Temperature (°C)
X_F^{Bt}
X_{Cl}^{Ap}
$X_{Fe}^{Bt} = 1$
$X_{Fe}^{Bt} = 0$
X_F^{Melt} increase
X_{Cl}^{Melt} increase

Fig. 8

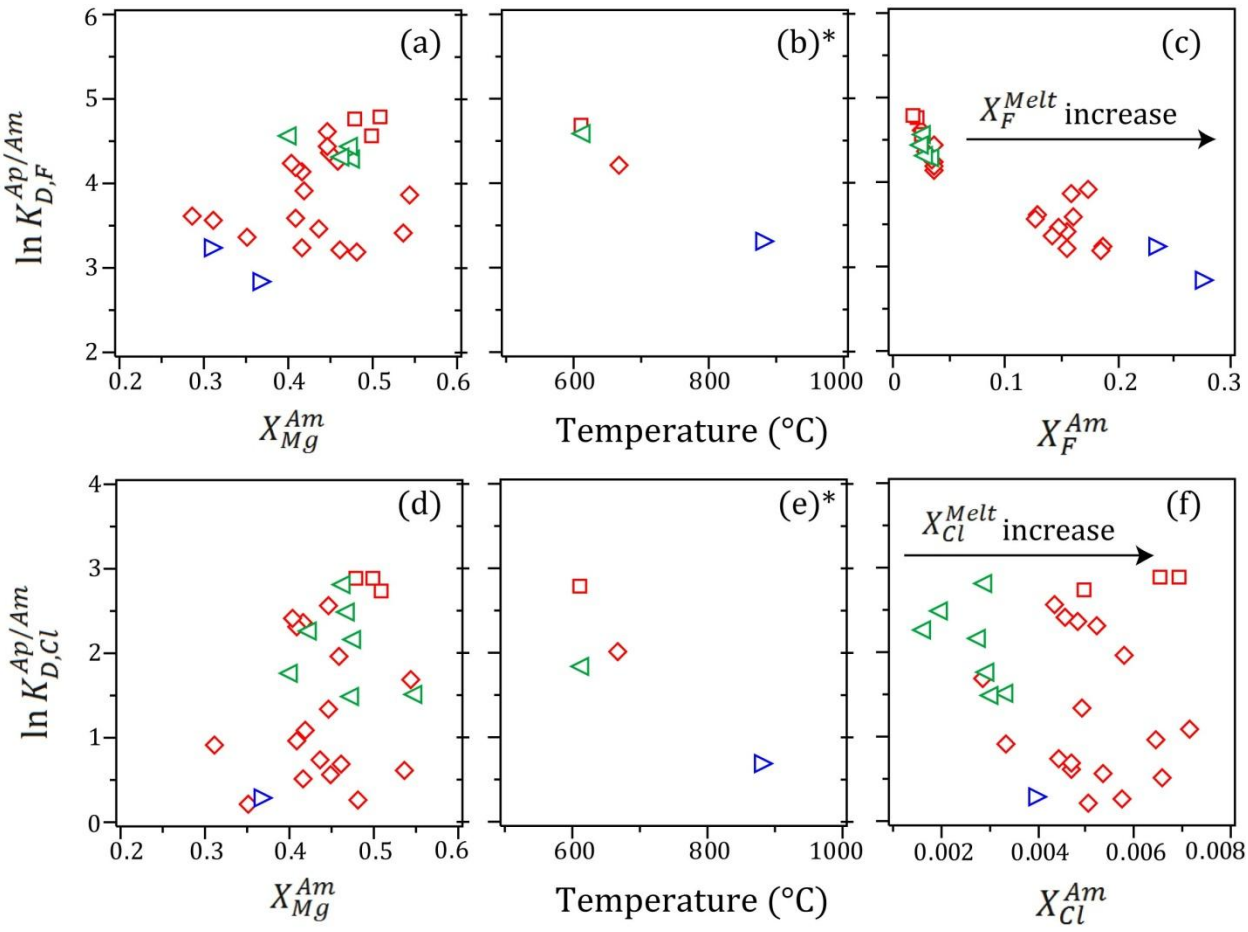
(a)
(b)*
(c)
(d)
(e)*
(f)
$\ln K_{D,F}^{Ap/Am}$
$\ln K_{D,Cl}^{Ap/Am}$
X_{Mg}^{Am}
Temperature (°C)
X_F^{Am}
X_{Cl}^{Am}
X_F^{Melt} increase
X_{Cl}^{Melt} increase

Fig. 9

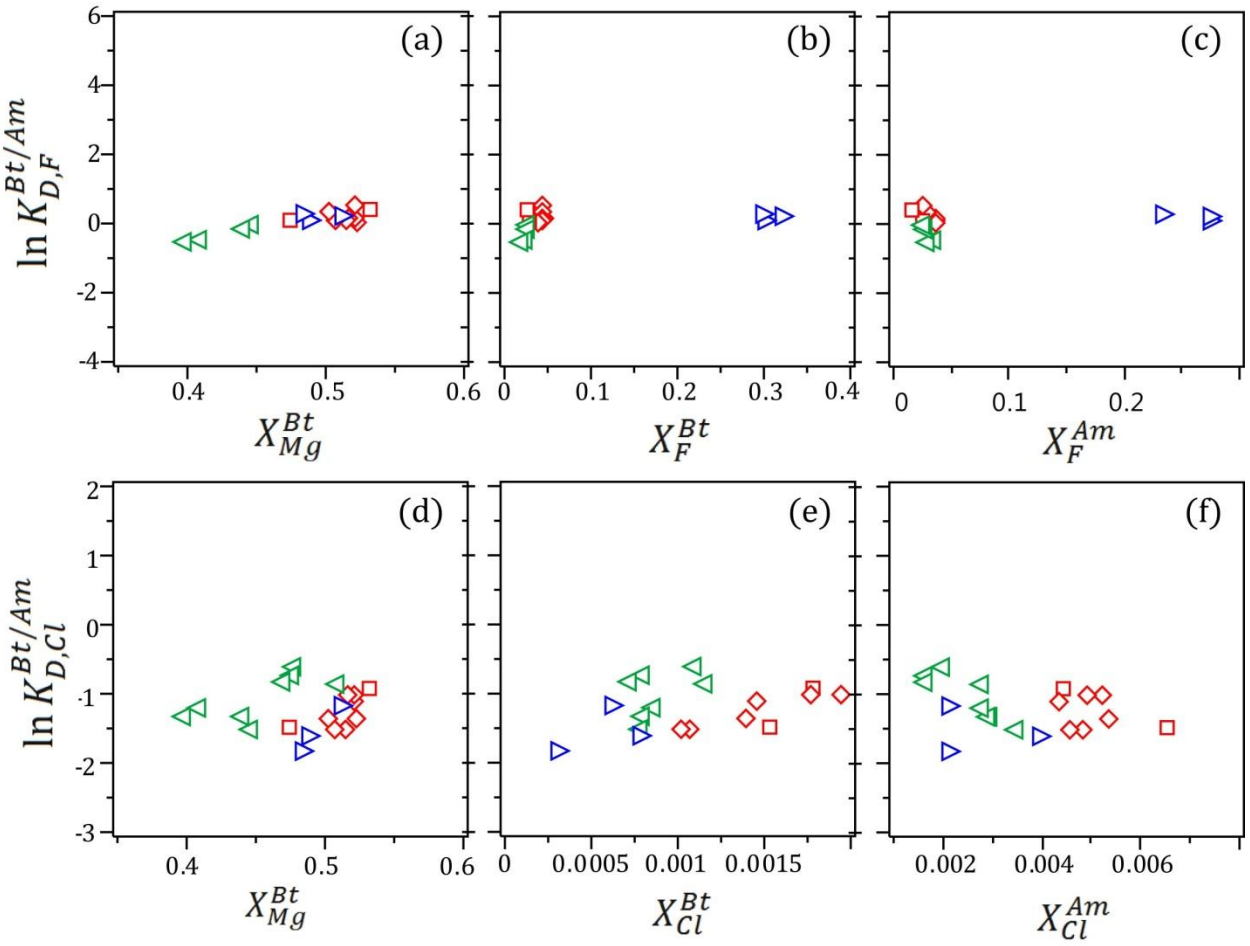
(a)
(b)
(c)
(d)
(e)
(f)
$\ln K_{D,F}^{Bt/Am}$
$\ln K_{D,Cl}^{Bt/Am}$
X_{Mg}^{Bt}
X_{F}^{Bt}
X_{F}^{Am}
X_{Mg}^{Bt}
X_{Cl}^{Bt}
X_{Cl}^{Am}

Fig. 10

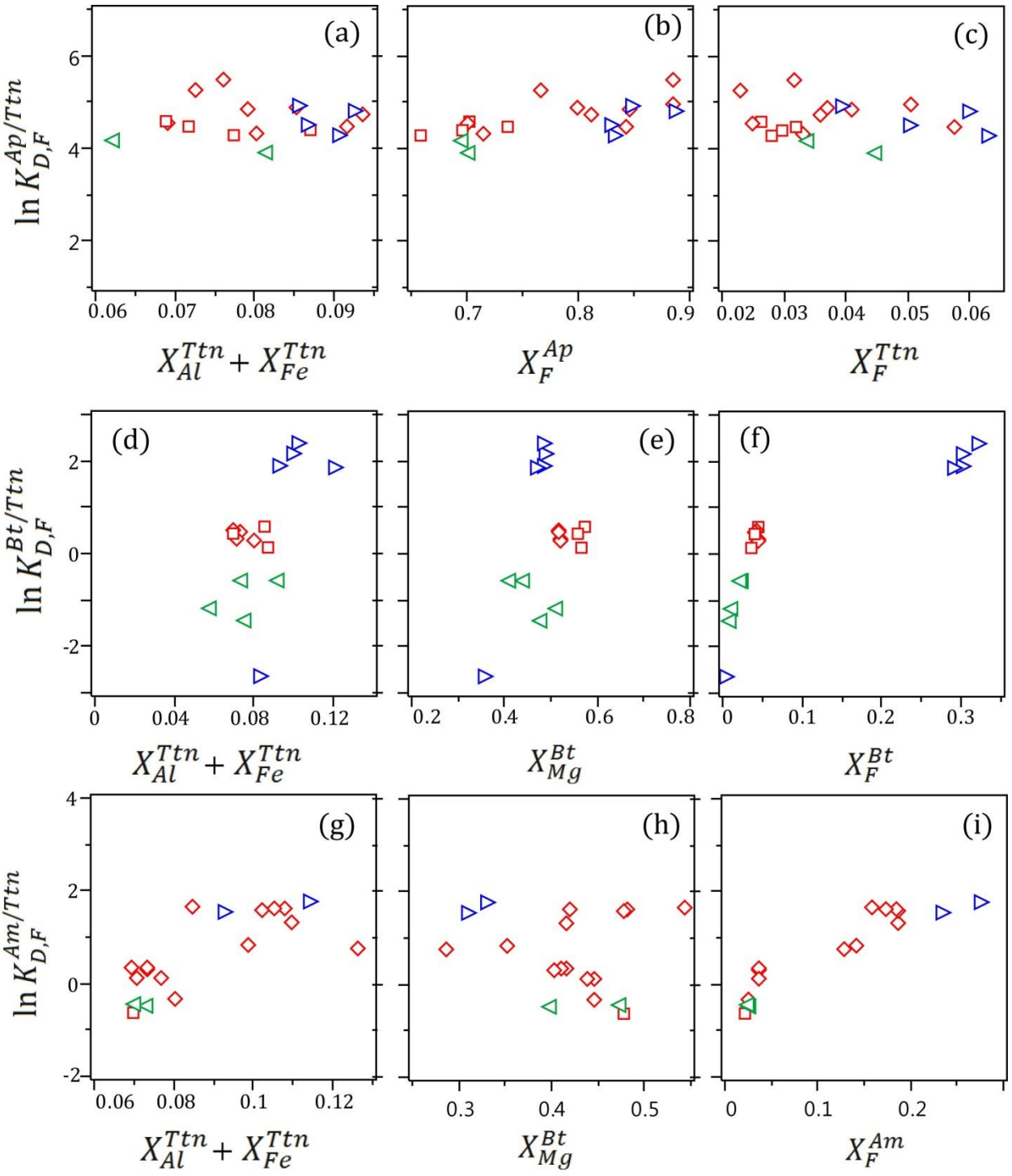
(a)
(b)
(c)
(d)
(e)
(f)
(g)
(h)
(i)
$\ln K_{D,F}^{Ap/Ttn}$
$\ln K_{D,F}^{Bt/Ttn}$
$\ln K_{D,F}^{Am/Ttn}$
$X_{Al}^{Ttn} + X_{Fe}^{Ttn}$
X_F^{Ap}
X_F^{Ttn}
X_{Mg}^{Bt}
X_F^{Bt}
X_F^{Am}

Fig. 11

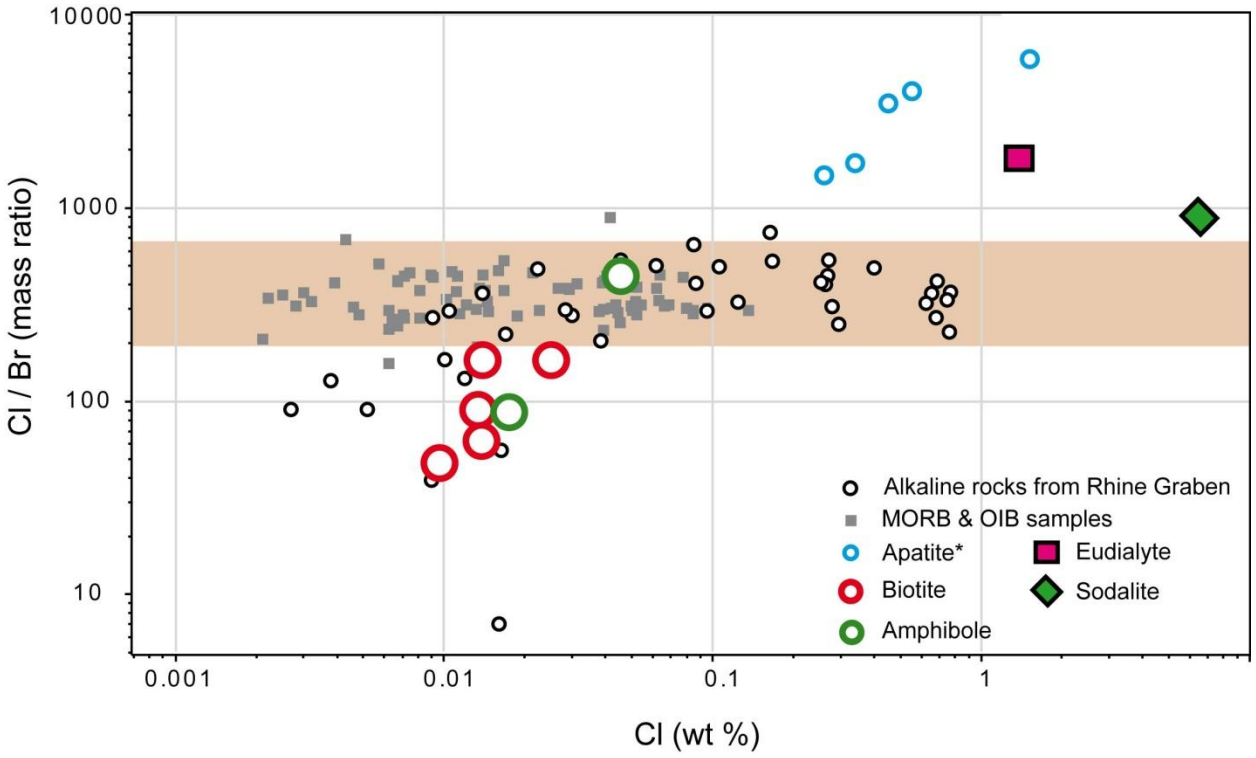
10000
1000
100
10
Cl / Br (mass ratio)
0.001
0.01
0.1
1
Cl (wt %)
Alkaline rocks from Rhine Graben
MORB & OIB samples
Apatite*
Biotite
Amphibole
Eudialyte
Sodalite

Table 1: Summary of the halogen-bearing mineral assemblages (distribution and abundances) observed in the various Tamazeght rocks.

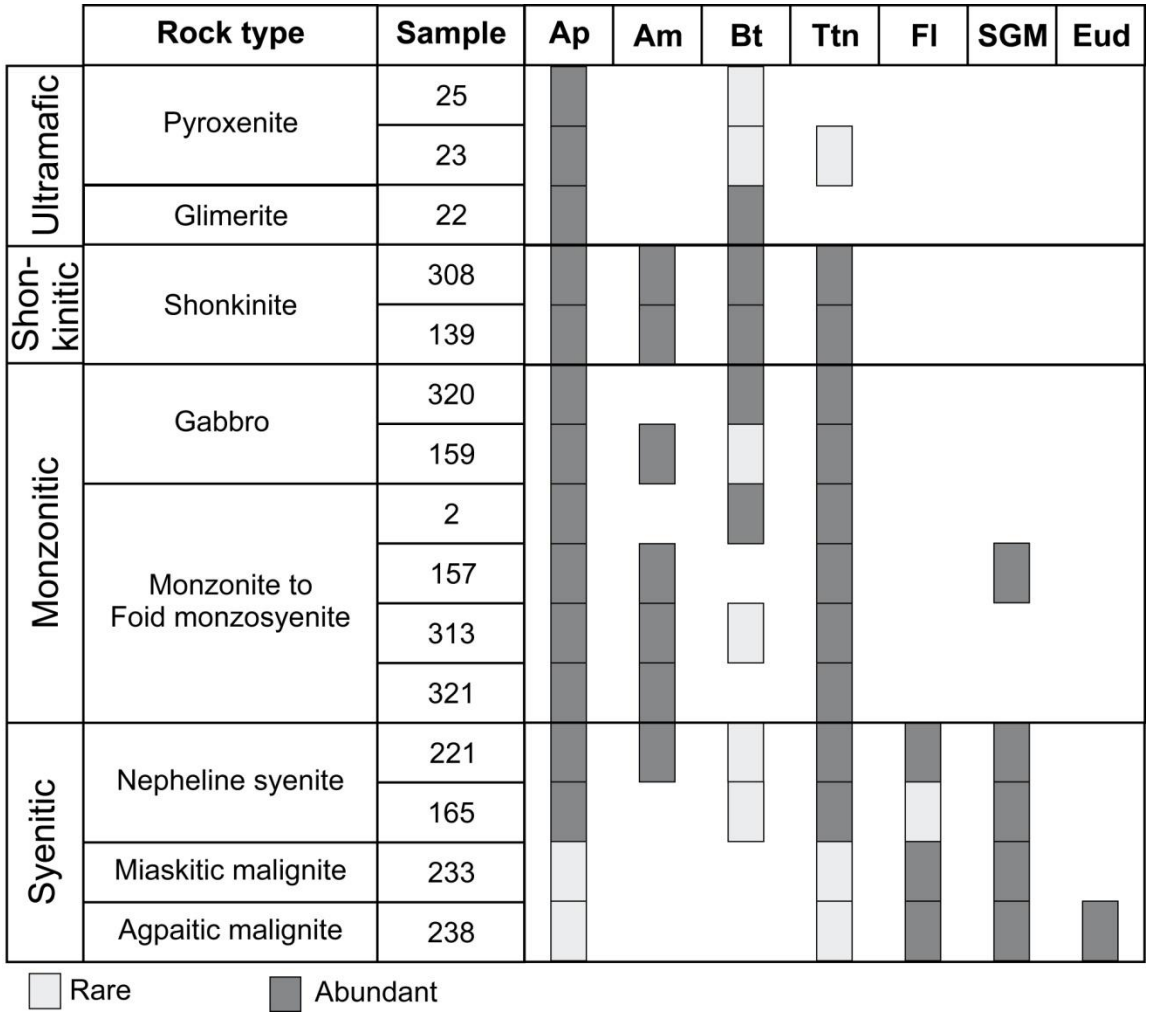

Table 2: Average halogen contents of apatite, biotite, amphibole, titanite, sodalite and eudialyte from the Tamazeght complex, Morocco.

	Ultramafic			Shonkinitic		Monzonitic						Syenitic			
	TMZ25	TMZ23	TMZ22	TMZ308	TMZ139	TMZ320	TMZ159	TMZ2	TMZ157	TMZ313	TMZ321	TMZ221	TMZ165	TMZ233	TMZ238
Apatite	n=21	n=22	n=46	n=22	n=13	n=28	n=36	n=26	n=21	n=19	n=35	n=21	n=23	n=11	n=3
F (wt%)	2.9	2.8	2.8	2.3	2.6	2.7	2.5	3.1	3.2	2.7	3.2	3.4	3.0	3.1	3.2
Cl (µg/g)	100	120	90	560	470	1430	1810	3650	90	790	110	b.d.l.	b.d.l.	b.d.l.	b.d.l.
Br (µg/g)	n.a.	n.a.	n.a.	n.a.	n.a.	n.a.	n.a.	n.a.	n.a.	n.a.	n.a.	n.a.	n.a.	n.a.	n.a.
Biotite	n=9/4	n=10/4	n=13/4	n=14/4	n=9/4	n=16/4	n=6/4	n=10/4	—	n=13/4	—	n=17/4	n=23/4	—	—
F (wt%)	1.96	1.44	1.12	b.d.l.	0.15	0.32	0.19	1.83	—	0.33	—	2.61	b.d.l.	—	—
Cl (µg/g)	135	95	120	125	140	100	280	1520	—	235	—	65	90	—	—
Br (µg/g)	2.0±0.3	1.5±0.5	1.9±0.2	0.8±0.1	b.d.l.	b.d.l.	n.a.	b.d.l.	—	1.5±0.5	—	n.a.	n.a.	—	—
Amphibole	—	—	—	n=9/4	n=12/5	—	n=8/5	—	n=10/5	n=15/5	n=15/5	n=6/5	—	—	—
F (wt%)	—	—	—	b.d.l.	0.09	—	0.08	—	0.60	0.15	0.63	1.09	—	—	—
Cl (µg/g)	—	—	—	180	250	—	390	—	315	400	440	180	—	—	—
Br (µg/g)	—	—	—	b.d.l.	b.d.l.	—	b.d.l.	—	b.d.l.	b.d.l.	1.0±0.2	2.1±0.7	—	—	—
Titanite		n=12		n=23	n=34	n=15	n=27	n=6	n=26	n=23	n=29	n=20	n=15	n=12	n=11
F (wt%)	—	0.03	—	0.18	0.34	0.25	0.37	0.32	0.38	0.28	0.41	0.46	0.49	0.71	0.75
Cl (µg/g)	—	n.a.	—	n.a.	n.a.	n.a.	n.a.	n.a.	n.a.	n.a.	n.a.	n.a.	n.a.	n.a.	n.a..
Br (µg/g)	—	n.a.	—	n.a..	n.a.	n.a.	n.a..	n.a.	n.a.	n.a.	n.a.	n.a.	n.a.	n.a.	n.a.
Sodalite*	—	—	—	—	—	—	—	—	—	—	—	—	—	—	—
F (wt%)	—	—	—	—	—	—	—	—	n.a.	—	—	n.a.	—	n.a.	n.a..
Cl (wt%)	—	—	—	—	—	—	—	—	6.7	—	—	6.1	—	6.4	6.4
Br (µg/g)	—	—	—	—	—	—	—	—	n.a.	—	—	n.a.	—	n.a.	76±2
Eudialyte#	—	—	—	—	—	—	—	—	—	—	—	—	—	—	n=14
F (wt%)	—	—	—	—	—	—	—	—	—	—	—	—	—	—	n.a.
Cl (wt%)	—	—	—	—	—	—	—	—	—	—	—	—	—	—	1.18±0.03
Br (µg/g)	—	—	—	—	—	—	—	—	—	—	—	—	—	—	6.6±0.7

* Data from Marks et al. (2008), # Data from Schilling et al. (2009), n.a. = not analyzed, b.d.l. = below detection limit

Table 3: Estimation of F and Cl abundances in the Tamazeght magmas.

Sample	T(° C)	$lnK_D^{Ap/Bt}$	Melt[a]		Melt[b]		Melt[c]		Melt[d]
			F (µg/g)	Cl (µg/g)	F (µg/g)	Cl (µg/g)	F (µg/g)	Cl (µg/g)	Log(Cl/OH)
TMZ25	950	2.4	8450	120	2120	130	2880	90	
TMZ23	905	2.7	8280	150	2070	160	2370	60	
TMZ22	870	2.9	8120	120	2020	120	1940	80	
TMZ308	390	6.8	6700	700	1600	750	30	100	-3.9
TMZ139	610	4.8	7780	590	1910	620	420	110	-3.2
TMZ320	630	4.2	7870	1790	1950	1900	590	790	
TMZ159	609	4.5	7420	2260	1810	2380	400	230	-2.9
TMZ2	827	3.2	9050	4560	2300	4830	3330	1250	
TMZ157			9500	110	2430	120			
TMZ313	667	4.1	7910	990	1950	1040	690	190	-2.8
TMZ321			9500	140	2430	150			
TMZ221	882	3.1	9950	<50	2570	<50	5930	50	-2.6
TMZ165	307	8.8	8860	<50	2290	<50	20	40	
TMZ233			9150	<50	2460	<50			
TMZ238			9330	<50	2500	<50			

a Calculated from apatite compositions according to the model of Mathez and Webster (2005)

b Calculated from apatite compositions according to the model of Webster et al. (2009) and Zhang et al. (2012)

c Calculated from biotite compositions according to the model of Icenhower and London (1997)

d Calculated from amphibole compositions according to the model of Sato et al. (2005)